Summer 8-31-2003

Issues of seismic response and retrofit for critical substation equipment

Seyed Ali Hashemi Nezhad Ashrafı
New Jersey Institute of Technology

ABSTRACT

ISSUES OF SEISMIC RESPONSE AND RETROFIT FOR CRITICAL SUBSTATION EQUIPMENT

by
Seyed Ali Hashemi Nezhad Ashrafi

This study focuses on means to reduce the seismic hazard for transformer-bushing systems and different issues of the response and rehabilitation of transformers. The primary means of seismic mitigation investigated is the use of the Friction Pendulum System (FPS) bearings to seismically isolate transformers. This is done by developing a finite element model representing the behavior of FPS bearings and implementing this model on to ADINA finite element package for further use in analytical studies. This model is used to study the behavior of isolated primary-secondary systems and the effects of parameters like different FPS radii or vertical excitations. Also studied are the effects of isolation on forces applied to the foundations and the corresponding design of foundations compared to the commonly used fixed-base forces. Further, the interaction of transformer-bushings with interconnecting equipment in the substation is studied and corresponding graphs indicating the amount of required slack in connecting cables are presented. Finally, the behavior of internal components of transformers under seismic excitation has been studied. Possible failure and damage modes are identified and a model is developed and analyzed to assess damage risk.

ISSUES OF SEISMIC RESPONSE AND RETROFIT FOR CRITICAL SUBSTATION EQUIPMENT

by
Seyed Ali Hashemi Nezhad Ashrafi

A Thesis
Submitted to the Faculty of
New Jersey Institute of Technology
In Partial Fulfillment of the Degree of
Master of Science in Civil Engineering

Department of Civil and Environmental Engineering

August 2003

APPROVAL PAGE

ISSUES OF SEISMIC RESPONSE AND RETROFIT FOR CRITICAL SUBSTATION EQUIPMENT

Seyed Ali Hashemi Nezhad Ashrafi

M. Ala Saadeghvaziri, Thesis Advisor — Date
Professor of Civil and Environmental Engineering, NJIT

William R. Spillers, Committee Member — Date
Distinguished Professor of Civil and Environmental Engineering, NJIT

Methi Wecharatana, Committee Member — Date
Professor of Civil and Environmental Engineering, NJIT

BIOGRAPHICAL SKETCH

Author: Seyed Ali Hashemi Nezhad Ashrafi

Degree: Master of Science

Date: August 2003

Undergraduate and Graduate Education:

- Master of Science in Civil Engineering,
  New Jersey Institute of Technology, Newark, NJ, 2003

- Bachelor of Science in Civil Engineering
  Sharif University of Technology, Tehran, Iran, 2000

Major: Civil Engineering

Presentations and Publications:

Ashrafi, Ali, "Analytical Study on Rehabilitation of Critical Electric Power System Components", Student Research Accomplishments 2001-2002, Multidisciplinary Center for Earthquake Engineering Research, 2002.

Ashrafi, A., Saadeghvaziri, M. Ala, "Response of Transformer Internal Components under Earthquakes", Internal Report for Multidisciplinary Center for Earthquake Engineering Research, May 2003.

Saadeghvaziri, M. Ala, Ashrafi, A., "Analytical Study on Rehabilitation of Critical Electric Power System Components", MCEER site visit by National Science Foundation, June 2003.

Ersoy, Selahattin, Ashrafi Ali, "Seismic Response of Transformer-Bushing Systems and their Rehabilitation Using Friction Pendulum System", Multi-Disciplinary Center for Earthquake Engineering Research Annual Meeting, Poster Session, March 2002.

To my mother for her loving support and devotion, and to the memory of my father

ACKNOWLEDGMENT

I would like to express my deep appreciation to Prof. M. Ala Saadeghvaziri for his personal and moral support, excellent technical supervision, and helpful guidance during this work. My gratitude also goes to my committee members, Prof. William R. Spillers and Prof. Methi Wecharatana for their constructive advice.

The financial support for this work was provided by the National Science Foundation through the Multidisciplinary Center for Earthquake Engineering Research (MCEER). This support is greatly appreciated.

TABLE OF CONTENTS

TABLE OF CONTENTS
(Continued)

Chapter **Page**

LIST OF TABLES

LIST OF FIGURES

LIST OF FIGURES
(Continued)

LIST OF FIGURES
(Continued)

LIST OF FIGURES
(Continued)

Figure **Page**

CHAPTER 1

INTRODUCTION

Electric substations are among the most important parts of any electric power network. In societies deeply dependent on electric energy, any damage to these substations or anything interrupting their functioning has immense adverse effects on the society. Such effects include economic damage, disruption of life, interruption in provision of services, and safety problems. Especially in case of earthquakes, the uninterrupted functioning of electric power systems is an integral condition for all activities aimed at recovery, restoration, and reconstruction of the seismically damaged environment.

This thesis deals with different issues of behavior and improvement of electric substations under earthquake conditions. Transformers and bushings are diagnosed as the most important components of an electric substation. Hence, the study is focused on means to reduce seismic hazard of transformer-bushing systems and different issues concerning the response and rehabilitation of transformers. The primary means of seismic mitigation chosen here is the use of the Friction Pendulum System to seismically isolate transformers. This job is done by the development of a finite element model representing the behavior of FPS bearings and implementing it in the ADINA finite element package for further use in analytical studies. This element is used to study the behavior of the isolation system on primary-secondary system response. Also, the effects of isolation on forces applied to the foundation and the corresponding design of foundation are studied. Furthermore, the interaction of transformer-bushing with interconnecting equipment in the substation is studied and corresponding graphs providing the amount of required slack

in connecting cable are presented. Finally, the behavior of internal components of transformers under seismic excitation has been studied.

1.1 The Performance of Electric Substations Under Earthquakes

An electric power system consists of five major components: the power generating facilities, transmission and distribution lines, transmission and distribution substations, control and data acquisition systems, and ancillary facilities and functions. Figure 1.1 shows a typical electric substation. Electric substations that are nodes in this network have different functions including [Ersoy, 2002]:

- Protection of transmission and distribution lines and the equipment within the substation.
- Triggering other devices to isolate the lines or the equipment in abnormal operating conditions.
- Transfer of power between different voltage levels through use of power transformers.
- Reconfiguration of the power network by opening transmission lines or partitioning multi-section buses.

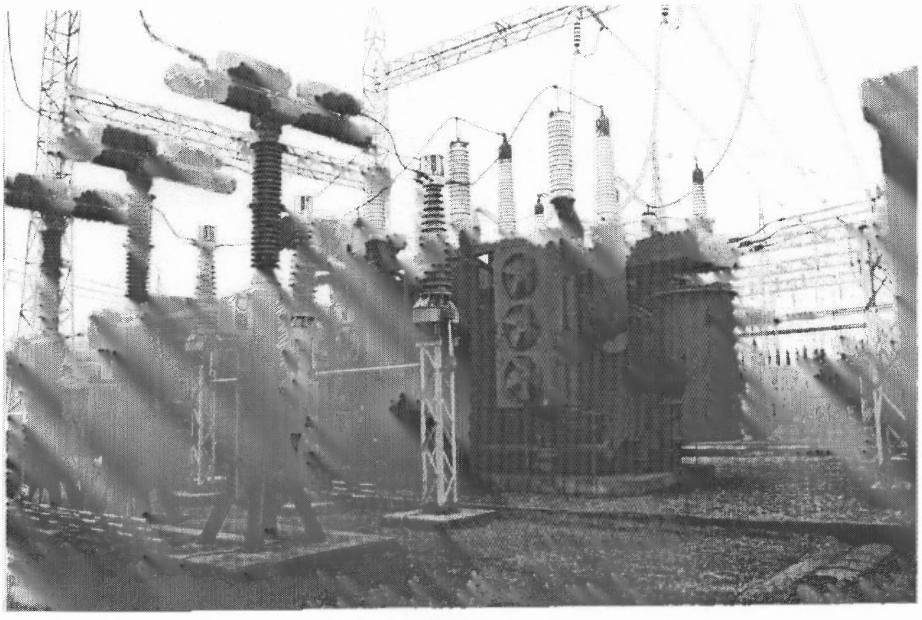

Figure 1.1 Typical substation [Ersoy, 2002].

A key component of a substation is the transformer. A power transformer is the single largest capital item in a substation, comprising almost 60% of the total investment [Woodcock, 2000]. A transformer is a tank containing elements such as a core, coils, and mineral oil and supporting bushings and other electric components [Ersoy, 2002]. These components include sudden pressure and protective relays, anchorage, radiators, bushings, conservators, lightning arrestors, tertiary bushings, and surge arrestors. Sometimes, there are other attachments to the transformer such as reservoir and cooling fans. Figure 1.2 shows a typical transformer and its components. More information about the internal components of transformers is provided in Chapter 5.

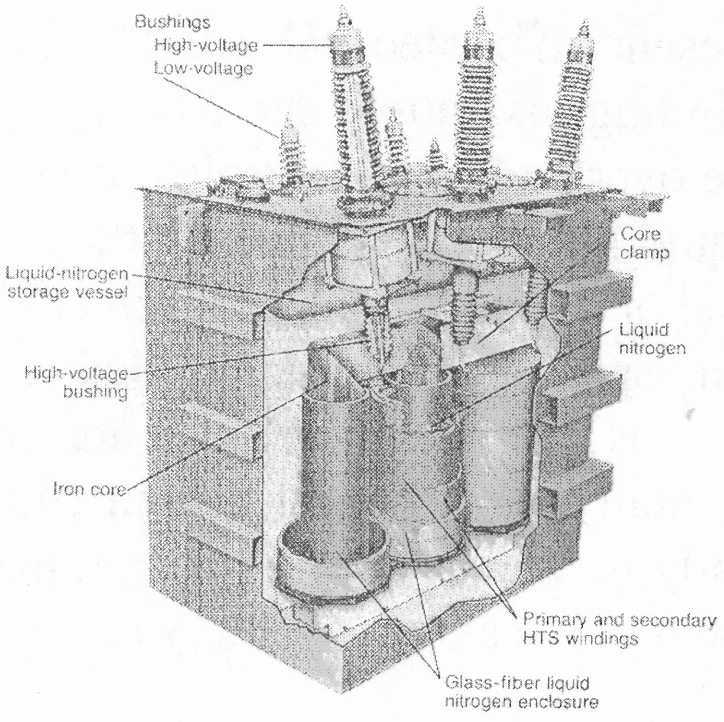

Figure 1.2 Typical transformer and its components [Pansini, 1999].

Bushings are insulated conductors providing electrical connection between the transformer and high-voltage lines. Typically, there is a bushing on top of the transformer above each leg of the core passing through the coils. The most common transformers are three-phase, meaning there will be three bushings above the transformer [Heathcote, 1998]. Figure 1.3 shows a longitudinal section of a 550 kV porcelain bushing. A bushing consists of a conductor passing through an insulating collar, usually made of porcelain. There is mineral oil inside the bushing providing more insulation. The bushing is connected to the transformer through its flange. The bushing is prestressed through the dome on its top. There are springs between this dome and the top porcelain, ensuring uniform distribution of prestressing stresses.

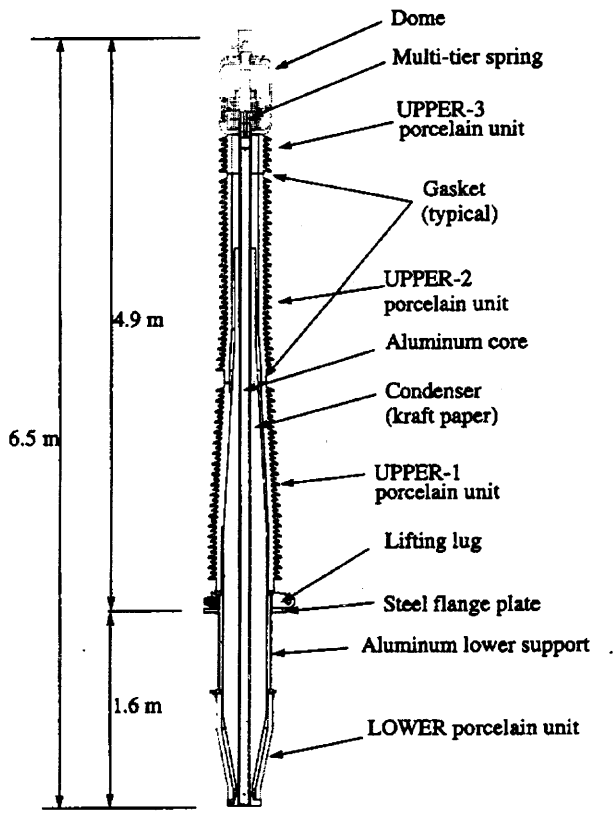

Figure 1.3 Longitudinal section of a 550 kV porcelain bushing [Gilani, 1999(b)].

In past earthquakes, such as the 1994 Northridge earthquake and 1999 Izmit earthquake, electric power systems experienced failures [Ersoy, 2002]. The observed failures in power transformers cab be categorized as:

- Failure of unrestrained transformers.
- Anchorage failure of transformers.
- Conservator failure of transformers.
- Foundation failure of transformers.
- Damage to control boxes.

The first two are the most common modes of failure for transformers. These failures are depicted in Figures 1.4 and 1.5. Unrestrained transformers can be overthrown by earthquake. Restraining them requires considerable anchorage that can carry large forces of seismic excitation including overturning moments. Likewise, the foundation should be designed to sustain such high loads. In addition to these mechanical failures, the internal components of the transformers can sustain damages that impede electric functioning of transformer. These failure modes are extensively discussed in Chapter 5. If no damage is observed in the transformer and the earthquake intensity is low to moderate, the transformer is usually put back to service after a high-potential test for possible internal failures.

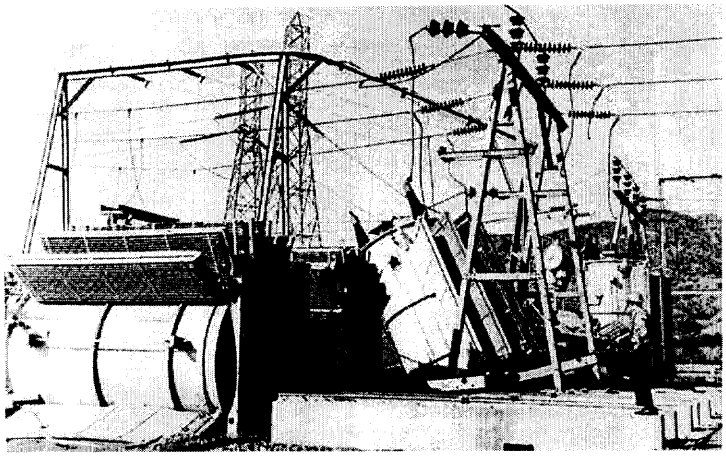

Figure 1.4 Damage to a rail-mounted transformer [ASCE, 1999].

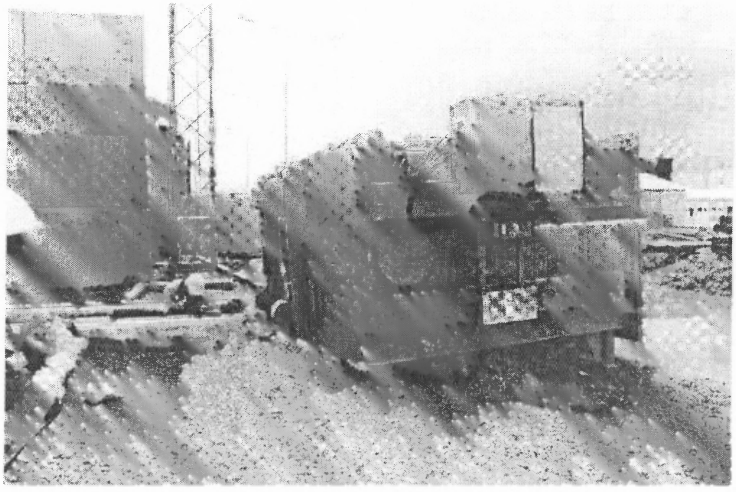

Figure 1.5 Transformer overturned due to failure of anchorage [MCEER, 2000].

Bushings may sustain damages as well. The major damages to bushings can be classified as oil leak due to gasket failure, and fracture of porcelain body due to interaction between bushing and the interconnecting equipment. Previous studies have shown that amplification of ground input because of flexibility of transformer can be one of the major sources of damages observed in bushings. While tests of bushings on rigid frames show high resistance of bushings, failure may occur when the bushing is mounted on a flexible frame. This phenomenon is observed both in experimental studies [Gilani, 1999(a), 1999(b)] and analytical studies [Ersoy, 2002].

1.2 Issues Investigated Under This Research Study

The second chapter of the thesis is dedicated to behavior of FPS bearings. A thorough study of the experimental and analytical work done on FPS is followed by theoretical representation of how FPS behaves under excitations. Then the details of the finite element model developed to represent this behavior are explained. The steps to

implement this element into ADINA in order to enable us to do finite element analysis of the isolated structure are explained with great detail and special focus on how to deal with numerical nuances of the model. In order to verify this model, numerous time-history analyses of behavior of rigid masses and flexible structures are performed and compared to analytical or experimental results from different analysis methods or different sources. This element is used to study the behavior of isolated primary-secondary systems. A very simple model is used to consider the effect of isolation with FPS bearings on seismic behavior of a wide range of primary and secondary systems with different frequency and mass properties, FPS friction coefficients and radii. All effects including large displacement effects and effects of vertical excitation on the response are studied.

Chapter 3 studies the effects of FPS on foundation design. The design of foundation is done for several cases of isolated transformers. These designs are compared to that of fixed-base transformers. The differences in foundation size and cost are assessed.

Chapter 4 involves a brief study on interaction of transformer-bushing system with other interconnecting equipment in an electrical power station. A simplified model is used to consider the effects of interaction. The results are also compared to the results from previous studies with a simpler model for FPS. The graphs are provided showing the amount of slack required for different levels of peak ground acceleration and FPS radius.

The fifth chapter investigates the seismic behavior of internal components of transformers. A fairly detailed explanation of the internal components is presented. Four

possible modes of failure/damage are identified for the internal components, two of which are detected to be of more concern. The prestressing force in core is identified as the critical criterion for these failure modes and several analyses are performed to determine the level of ground excitation that can cause loss of prestressing. Again, effect of use of FPS on reducing the hazard of damage to the internal components is studied and it is shown to be an effective rehabilitation tool.

Finally, Chapter 6 presents the conclusions.

CHAPTER 2

USE OF FRICTION PENDULUM SYSTEM IN SEISMIC ISOLATION OF POWER TRANSFORMERS

Among different methods of mitigation of seismic hazards known and utilizes so far, base isolation is one of the most effective ways with multiple advantages over the traditional seismic design methods. The general idea in base isolation is to partially separate the base of structure from ground excitations and limit the amount of excitation and force absorbed by the structure. Base isolation can be done for a whole structure, parts of a structure like the roof, or secondary systems inside the structure. Base isolation mechanism usually involves two behavioral characteristics of providing a restoring force and a damping system [Fan, 1990]. They usually tend to move the period of structure to higher periods where the earthquake does not have much energy, hence reducing the amount of energy imparted into the system [Fan, 1990].

Amidst different base isolation systems, a wide category of them makes use of friction as at least one of the behavioral characteristics. Frictional systems have the advantage that they provide a limit on how much force can be transmitted to the structure depending on their friction coefficient. They are also less sensitive to the frequency content of ground input, hence making them proper for use in situation with different ground characteristics [Mokha, 1990]. They also provide some initial resistance to smaller lateral forces [Mokha, 1990] such as wind. On the other hand, since their involvement entails sliding of the structure, in absence of a recentering mechanism, they tend to require the capacity for large displacements in the structure that is being isolated

and there might be substantial permanent displacement after the earthquake. This could pose a problem for structures if they are connected to other structures and equipment and should be taken into consideration if frictional isolation systems are to be used. Another observed feature of frictional systems is that they tend to produce higher frequencies in the response that could potentially excite higher modes of the structure or affect the secondary systems with higher frequencies [Fan, 1990]. The other special aspect of friction systems is that their response is affected by vertical ground input and vertical response of the structure due to their dependence on the amount of normal force in friction surface.

Friction Pendulum System is a very effective system among the frictional systems used for seismic mitigation. Friction Pendulum System (FPS) has a spherical sliding surface. The curvature of the surface provides the structure with a restoring force due to its own weight. This effect is more pronounced in higher displacements [Mokha, 1990]. Hence, FPS tends to provide an ever-increasing force as the displacement of the slider increases. This will have the effect of reducing the maximum displacement incurred and having a small permanent displacement in the bearing. This increased force will on the other hand translate into higher shear forces. The FPS bearings have several advantages such as their fixed period. Since the amount of the recentering force is proportional to the vertical load on FPS, the period of the system is independent of mass [Mokha, 1990]. Also, the center of stiffness will be the same as the center of mass, hence preventing torsional movements in structures based on FPS [Mokha, 1990]. More details of this kind of base isolation selected for seismic rehabilitation of transformers under this study are presented in the following section.

2.1 Friction Pendulum System

The Friction Pendulum System (FPS) is an effective base isolation system used for reducing seismic effects on a structure. It consists of an articulated slider sliding on a stainless steel spherical surface covered with low friction material [EPS, 1996] and can be used with the surface being upward or downward. Studying the behavior of FPS bearings has a history of more than 15 years and includes numerous analytical and experimental works [Zayas, 1987].

There are a series of experimental studies performed on FPS. A report was published in 1986 on compression-shear testing of model FPS bearings and shake table tests of model two-story steel frame structures [Zayas, 1987]. This report is followed by another one in 1989 containing feasibility and performance studies on use of FPS for improving seismic behavior of new and existing buildings [Zayas, 1989]. Shake table tests of scaled six-story steel moment frame were performed in 1990 [Mokha, 1990]. Compression-shear testing was done on full size 2.0 second period FPS bearings used in seismic retrofit of a four-story wooden apartment building in 1991 [Zayas, 1991]. Use of Friction Pendulum System for seismic isolation of bridges was studied experimentally and analytically in 1993 [Constantinou, 1993]. A comprehensive study of the behavior of friction surface under different normal force and speeds was performed in 1993 [Zayas, 1993]. FPS was used to perform shake table tests of a quarter model of a seven-story steel moment and braced frames [Al-Hussaini, 1994]. The behavior of computer equipment on FPS was studied in 1994 [Lambrou, 1994]. More extensive compression-shear tests of full size FPS bearings were continued and 20,000-cycle wear tests of the bearing liner were conducted in Earthquake Protection Systems, Inc. in 1996 [Zayas, 1996].

Constantinou performed research on longevity and reliability of sliding seismic isolation systems at the same year [Constantinou, 1996]. A history of all the experimental work done on FPS is presented in a technical report by Earthquake Protection Systems, Inc. [EPS, 1996].

Different approaches have been used to analytically model the behavior of structures isolated with FPS bearings. The most comprehensive program developed having this analytical capability is the series of 3D-BASIS software developed by Reinhorn in MCEER. This software group includes 3D-BASIS [Nagarajaiah, 1989, 1991], 3D-BASIS-M [Tsopelas, 1991], 3D-BASIS-ME [Tsopelas, 1994], and 3D-BASIS-TABS [Nagarajaiah, 1993; Reinhorn, 1994]. These software are designed for analysis of three-dimensional structures isolated using different isolation mechanisms including FPS. Different versions of the software provide for special needs such as analysis of single and multiple structures and liquid storage tanks. They provide the user with a series of options in modeling the structure including inputting the characteristics of the model, or modeling the structure through ETABS [Reinhorn, 1994]. They are, however, restricted to linear structures, condense the structure into 3 degrees of freedom per floor (two lateral displacement and one torsion) and cannot consider the vertical behavior of the structure. Only 3D-BASIS-ME has the option to partially consider the effects of vertical ground motion through modification of the gravity constant g to $g + \ddot{u}_g$ and calculating the normal force change due to overturning moments. However, the effect of structural flexibility on normal force change is ignored [Tsopelas, 1994]. 3D-BASIS uses pseudo-force method for computing the effects of isolation systems. There have been other direct attempts in finite element modeling of FPS as well. Tsai has done a

finite element formulation for friction pendulum seismic isolation systems considering the effect of local bending moments [Tsai, 1997]. Almazan et. al. also have modeled FPS and used their model through MATLAB to study effect of different parameters including vertical excitation in behavior of structures isolated with FPS [Almazan 1998, 2002].

These available analytical tools have shortcomings that justify development of a finite element model of FPS that can be implemented in a finite element package. Study of seismic behavior of isolated transformer-bushing requires a complex nonlinear structural model that is not offered by these tools. The models by Almazan and Tsai are not part of a finite element package allowing such modeling, while the family of 3-D BASIS software permits a linear model that is limited to linear elements and condenses the structure into a model with three degrees of freedom per floor. In addition, 3D-BASIS does not consider the effects of vertical ground excitation and vertical response of the structure (except partially by 3D-BASIS-ME).

The finite element package ADINA provides the user with the capability of defining his own element while offering him access to a rich library of elements and material models. The formulation of FPS presented by Tsai and Almazan is not consistent with the format of the user-defined element subroutine in ADINA. Hence, a finite element model is developed by the author to be used in ADINA to model behavior of structures isolated with FPS.

2.2 Formulation of the Behavior of FPS and Its Finite Element Modeling

2.2.1 Theoretical Model for Sliding

The basic equation determining the friction force in one direction is

$$F_f = \mu NZ \tag{2.1}$$

where μ is the friction coefficient, N is the Normal force and Z is a function between -1 and 1 calculated from

$$Y\dot{Z} + \gamma\left|\dot{U}_b\right|Z|Z|^{\eta-1} + \beta\dot{U}_b|Z|^{\eta} - A\dot{U}_b = 0 \tag{2.2}$$

where U_b is the displacement of the slider [Constantinou, 1990]. Experimental observations on Teflon-steel interfaces suggest a very small elastic displacement before sliding that is represented by a value of Y of about 0.005 to 0.02 inch. The value of η = 2, with A = 1 and $\beta + \gamma = 1$ ($\beta = 0.1$, $\gamma = 0.9$) produces loops of friction forces versus displacement that are in good agreement with experimental results. Experiments also show that the value of μ is dependent on velocity of sliding [Mokha, 1993].

$$\mu = -(\mu_{\max} - \mu_{\min})e^{-\alpha|V|} \tag{2.3}$$

where $\mu_{\max}$ and $\mu_{\min}$ are the maximum and minimum values of friction coefficient, α is the constant determining the rate of change with velocity, and V is the velocity.

Two-dimensional friction force can be determined by the following set of equations [Mokha, 1993]

$$F_{fx} = \mu NZ_x \tag{2.4}$$

$$F_{fy} = \mu NZ_y \tag{2.5}$$

where

$$\dot{Z}_x = -\frac{\gamma}{Y}\left|\dot{U}_{bx}Z_x\right|Z_x - \frac{\beta}{Y}\dot{U}_{bx}Z_x^2 - \frac{\gamma}{Y}\left|\dot{U}_{by}Z_y\right|Z_x - \frac{\beta}{Y}\dot{U}_{by}Z_xZ_y + \frac{A}{Y}\dot{U}_{bx} \tag{2.6}$$

$$\dot{Z}_y = -\frac{\gamma}{Y}\left|\dot{U}_{by}Z_y\right|Z_y - \frac{\beta}{Y}\dot{U}_{by}Z_y^2 - \frac{\gamma}{Y}\left|\dot{U}_{bx}Z_x\right|Z_y - \frac{\beta}{Y}\dot{U}_{bx}Z_xZ_y + \frac{A}{Y}\dot{U}_{by} \tag{2.7}$$

At the time of sliding, Z is either equal to 1 or -1. Therefore, instead of solving these involved differential equations that is a tedious process, a simpler hysteresis model for Z is considered with bilinear elasto-plastic behavior. The slope in non-sliding phase can be calculated as $\frac{1}{Y}$ and the slope in sliding phase is equal to zero. Figure 2.1 shows this behavior in one-directional friction.

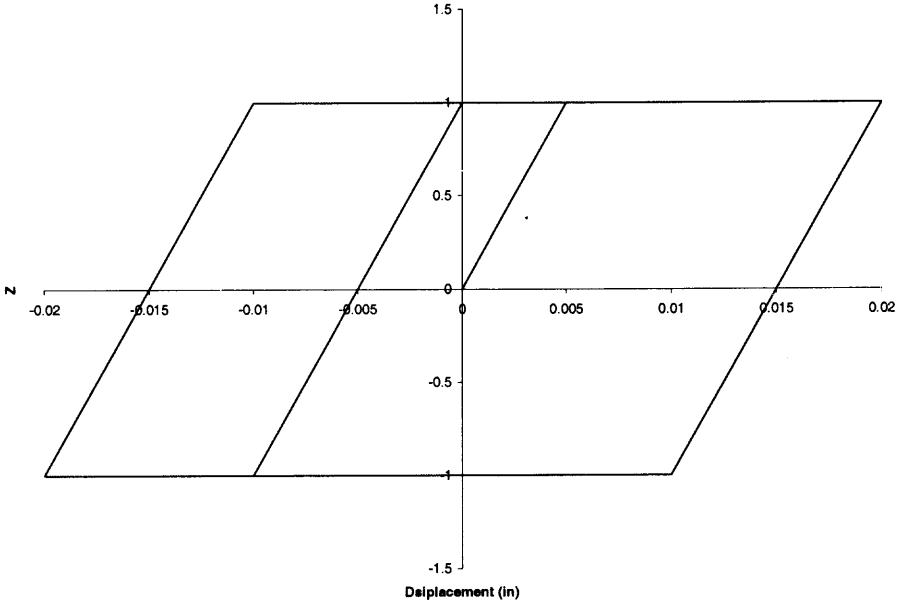

Figure 2.1 Assumed hysteresis behavior of Z in one direction.

The value of Z for 2-D case is calculated as below. There can always be assumed a circle with the radius for Y inside which the slider is experiencing elastic displacement and outside which sliding happens. The slider is where the slider would be if no force

was applied to it. The norm of Z on and outside the circle is 1 and it is reduced linearly to 0 as the slider moves from the boundary inward to the center. The direction of this Z vector is always along the vector connecting the center of the circle to the slider location (outward) and the values of Z_x and Z_y are the components of Z in x and y directions. When slider is moving inside this circle, the position of the circle does not change. However, when the slider moves outside the circle, it moves the circle along in a way that at the end of the time step in which it slides, it is on the boundary of the new circle and the center of the circle is aligned with the direction of sliding. Figure 2.2 shows this schematically for different situations. The thick lines show the position of slider and the neutral center at the last converged time step and the thin lines show the positions at the current time step. The first and second rows of the figure respectively represent the situation where the slider has been or has not been sliding at the last time step. If the slider slides in the current step, it will change the position of the neutral center and move the non-sliding circle with it. In any case, the values Z_1 and Z_2 are calculated as

$$Z_1 = U_1 / Y \tag{2.8}$$

$$Z_2 = U_2 / Y \tag{2.9}$$

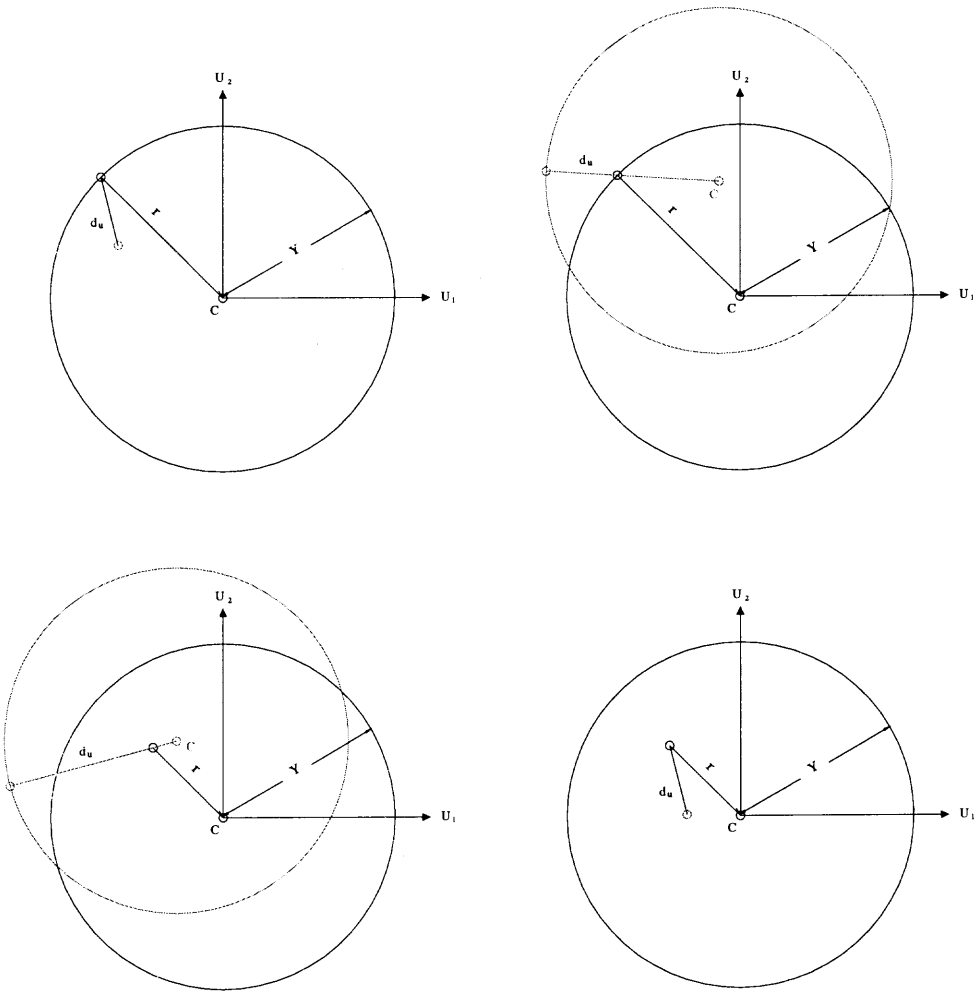

Figure 2.2 2-D behavior of the model for Z.

2.2.2 The Finite Element Formulation

Figures 2.3 and 2.4 show a typical FPS bearing. Figure 2.5 shows a schematic graph of the bearing with active forces sketched. As observed, the FPS consists of a sliding surface with a certain curvature, and an articulated slider. The finite element developed for FPS consists of 2 nodes with 3 translational degrees of freedom in each node. The first node represents the sliding surface while the second node represents the articulated slider. There are small values of moment involved for keeping the static balance that are ignored here. Since the element is being implemented in ADINA as part of this study, it is

required to add 3 rotational degrees of freedom to each node. However, all forces in these nodes and all the stiffness components related to them are equal to zero.

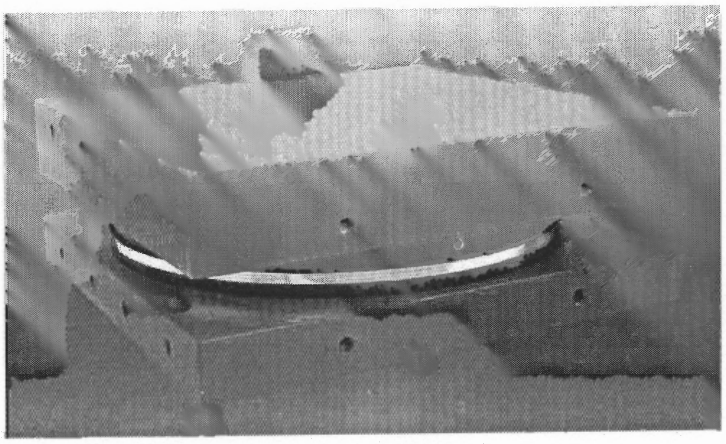

Figure 2.3 Picture of a typical FPS bearing [Ersoy, 2002].

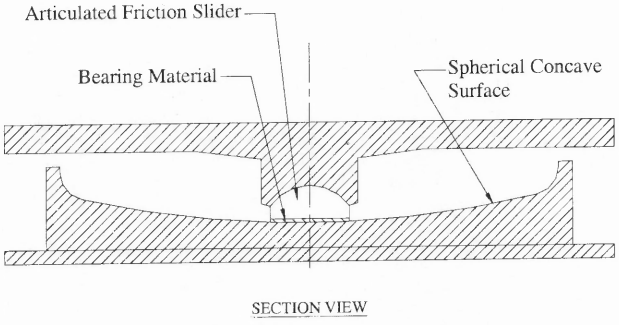

Figure 2.4 Sketch of a typical FPS bearing [Ersoy, 2002].

The global degrees of freedom are

$$U = \begin{bmatrix} u_{11} \\ u_{12} \\ u_{13} \\ u_{21} \\ u_{22} \\ u_{23} \end{bmatrix} \tag{2.10}$$

where the first subscript refers to the corresponding node and the second subscript shows the corresponding direction. The first two directions are horizontal and the 3rd direction is vertical. Two local coordinates are used to describe the position and behavior of the slider more easily. The first is

$$X = \begin{bmatrix} x_1 \\ x_2 \\ x_3 \end{bmatrix} = \begin{bmatrix} u_{21} - u_{11} \\ u_{22} - u_{12} \\ u_{23} - u_{13} \end{bmatrix} \tag{2.11}$$

that describes position of the slider relative to the sliding surface.

However, there is a need for another set of coordinates that can reflect the sliding behavior of the slider that occurs in a plane tangent to the surface at each point in time. These are the coordinates that should be used in the relations determining friction forces. After determining the forces, they are transformed into forces in global coordinates. The first of these coordinates, called v_1 is the vector in the tangent plane that has no x_2 component and is in the direction with positive x_1 component. The second vector is the tangent vector perpendicular to v_1 and the third vector is the normal vector with positive

x_3 component. The direction of v_2 is chosen in a way to make this a right-hand coordinate system. The coordinates of these vectors in X coordinate system are as follows:

$$v_1 = \begin{pmatrix} 1/\sqrt{1+\tan(\phi)^2 * \cos(\theta)^2} \\ 0 \\ \sqrt{1-v_{11}{}^2} * sign(\cos(\theta)) \end{pmatrix} \tag{2.12}$$

$$v_3 = \begin{pmatrix} -\sin(\phi) * \cos(\theta) \\ -\sin(\phi) * \sin(\theta) \\ \cos(\theta) \end{pmatrix} \tag{2.13}$$

$$v_2 = v_3 \times v_1 \tag{2.14}$$

The angles ϕ and θ in these equations are the angles between slider (node2) and vertical and x-axis in spherical coordinates.

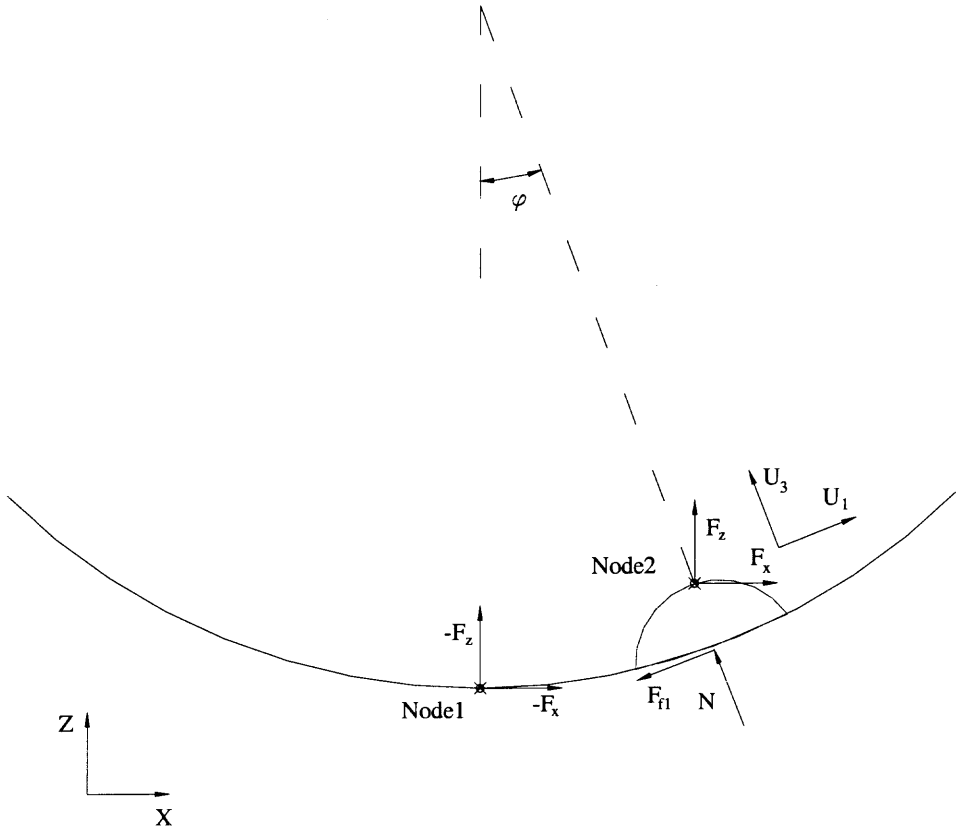

Figure 2.5 Diagram of the forces in FPS (only in-plane forces are shown).

To calculate the forces in the element in each time step based on the position of the nodes, the normal force should be first determined. To this end, a k_{normal} with high stiffness is considered to simulate the stiffness of the FPS surface in normal direction. A high damping close to the critical damping (damping ratio of 20%~90%) is also applied in this normal direction to prohibit excessive vibration in vertical direction causing unreal changes in normal force. Using this stiffness, the normal force at each time is determined based on the distance of slider from the surface (this is a nominal distance and as long as the stiffness is high enough and the tolerance is picked accordingly, it does not affect the

results). Defining z_{surf} as the third component of the position of the point in the surface under slider in X coordinates, we have

$$N = -k_{normal} * z_{normal,n+1} - c * vel_{normal} \tag{2.15}$$

Friction force at each moment is determined using the calculated normal force and the value of Z at the moment. Defining components of Z in v_1 and v_2 direction as Z_1 and Z_2, the friction force applied by surface to the slider in these directions are equal to:

$$F_{f1} = -\mu N Z_1 \tag{2.16}$$

$$F_{f2} = -\mu N Z_2 \tag{2.17}$$

The external force at node2 of FPS can be calculated as:

$$\begin{pmatrix} F_x \\ F_y \\ F_z \end{pmatrix} = -\overbrace{\begin{Bmatrix} v_1 v_2 v_3 \end{Bmatrix}}^{} \begin{pmatrix} F_{f1} \\ F_{f2} \\ N \end{pmatrix} \tag{2.18}$$

The stiffness matrix for the FPS element should satisfy the equation

$$K\Delta X = \Delta F \tag{2.19}$$

It is defined as a diagonal matrix as follows:

$$K = \begin{bmatrix} T & 0 & -T & 0 \\ 0 & 0 & 0 & 0 \\ -T & 0 & T & 0 \\ 0 & 0 & 0 & 0 \end{bmatrix} \tag{2.20}$$

$$T = \begin{bmatrix} \Delta F_{x1} / \Delta x_1 & 0 & 0 \\ 0 & \Delta F_{x2} / \Delta x_2 & 0 \\ 0 & 0 & \Delta F_{x3} / \Delta x_3 \end{bmatrix} \tag{2.21}$$

The details of these calculations are explained in the appendix.

2.3 Behavior of Fixed and Isolated Primary-Secondary Systems

The behavior of a transformer, isolated by FPS and modeled as a rigid mass, has previously been studied [Ersoy, 2002]. There are also studies on effect of base isolation of structures on secondary systems. It was found that use of base isolation generally reduces the peak responses of secondary systems [Fan, 1990]. Laminating rubber bearings were found to be more effective in a wide range of frequencies compared to friction isolators (pure friction, and resilient friction). Using a simple model for friction that show stick-slip behavior, it was observed that the frictional base isolation systems generate high frequencies in the structural responses. The resilient-friction isolation was observed to be more effective than pure friction isolation in most of the times. It was also found that use of isolation systems should be avoided in regions with low frequency energy content. These results are reaffirmed in another publication [Fan, 1992]. Another study showed effectiveness of base-isolation of primary system for reducing the secondary system response for all earthquakes, except those with very low frequency content This study was performed using laminated rubber bearings [Kim, 1993].

To study the effects of FPS on secondary systems, a primary-secondary system was parametrically studied for both fixed and isolated cases. The more accurate friction

model, articulated in Chapter 2, is used to model friction. The flexibility of primary system is considered in the model because of its effects on FPS and secondary system response. The primary system has three degrees of freedom, two horizontal and one vertical. The secondary system has two horizontal degrees of freedom and has the same vertical displacement as that of the primary system. All elements have linear elastic force-displacement behavior. The vertical degree of freedom is considered for the primary system to make possible the study of vertical excitation of the primary system, that can change normal force, and hence the friction force. Change in frequency content of this force can be expected, especially close to vertical frequency of the primary system. This may amplify the response of secondary systems having similar frequencies.

Figure 2.6 shows a 2-D diagram of the model considered. The model has the same characteristics in the other horizontal direction. The weight of primary system is equally divided between its top and bottom nodes. Primary system is taken to be much heavier than the secondary system. Since the focus of this study is on transformers and bushings, the physical characteristics of the model are chosen in a range close to actual transformer-bushing systems. Also, the words transformer and bushing might be used instead of primary system and secondary system in this chapter.

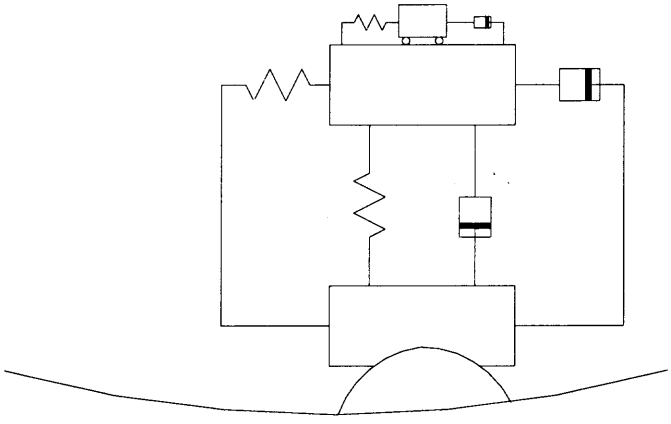

Figure 2.6 Primary-secondary model.

Tables 2.1 and 2.2 show the physical characteristics of the primary and secondary systems used in the model. TT1 has the same characteristics as transformer type 25 MVA – 650 HV BIL. BUS1 has the same frequency as a 196 kV bushing fixed at base [Ersoy, 2002]. The structure of 230 kV bushings is also similar to 196 kV bushings [Gilani, 1999(a)]. BUS3 can represent the same bushing mounted on TT1 [Ersoy, 2002]. BUS2 represents a 550 kV bushing fixed at base [Gilani, 1999(b)]. TT4 and TT6 are included to study the effects of vertical frequency of transformer on different responses. However, it should be kept in mind that the vertical frequency of an actual transformer is considerably higher than its horizontal frequency, and cases like TT4 are not found in reality.

Table 2.1 Properties of the Primary Systems Studied

Primary	Horizontal frequency (Hz)	Vertical frequency (Hz)	Mass (kips)	Damping ratio
TT1	14.0	26.1	179	2%
TT2	8.0	16.0	773	2%
TT4	14.0	14.0	179	2%
TT6	14.0	21.0	179	2%

Table 2.2 Properties of the Secondary Systems Studied

Secondary	Frequency (Hz)	Mass (kips)	Damping ratio
BUS1	16.0	0.69	2%
BUS2	8.0	4.23	2%
BUS3	11.0	0.69	2%
BUS4	10.5	0.69	2%
BUS5	10.0	0.69	2%
BUS6	9.5	0.69	2%
BUS7	9.0	0.69	2%
BUS8	7.0	4.23	2%
BUS9	6.0	4.23	2%
BUS10	5.0	4.23	2%
BUS11	12.0	0.69	2%
BUS12	14.0	0.69	2%

Table 2.3 shows the data related to several analyses performed. The analyses are performed for El Centro earthquake with 1g PGA in two horizontal directions and a PGA of 0.8g in vertical direction according to IEEE [IEEE, 1998].

Table 2.3 Characteristics of the Primary-Secondary Systems Studied

Case	Primary	Secondary	Support
1	1	1	FPS, R = 60 in
2	1	3	FPS, R = 60 in
3	1	4	FPS, R = 60 in
4	1	5	FPS, R = 60 in
5	1	6	FPS, R = 60 in
6	1	7	FPS, R = 60 in
7	1	11	FPS, R = 60 in
8	1	12	FPS, R = 60 in
9	1	1	Fixed
10	1	3	Fixed
11	1	4	Fixed
12	1	5	Fixed
13	1	6	Fixed
14	1	7	Fixed
15	1	11	Fixed
16	1	12	Fixed
17	2	1	FPS, R = 60 in
18	2	2	FPS, R = 60 in
19	2	3	FPS, R = 60 in
20	2	4	FPS, R = 60 in
21	2	5	FPS, R = 60 in
22	2	6	FPS, R = 60 in
23	2	7	FPS, R = 60 in
24	2	8	FPS, R = 60 in
25	2	9	FPS, R = 60 in
26	2	10	FPS, R = 60 in
27	2	11	FPS, R = 60 in
28	2	1	Fixed
29	2	2	Fixed
30	2	3	Fixed
31	2	4	Fixed
32	2	5	Fixed
33	2	6	Fixed
34	2	7	Fixed
35	2	8	Fixed
36	2	9	Fixed
37	2	10	Fixed
38	2	11	Fixed
39	1	1	FPS, R = 30 in
40	1	3	FPS, R = 30 in
41	1	4	FPS, R = 30 in
42	1	5	FPS, R = 30 in
43	1	6	FPS, R = 30 in
44	1	7	FPS, R = 30 in
45	1	11	FPS, R = 30 in
46	1	12	FPS, R = 30 in
47	4	1	FPS, R = 60 in
48	4	3	FPS, R = 60 in
49	4	4	FPS, R = 60 in

Table 2.3 Characteristics of the Primary-Secondary Systems Studied (Continued)

Case	Primary	Secondary	Support
50	4	5	FPS, R = 60 in
51	4	6	FPS, R = 60 in
52	4	7	FPS, R = 60 in
53	4	11	FPS, R = 60 in
54	4	12	FPS, R = 60 in
55	4	1	Fixed
56	4	3	Fixed
57	4	4	Fixed
58	4	5	Fixed
59	4	6	Fixed
60	4	7	Fixed
61	4	11	Fixed
62	4	12	Fixed
63	6	1	FPS, R = 60 in
64	6	3	FPS, R = 60 in
65	6	4	FPS, R = 60 in
66	6	5	FPS, R = 60 in
67	6	6	FPS, R = 60 in
68	6	7	FPS, R = 60 in
69	6	11	FPS, R = 60 in
70	6	12	FPS, R = 60 in
71	6	1	Fixed
72	6	3	Fixed
73	6	4	Fixed
74	6	5	Fixed
75	6	6	Fixed
76	6	7	Fixed
77	6	11	Fixed
78	6	12	Fixed

Figure 2.7 shows the bushing relative displacement for different radii of FPS. The primary system TT1 is used in these analyses. As expected, the FPS with lower radius causes more displacement (and more force) in the bushing. For comparison, it should be said that a 230 kV bushing with a frequency in the range of 11~14 Hz depending on its support experiences failure in relative displacements between 0.3~0.35 in [Gilani, 1999(a)]. Lower frequencies belong to bushings with higher capacities and larger structures that will have higher allowable displacements. The results in this figure are all under 0.3 in, showing that use of FPS prevents any damage to the bushings.

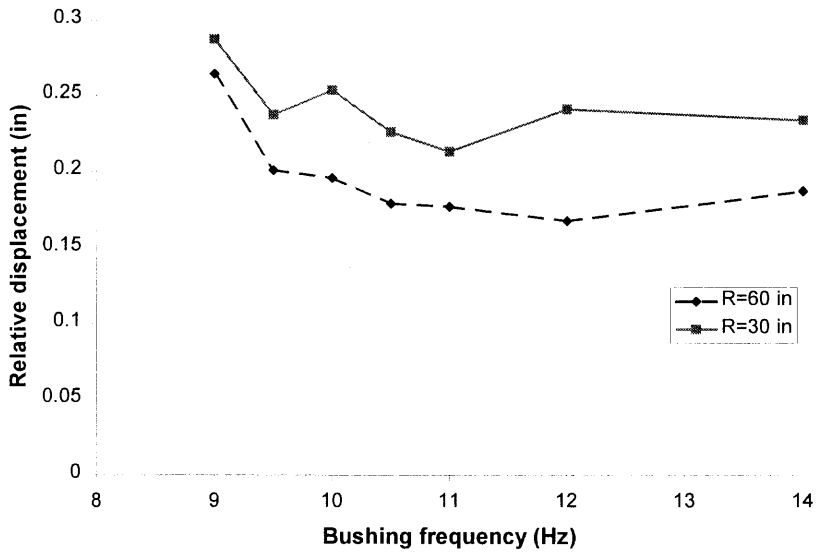

Figure 2.7 Bushing response for TT1.

Figure 2.8 shows effect of vertical frequency of transformer on the bushing response and compares this with the fixed-base response. The notations TT1, TT6, and TT4 refer to transformers with the same horizontal frequency. The vertical to horizontal frequency ratio for these transformers are 1.86, 1.5, and 1.0, respectively. The horizontal frequency of transformer is 14 Hz. As can be seen, the closer the vertical frequency is to the horizontal frequency, the higher the bushing response. This amplification can particularly be observed for the case when vertical frequency is equal to horizontal frequency. However, the FPS is still effective in reducing the bushing response compared to the fixed-base case.

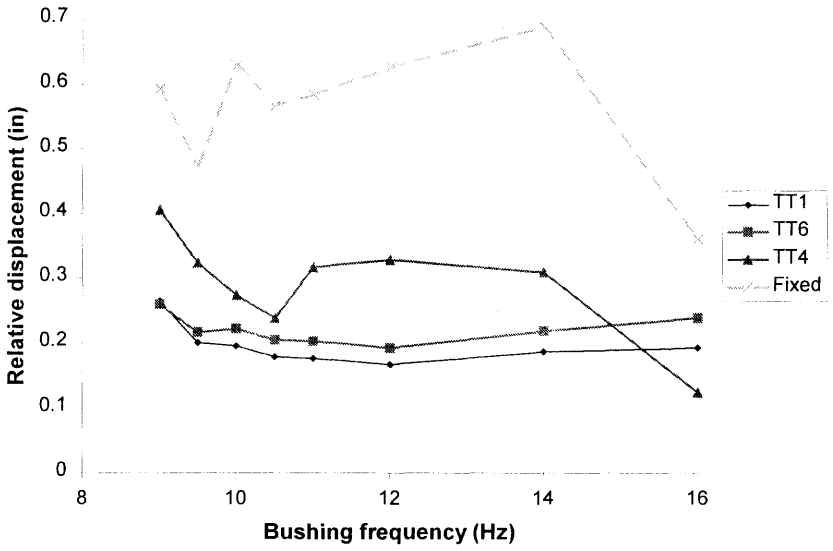

Figure 2.8 Effect of vertical frequency and support fixity on bushing response.

Figure 2.9 shows the bushing response for bushings mounted on another transformer with a horizontal frequency of 8 Hz. Again, the FPS is effective in reducing the bushing response, especially for lower frequencies. This is due to higher response of bushings with low frequencies in general. Base isolation is particularly effective when bushing has a frequency close to transformer, because FPS prevents the amplification of bushing response.

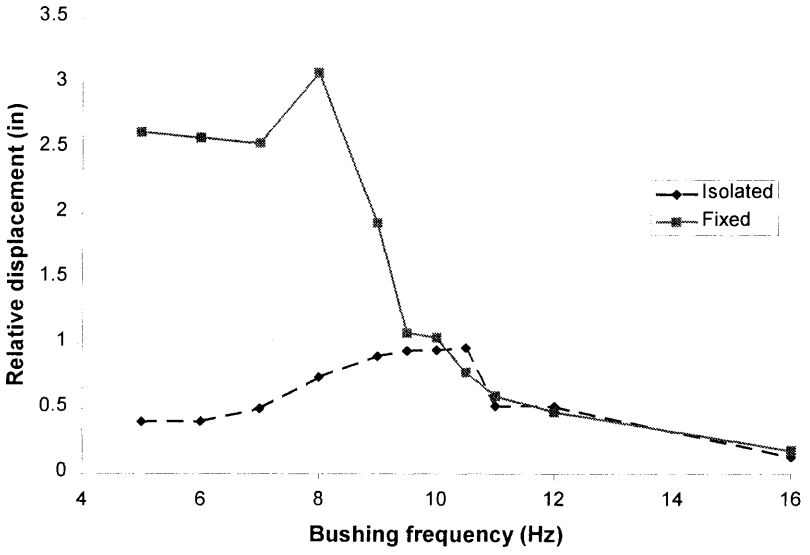

Figure 2.9 Bushing response for TT2.

Figure 2.10 compares the bushing response of isolated systems for two different transformers. TT1 has a horizontal frequency of 14 Hz while TT2 has a frequency of 8 Hz. As observed, the response for TT2 is usually higher than that of TT1. This can probably be attributed to the fact that its frequency is closer to the frequency range where the earthquakes have most of their energy. However, higher voltage transformers require higher voltage bushings. Higher voltages mean larger dimensions, lower frequencies, and more displacement capacities for both transformers and bushings. Therefore, transformers with lower frequencies often have bushings with higher displacement capacities as well. While bushings on TT1 are definitely safe, it cannot be directly determined from this graph whether bushings on TT2 will fail or not. This should be determined based on the specific frequency and allowable displacement of such bushings. However, it is very probable that the higher displacement capacity of such bushings will cover the increase in their response.

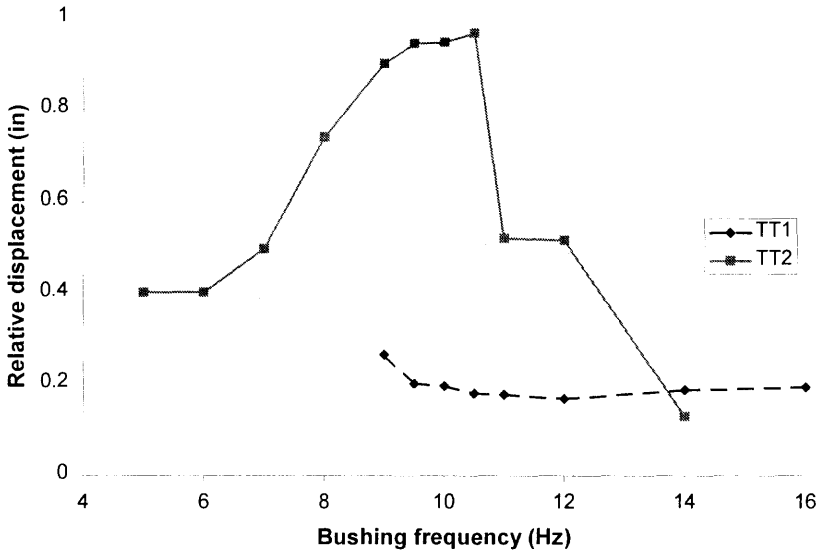

Figure 2.10 Effect of transformer frequency on bushing response.

Figure 2.11 compares the vertical force at support for different isolated and fixed systems. The frequency of bushing does not have much effect, because its weight is small compared to that of the transformer. It can be seen that closeness of vertical and horizontal frequency of transformer will result in increase in vertical force. For fixed TT4 and TT6, tension can be observed at times in the support. The isolated systems for these cases experience uplift, though it is very brief in the case of TT6.

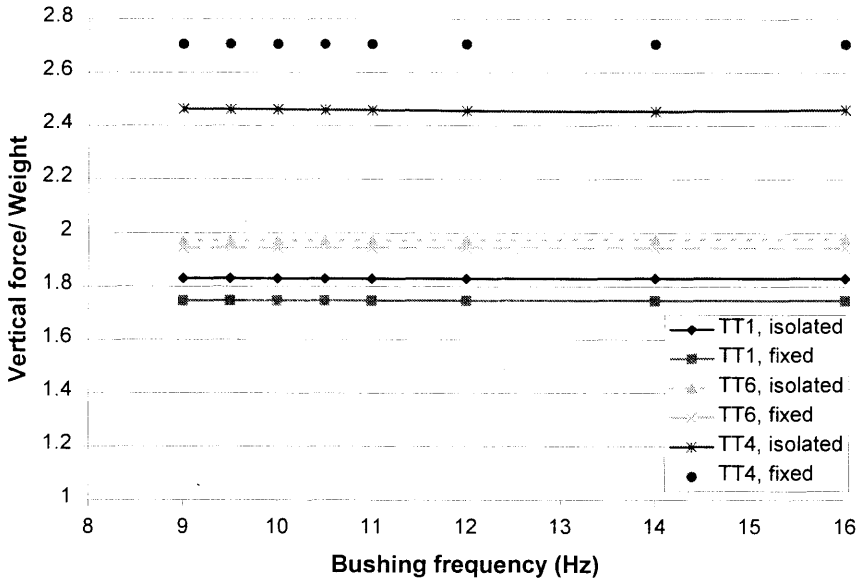

Figure 2.11 Vertical force at support.

Figures 2.12 and 2.13 compare the base shear force in the two horizontal directions. The effect of vertical frequency of transformer can be observed through the difference between response of TT1, TT6, and TT4 while the effect of isolation can be seen comparing the forces with those of fixed-base case. As can be seen, the isolation has been more effective in one direction (designated as x-direction). If the vertical and horizontal frequencies of the transformer are too close to each other, considerable increase in shear force is observed. However, the shear forces are still much less than those of fixed-base system in x-direction. In y-direction, FPS has been less effective in reducing base shear. For TT4, the shear force in y-direction in isolated system is higher than the fixed-base case due to the increase in normal force. However, it should be emphasized that the proximity of vertical and horizontal frequency of TT4 is unrealistic. The response of TT1 and TT6 that show efficacy of FPS are more representative of the behavior of actual isolated structures. It should be noted that the forces are presented in

terms of the ratio of shear force over weight, not normal force. The normal forces are about twice higher than the weight, as mentioned previously.

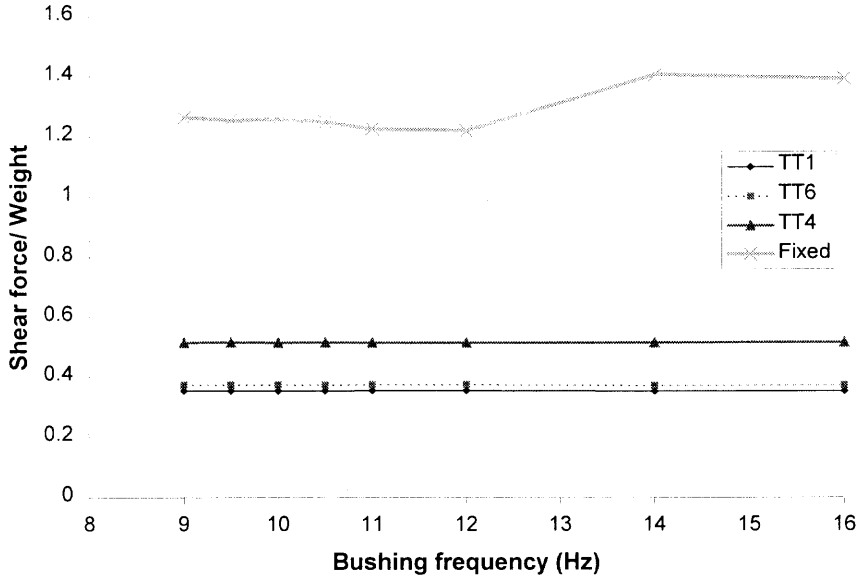

Figure 2.12 Effect of vertical frequency and support fixity on shear force in x-direction.

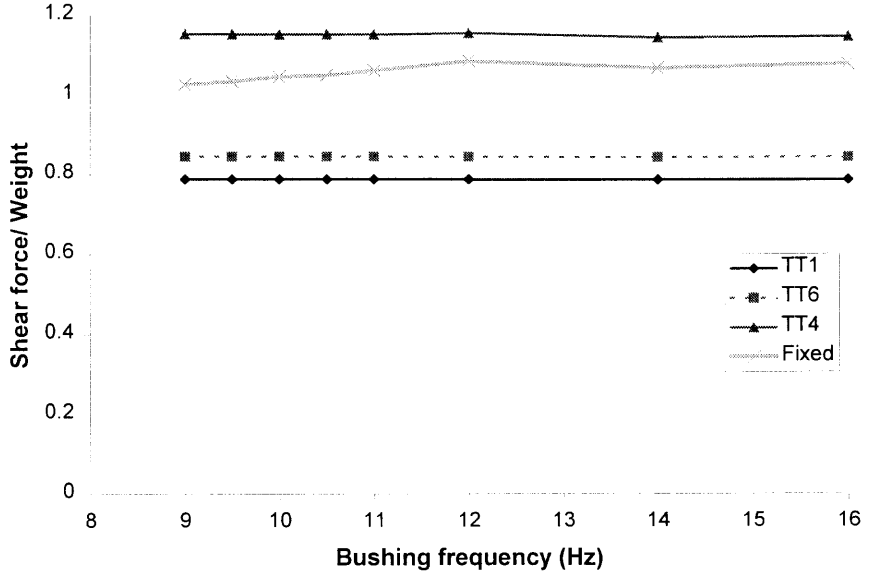

Figure 2.13 Effect of vertical frequency and support fixity on shear force in y-direction.

Figures 2.14 and 2.15 show base shear force for TT1 in both directions for two different FPS radii. The forces for R = 30 in are higher in both directions, but the difference is more in x-direction. In all these cases, the y-direction is the direction in which FPS slider moves the most. That is why FPS shows a higher resistance in this direction due to higher restoring forces and higher stiffness caused by the changed slope of the surface. The difference of response in y-direction between different radii is less, because they are closer to the response of a fixed-base system.

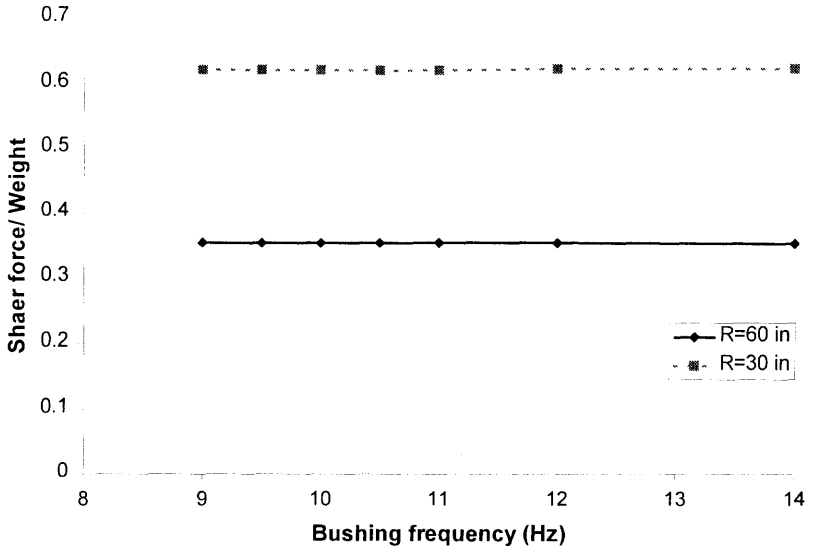

Figure 2.14 Shear force in x-direction for TT1.

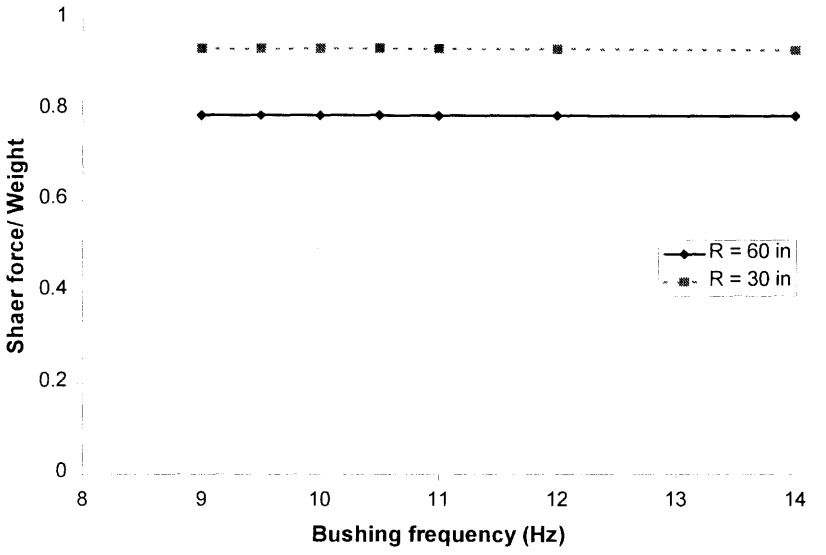

Figure 2.15 Shear force in y-direction for TT1.

Figure 2.16 shows the same trends when comparing response of two different transformers. While response of TT2 that has a lower frequency is always more than TT1, the difference is more pronounced in x-direction compared to y-direction. Comparing this to Figure 2.17 that depicts fixed-base response of these two systems yields an interesting point. The most critical component of earthquake for a fixed-base structure might be different from an isolated structure. While the x-direction is much more critical in fixed-base cases, it is the y-component that has the most effect on response of the isolated structure. Such an observation can have different reasons. Richness of an earthquake in terms of frequencies close to natural frequency of a structure is the most important factor determining response of the structure. Therefore, having the same peak ground acceleration, the earthquake components with frequency content closer to natural frequency of the structure will have the most effect on it. However, in an isolated structure, proximity of the earthquake frequency content to

natural frequency of the FPS is also an important factor. Moreover, the number and duration of times when the ground acceleration surpasses the sliding threshold of FPS is an important factor determining the amount of sliding and restoring force. Hence, it is possible that the earthquake component more effective on an isolated structure is different from the component more effective on the fixed structure.

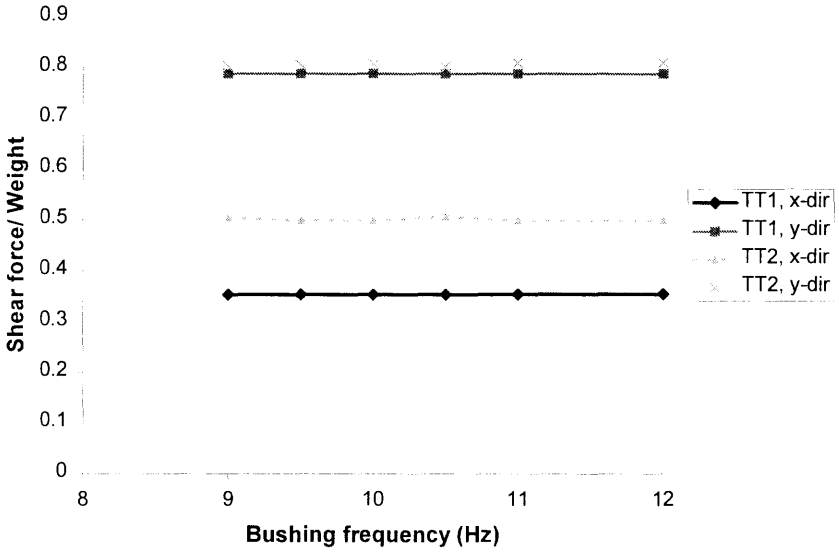

Figure 2.16 Effect of transformer frequency on shear force in isolated systems.

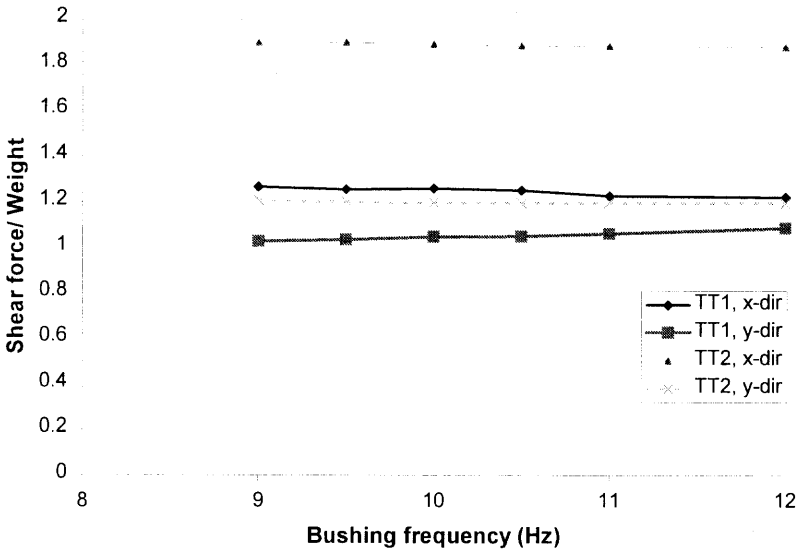

Figure 2.17 Effect of transformer frequency on shear force in fixed-base systems.

In summary, it can be said that these studies show effectiveness of FPS for reducing response of secondary system for all ranges of primary and secondary system frequencies. This is evident even when primary and secondary systems have the same frequencies. Efficiency of FPS in reducing the secondary system response, even for high frequencies, can probably be attributed to the more accurate model used for friction, that does not generate artificial high frequencies in the response.

The isolation is also effective in reducing the shear force and response of primary system (since base shear is essentially equal to force in primary system). This however, does not necessarily mean that response of bushing will remain in allowable range for all cases. Such determination should be made based on these results, having the exact information about displacement capacity of a particular type of bushing. Closeness of the vertical and horizontal frequencies of a primary system can increase the secondary response and base shear. This effect, however, is limited for the practical values of

frequencies of transformers. Also it should be noted that results of this work were intended for use for transformer-bushing systems and frequency range and mass proportions were chosen accordingly. The behavior trends might change if the structure of interest has primary or secondary systems of much lower frequencies such that they are close to frequency of the FPS.

CHAPTER 3

EFFECT OF ISOLATION ON FOUNDATION DESIGN OF TRANSFORMERS

Transformers are very heavy equipment subject to enormous forces under earthquake. As mentioned in Chapter 1, failure of foundation of transformers under earthquake is one of the major modes of damage in an electrical substation. Proper design of foundation to withstand large vertical and lateral loads and moments is an integral part in seismic design of the substation.

Enormity of the seismic loads requires very large foundations for transformers that are very costly. Use of FPS can help reduce the loads, hence reducing the cost of foundation. This can be a very considerable saving, justifying use of FPS by itself.

3.1 Seismic Design of Foundations in Electrical Substations

Pile-type foundations supporting equipment in electrical substations should be designed to the loads found in the qualification process for the equipment and support [IEEE, 1998]. Pad-type foundations may be designed using lower loads than required by the qualification of the equipment and support. These types of foundations can be analyzed to the requirements of equation

$$F_p = ZIC_pW_p \tag{3.1}$$

which comes from the Uniform Building Code (UBC), where $C_p = 0.75$.

The electrical substation equipment are designed based on the seismic performance level expected of them. There are three performance levels (PL) suggested in IEEE. These include high seismic PL, moderate seismic PL, and low seismic PL.

Equipment that is shown to perform acceptably in ground shaking up to the desired performance level is said to be seismically qualified to that level. High seismic performance level is chosen for this study [IEEE, 1998].

It is often impractical or not cost-effective to test the equipment to the actual high or moderate performance levels. Hence, the equipment might be tested at 50% of the PL and the analyses are performed at this level as well for consistency. This reduced level is called RRS. The equipment tested or analyzed to the RRS level is expected to have acceptable performance at the PL. Stresses in brittle components like porcelain and cast aluminum are compared to 50% of their ultimate strength and stresses in ductile materials such as steel and ductile aluminum shall not exceed their allowable stresses. These requirements mean that under PL, the brittle material shall not exceed its ultimate strength and the ductile material may experience some yielding [IEEE, 1998].

The same approach is used for foundation as specified before. These RRS level loads are what the foundation should be designed for so that it does not exceed its capacity under the corresponding PL. This means that the foundation should have an ultimate capacity at least equal to the loads under PL [IEEE, 1998]. Since use of FPS introduces nonlinear behavior, the loads under PL, rather than twice the loads under RRS, are used to check the design of foundation. Also, to be able to compare the results for pad-type and pile-type foundations, both are designed to carry these loads and equation 2.1 is not used for pad-type foundations.

Results of the analysis on the TT1 transformer from Chapter 2 are used for foundation design. In addition to the high seismic performance level with PGA of 1.0g in horizontal directions and 0.8g in vertical direction, the medium seismic performance

level having accelerations half these values is used. The actual transformer used as the base for modeling TT1 has the horizontal frequencies 14.0 and 20.6 Hz. In Chapter 2, both frequencies were assumed equal to 14.0 Hz. Another set of analysis was performed based on the real frequencies; however, the effects on foundation forces are negligible. Therefore, the same results will represent the forces in the actual transformer.

The 1940 El Centro record is used for the analysis. The record used was recorded on a USGS type C ground [PEER, 2002]. This soil has an allowable stress of $q'_u = 1.0ksf$ [ICBO, 1997]. Since the safety factors considered are always higher than 2, an ultimate stress of $q_u = 2.0ksf$ is used in the analyses.

It is tried to avoid using piles in the design if possible. However, if the loading demands, piles are used to make design of a sufficient foundation with reasonable dimensions possible. The foundation is designed in a square shape to be able to withstand the forces if the direction of the earthquake is changed.

To calculate the moment at the level of the bottom of foundation, the moment caused by the lateral loads in this level is calculated. The point of effect of this load for transformers is chosen at 2/3 of height of the transformer, assuming triangular distribution of the load. For isolated transformers, this level is chosen as the middle of the transformer height since the transformer moves as a fairly rigid structure when isolated on FPS. Figure3.1 shows this difference schematically.

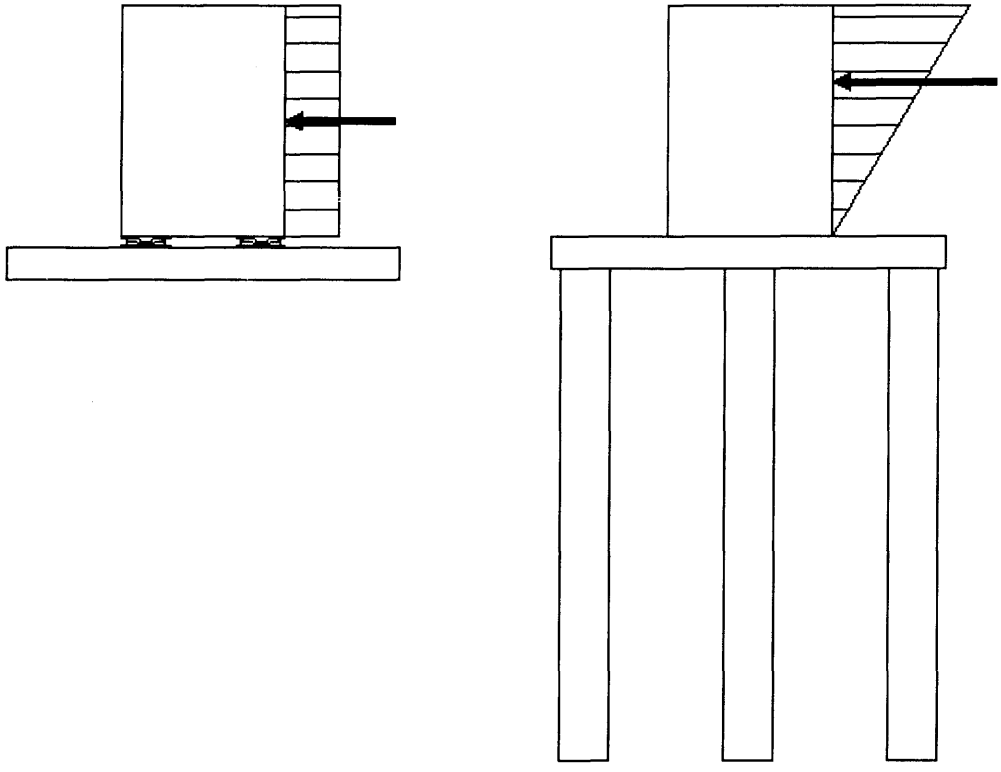

Figure 3.1 Distribution of lateral force on isolated and fixed transformers.

3.2 Foundation Design Results

Table 3.1 shows the cases used in foundation design. The weight of the transformer is 179 kips.

Table 3.1 Properties of the Cases Considered for Design of Transformer Foundations

Case	Support	PL	F_x (kips)	F_y (kips)	F_z (kips)	M_x (k-ft)	M_y (k-ft)
1	Isolated	High	63.0	141.0	327.5	1280.7	572.3
2	Fixed	High	249.0	194.0	315.7	2220.3	2849.8
3	Isolated	Moderate	35.4	45.9	259.0	416.9	321.6
4	Fixed	Moderate	124.5	97.0	246.0	1110.2	1424.9

The final acceptable design results for all cases are presented in Table 3.2.

Table 3.2 The Design Transformer Foundations

Case	B (ft)	L (ft)	D (ft)	Piles	Pile length (ft)	Pile diameter (ft)
1	24	24	2	-	-	-
2	24	24	2	9	30	3
3	17	17	2	-	-	-
4	24	24	2	9	15	3

As observed, a shallow foundation is sufficient to sustain the loads applied to the isolated transformer under moderate and high seismic performance levels. Meanwhile, fixed transformers need 9 piles of diameter 3' and length of 15'~30' to sustain the loads under the same seismic performance levels. The difference is due to higher point of effect for loads applied to a fixed transformer in addition to the fact that the value of these loads is also higher. The bigger moment arm puts a higher moment demand on the foundation that necessitates use of piles.

Based on limited data provided by LA Department of Water and Power (LADWP), design and construction of seismic foundation (i.e. piles) will add an additional cost of $50,000 to $100,000. Use of four FPS bearings will cost about $20,000 depending on volume and stroke required. Therefore, it appears that use of FPS bearings can be even justified on an initial cost basis. Further data should be collected in order to make a more accurate initial cost analysis. However, implied life-cycle benefits of FPS isolation are highlighted throughout this research project.

Details of design of a shallow foundation and a pile foundation are given before.

A Shallow Foundation Seismic Design:

A 24'×24'×2' Foundation is selected for Case 1. The eccentricities are calculated as

$$e_x = \frac{M_y}{F_z} = \frac{572.3}{327.5} = 1.7475 \quad ft$$

$$e_y = \frac{M_x}{F_z} = \frac{1280.7}{327.5} = 3.9105 \quad ft$$

Since $\frac{e_x}{B} = 0.073 < \frac{1}{6}$, $\frac{e_y}{L} = 0.163 < \frac{1}{6}$, the equivalent area of foundation is calculated using Figure 3.2

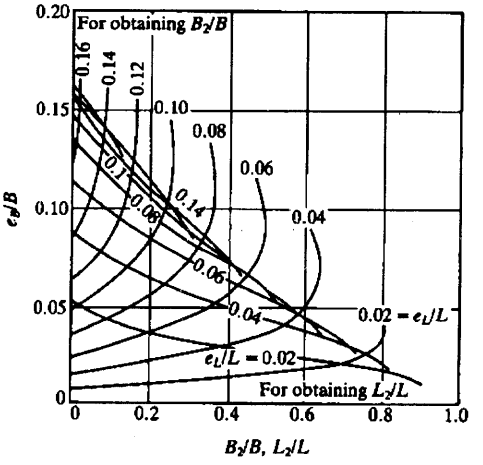

Figure 3.2 Effective area for foundation [Das, 1990].

$$\frac{B_2}{B} = 0.42$$

$$\frac{L_2}{L} = 0.0$$

$$A' = L_2 B + \frac{1}{2}(B + B_2)(L - L_2) = 408.96 \quad ft^2$$

To account for effect of the lateral load on foundation capacity, the load reduction factor is calculated from Figure 3.3

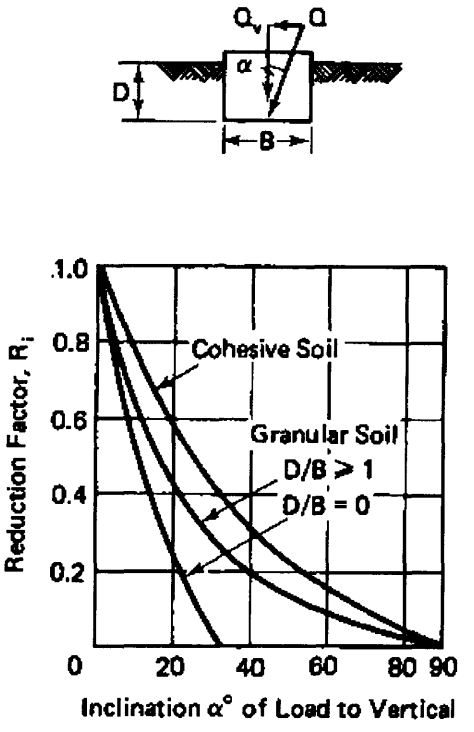

Figure 3.3 Inclined load reduction factors [Liu, 1987].

$$\alpha = a\tan(\frac{\sqrt{F_x^2 + F_y^2}}{F_z}) = 25.2°$$

$$R_i = 0.50$$

Hence, the capacity of foundation can be calculated as [Liu, 1987]:

$$Q_{ult} = R_i * A' * q'_u = 0.50 * 408.96 * 2.0 = 408.96 \quad kips > 327.5 \quad kips$$

A Pile Foundation Seismic Design:

A foundation of dimensions 24'×24'×2' with 9 piles of length 30' is used to support the transformer for Case 2. The load in individual piles in the group can be calculated as [Liu, 1987]:

$$Q = \frac{F_z}{n} \pm \frac{M_x y}{\sum y^2} \pm \frac{M_y x}{\sum x^2} \tag{3.2}$$

Using this equation, the maximum compressive and tensile forces can be calculated as 119.6 and 49.4 kips. To account for loss of efficiency in the pile group compared to individual piles, the group efficiency factor G_e is calculated as [Ersoy, 2001]

$$\frac{S}{B} = \frac{10}{3} = 3.33$$

$$G_e = 0.41$$

where S is the center to center distance of piles and D is the pile diameter. Considering this factor, the compressive and tensile capacity of the piles should be at least equal to 291.7 and 120.5 kips, respectively.

The pile capacity can be calculated as [Das, 1990]:

$$Q_u = Q_f + Q_t \tag{3.3}$$

where Q_f is the capacity from friction, and Q_t is the tip load.

$$Q_f = \alpha c_u pL \tag{3.4}$$

$$Q_t = 9 c_u A \tag{3.5}$$

where α is chosen from Figure 3.4.

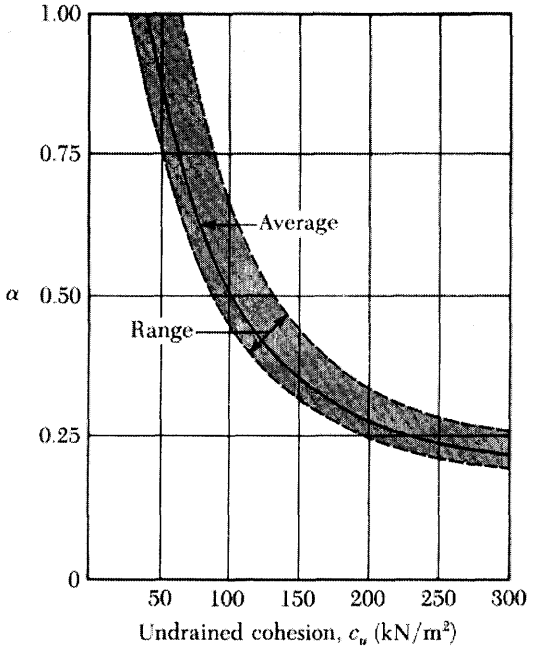

Figure 3.4 Variation of α with undrained cohesion of clay [Das, 1990].

c_u is the cohesion in soil that is half of the value of q'_u for undrained clay, p is the perimeter of the pile, and A is its area.

$$c_u = 1.0ksf = 47.94\,KN/m^2$$

$$\alpha = 1.0$$

$$Q_f = 1.0*1.0*(2\pi*1.5)*30 = 282.7 \quad kips$$

$$Q_t = 9c_uA = 9*1.0*(\pi*1.5^2) = 42.4 \quad kips$$

$$Q_u = 282.7 + 42.4 = 325.1 \quad kips > 291.7 \quad kips$$

The capacity of piles in tension can be calculated from

$$T_u = \alpha' c_u pL \tag{3.6}$$

$$\alpha' = 0.9 - 0.00625 c_u \quad (for \quad c_u \leq 80 \quad KN/m^2) \tag{3.7}$$

where c_u is in KN/m^2 .

$$\alpha' = 0.9 - 0.00625 * 47.94 = 0.600$$

$$T_u = 0.600 * 1.0 * (2\pi * 1.5) * 30 = 169.8 \quad kips > 120.5 \quad kips$$

The shear capacity of the piles is much higher than the applied load and can be calculated as [Fleming, 1992]:

$$P = 2nc_u SL = 2 * 9 * 1.0 * 10.0 * 30.0 = 5400 \quad kips >> 315.6 \quad kips$$

where n is the number of piles and L is the pile depth. Hence, the design is adequate to carry the loads and moments.

For comparison, if the foundation was used without piles, considering the combined effect of vertical and lateral load, the bearing capacity of the foundation would be 17.3 kips that is equal to 5.5% of the actual normal force of 315.7 kips. If the seismic load is reduced until this foundation is sufficient to carry the load, it is found that the seismic load is 0.16 times the original seismic load (0.16g in both horizontal directions, and 0.128g in vertical direction). Both the reduction in lateral load and the consecutive reduction in moment achieved by use of FPS explain such a significant gain in terms of foundation size.

CHAPTER 4

INTERACTION OF TRANSFORMER-BUSHING WITH INTERCONNECTING EQUIPMENT IN AN ELECTRICAL SUBSTATION

A transformer is only one element in an electric substation. The substation comprises several elements connected and performing together in order to achieve the defined electric function. When, as suggested in the previous chapters, a transformer is to be isolated, it will undergo large displacements under earthquake. However, the other interconnecting equipment are usually fixed and have small displacements in comparison. This means that interaction between transformer-bushing and the interconnecting equipment will be inevitable unless measures are taken to provide enough extra displacement capacity between these elements. It has been revealed in field investigations during recent earthquakes that this interaction may be largely responsible for the observed damage to connected electrical substation equipment [Der Kiureghian, 2001; Hong, 2001]. This chapter will study the effects of such interactions on response of different components and provide suggestions for a design that is safe for these elements.

4.1 Previous Studies on Interaction in an Electric Substation

In recent years, studies have been performed at University of California at Berkeley has done studies on seismic interaction in linearly connected electrical substation equipment and cable-connected equipment [Der Kiureghian, 2001; Hong, 2001]. The work on interaction through linear connection investigates the interaction between two equipment items connected by a linear spring-dashpot or spring-dashpot-mass element representing

a conductor bus [Der Kiureghian, 2001]. Each equipment item is modeled as a linear system with distributed mass, damping and stiffness properties and is characterized by a single degree of freedom through use of a prescribed displacement shape function. This study assumes a mass ratio of 2 between the two equipment and the frequency ratio of the heavy equipment to the light one ranges from 0.1 to 1. The frequencies of the connected system are respectively higher than the stand-alone frequencies of the individual equipment except for when both the equipment have the same frequency (that means no interaction).

It is found in this study that the interaction between the two equipment items may significantly amplify the response of the higher-frequency equipment item. The interaction increases as separation between the stand-alone equipment frequencies and stiffness of the connecting equipment increase. The interaction has amplification effect on response of the higher frequency equipment and de-amplification effect on response of the low frequency equipment. The relative displacement between the two equipment, which is also an indicator of the force in the connecting element, is always less than that of a system with no connecting element, suggesting that using that value for design of the connecting equipment will be conservative. Higher mass ratios (mass of the heavy equipment divided by the light one) will increase the interaction effect on the light equipment and decrease the effect on the heavy equipment since the heavy mass tends to dominate the behavior. Also, the force in the connecting equipment will increase with rising mass ratio. They found out that the interaction effects are not much sensitive to ground input frequency content. Overall, they observed amplification as high as 8 in the equipment with higher frequency in the cases they considered. At the end they suggest

decreasing the frequency gap by changing mass, stiffness or base-isolation, reduction in connecting equipment stiffness by providing flexible extension loops, or connecting the connecting element to a point close to top of the high-frequency equipment and near bottom of the low-frequency equipment [kiureghian, seismic linear].

In the study on cable-connected equipment, equipment connected with cables with different geometric configurations and amounts of slack are studies [Hong, 2001]. The flexibility and inertia of the cable is neglected. The results show that in absence of sufficient slack, the interaction effect can strongly amplify the responses of both equipment items. This amplification can be especially higher for the high-frequency equipment. A parameter β is defined that can roughly be said to be the ratio of the relative displacement of unconnected equipment to the existing slack. $\beta<1$ means that the slack in the cable is more than the relative displacement between the two stand-alone equipment. When both ends of the cable have the same elevation, choosing $\beta<1$ will significantly decrease the interaction, provided mass of the cable is relatively small. When the cable ends are at different levels, significant interaction might happen, even for values of β less than unity [Hong, 2001].

Valuable insight into interaction of two fixed-base equipment is provided through these studies. However, there are more factors that should be considered when studying the interaction of isolated transformer-bushing with interconnecting equipment. First of all, the nonlinear behavior of FPS is totally different from behavior of a linear system with the same period. Therefore, just increasing the transformer period and using the results of studies on linear equipment will not be correct. Also, the response of transformer and bushing should be taken into account since the connection is between top

of the bushing and the interconnecting equipment. In addition the mass of transformer is much higher than all the other equipment involved and it is expected to dominate the interaction. To study the interaction of isolated transformer-bushing without these deficiencies, Ersoy and Saadeghvaziri have used a simplified model [Ersoy, 2002].

A schematic picture of the model considered and its finite element representation are shown in Figures 4.1 and 4.2 In this model FPS is simulated using a nonlinear spring with kinematic bilinear material properties. The initial stiffness of the spring is $(\frac{\mu}{Y}+\frac{1}{R})W$ with W being the weight, R being the FPS radius, and Y being the elastic displacement parameter introduced in Chapter 2. The first term is because of friction while the second term is contribution of the restoring force due to curvature of the surface. The second term is almost negligible compared to the first term. The secondary stiffness of the element is $\frac{W}{R}$ because the friction force does not change anymore and small displacement assumption is made. Transformer, bushing, and the interconnecting equipment are each modeled as a linear spring. The connecting element is an element having the specified gap and working only in tension. The properties of transformer and bushing are chosen based on the results of finite element analyses [Ersoy, 2002]. The transformer has f = 14 Hz and bushing has a frequency of 10 Hz. Frequency of the interconnecting equipment is chosen to be 1 or 3 Hz. The model consists of lumped masses. The analyses are performed with infinite slack (no interaction), no slack, and a slack equal to half of the slack required to prevent interaction.

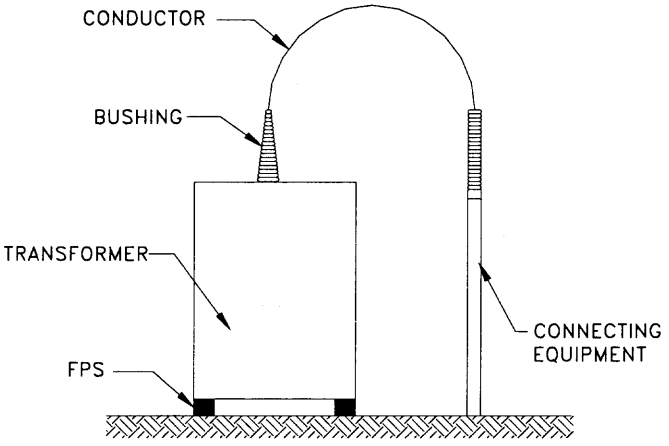

Figure 4.1 Physical model studied for interaction.

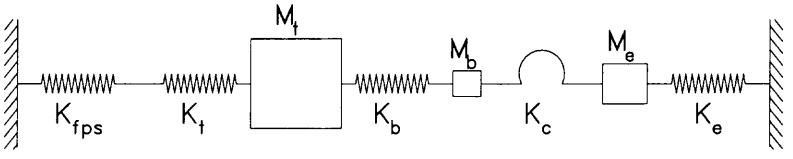

Figure 4.2 Simplified model used in prior studies.

The most important observation of this study was that the bushing forces always exceed their allowable value when there is interaction [Ersoy, 2002]. Without interaction, the force would always be less than allowable in the cases considered and the displacement of transformer and bushing is very close to that of the FPS. When there is no slack, the bushing force is higher for isolated transformer due to the much higher displacements. But, interaction does not affect the FPS response much because its behavior is dominated by the very large mass of transformer. The stiffness of the connecting cable is insignificant in the practical range considered. In the isolated case, it is seen that interaction basically happens when FPS tends to slide away from the interconnecting equipment and the cable is taut. When this happens, the big mass of

transformers pulls the bushing and the interconnecting equipment with it and the most severe forces in them are observed [Ersoy, 2002].

Based on these results, it has been suggested that enough slack should always be provided in order to prevent interaction that will result in failure of the bushing. Particularly, if FPS is to be used for rehabilitation, large amount of slack equal to sum of the maximum absolute displacement of FPS and interconnecting equipment should be provided [Ersoy, 2002]. The effect of slack ratio and frequency ratio of the interconnecting equipment to that of the FPS in cases when interaction occurs remains to be studied. The results of these studies are presented in the next section.

4.2 Simplified Model for Interaction Study

The studies done by Ersoy provide very good information on the effects of interaction on response of FPS, transformer, bushing, and the connecting equipment [Ersoy, 2002]. To continue that work, the same model used is used with the difference that the mass of transformer is divided between its bottom and top nodes (the nodes at the end of the FPS and transformer elements, respectively). This is because the stiffness of FPS is determined by the whole weight of the transformer, while the effective mass of the transformer in dynamic behavior is only a part of its whole mass. Because the absolute displacement of the whole transformer is almost the same due to predominance of the FPS displacement, equal distribution of the transformer mass between its top and bottom nodes is justified. This model is shown is Figure 4.3.

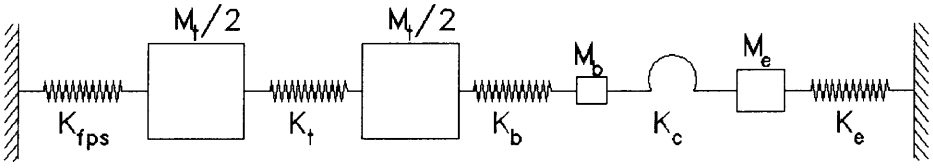

Figure 4.3 Simplified model used in this study.

A wider range of frequencies is considered to see how sensitive the interactions are to the frequency of different components. In order to study the effect of the relative frequency of the interconnecting equipment to that of the FPS, a frequency ratio of

$$FR = \frac{Interconnecting \quad frequency}{FPS \quad frequency} \tag{4.1}$$

is defined. The FPS frequency is used for this comparison instead of that of the transformer or bushing because the previous studies show that FPS displacement dominates the overall system response and that transformer and bushing have a displacement very close to it. To vary this ratio, the frequency of interconnecting equipment is changed. Since its mass is kept constant, this means that its stiffness is changed. However, in order to see what behavior a system with the same FR (as define by Equation 4.1) and a different interconnecting mass will have, the analyses are done for two different masses. The radius of R = 40 inch is used for FPS that means a period of 2.0 seconds for the isolation. A weight of 200 kips and frequency of 11 Hz for transformer and 5kips and 10 Hz for bushing are assumed. The strong horizontal component of the 1940 El Centro earthquake with a peak acceleration of 1.0g is applied to the model. Table 4.1 shows the interconnecting equipment characteristics for the cases studied.

Table 4.1 Interconnecting Equipment Characteristics for Studies on Effects of Frequency Ratio on Interaction

Case	Interconnecting Equipment Mass (kips)	FR
1	5	0.4
2	5	0.6
3	5	0.8
4	5	1.0
5	5	1.1
6	5	1.2
7	5	1.5
8	5	2.0
9	5	3.0
10	5	4.0
11	5	6.0
12	5	8.5
13	5	10.0
14	5	12.0
15	5	15.0
16	10	4.0
17	10	6.0
18	10	8.5
19	10	10.0
20	10	12.0
21	10	15.0

Figures 4.4 to 4.6 show the displacements of FPS and interconnecting equipment and relative displacement of the bushing for different ratios of FR. As can be seen, the response of FPS doesn't change for lower values of FR and then starts to increase. As mentioned before, this is because of the constancy of the interconnecting equipment mass. This results in unrealistically high stiffness for high values of FR, and low stiffness for very low FR values. The bushing response shows the change of bushing response for different FR values and it is minimum around FR = 1 with the minimum value of 0.32 in that is equal to the failure displacement of the 196 kV bushing (0.3~0.35 in) [Gilani, 1999(a)]. If there were enough slack to prevent interaction, the relative displacement of bushing would be slightly less than 0.05 in, that is acceptable. This shows that interaction has very adverse effects, even in frequency ratios that would result in little or no

interaction in linear systems. The interconnecting equipment displacement is a reflection of its stiffness that is dependant upon FR and is unrealistically high in low frequencies because of its very small stiffness.

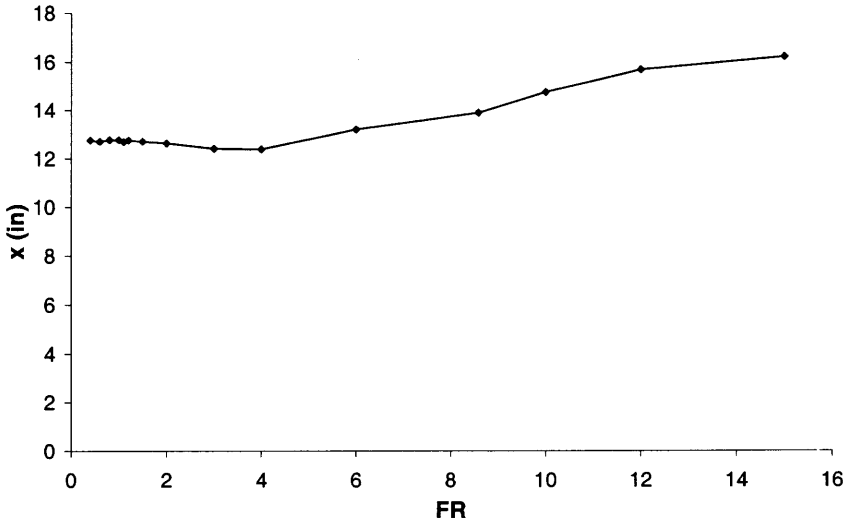

Figure 4.4 FPS displacement versus frequency ratio.

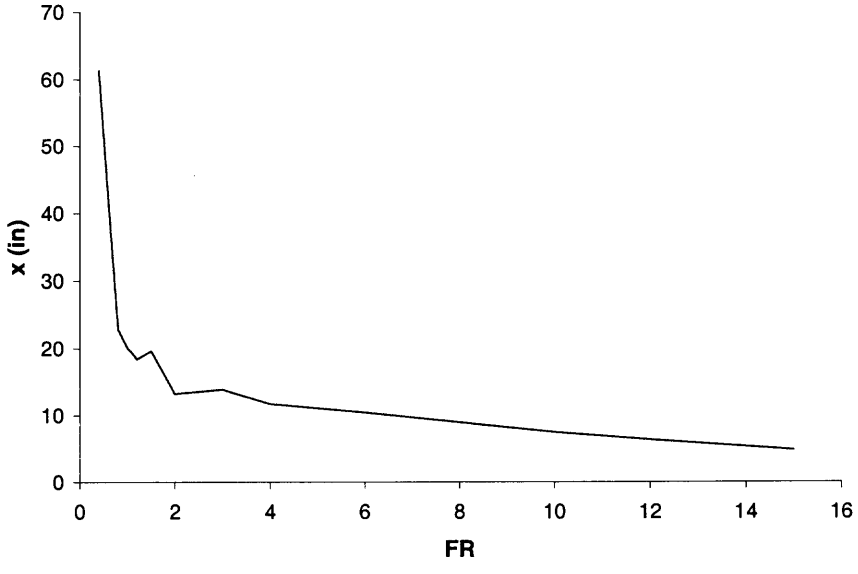

Figure 4.5 Displacement of interconnecting equipment versus frequency ratio.

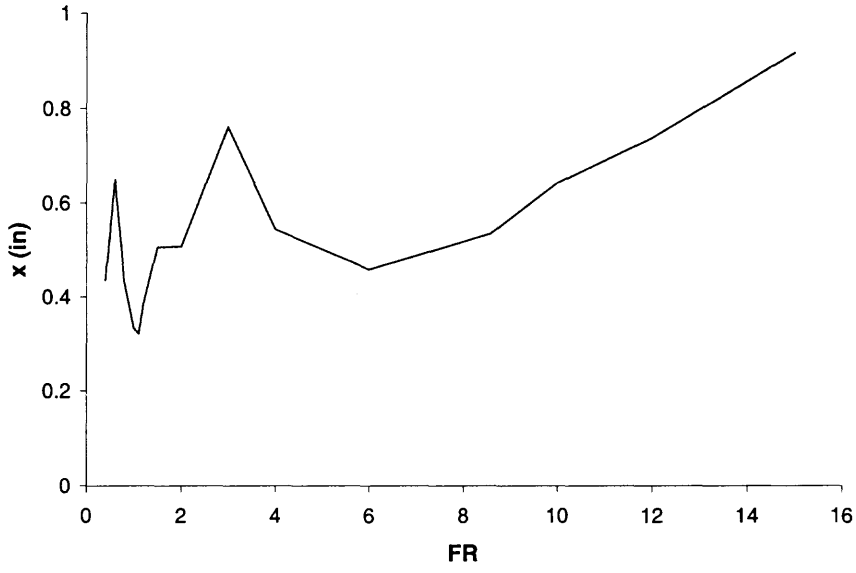

Figure 4.6 Relative displacement of bushing versus frequency ratio.

Figures 4.7 and 4.8 show the effect of the interconnecting mass on FPS and bushing response. The abbreviation INC in these figures and throughout this text refers to the interconnecting equipment. As observed, the interaction has more effect on FPS and bushing response when the interconnecting equipment has a higher mass.

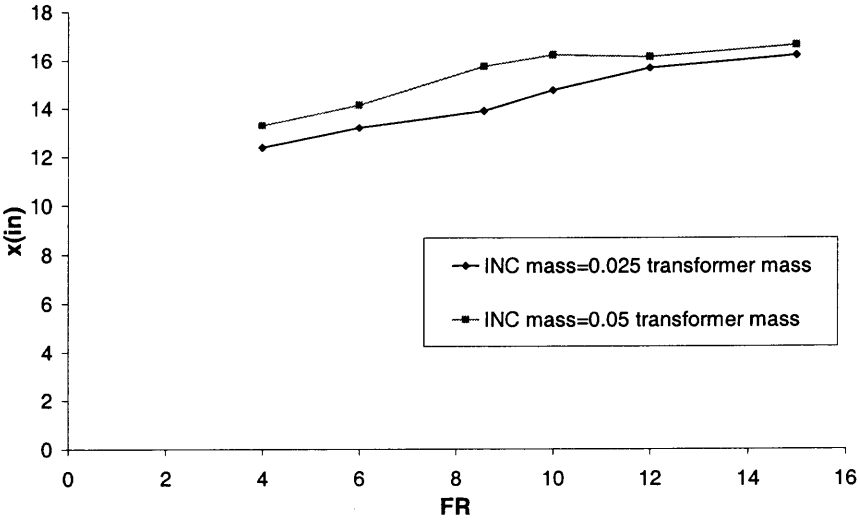

Figure 4.7 Effect of interconnecting equipment mass on FPS displacement.

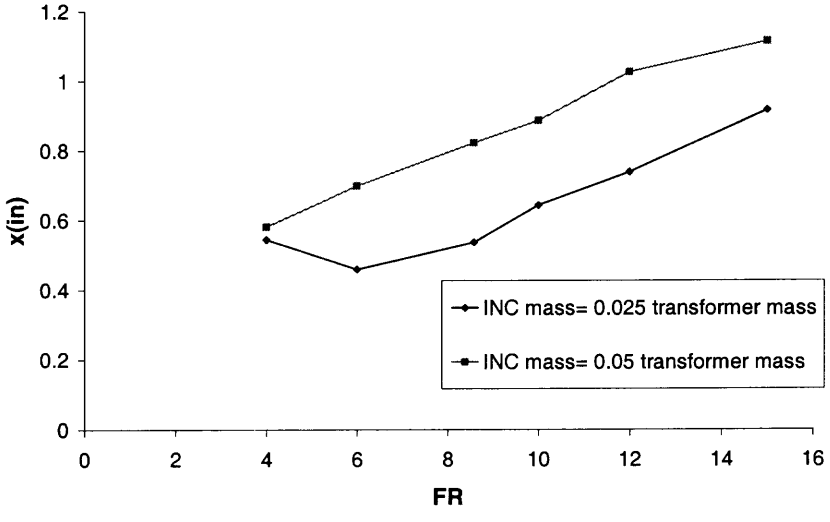

Figure 4.8 Effect of interconnecting equipment mass on relative displacement of bushing.

To study the effect of the amount of slack on interaction effects, another set of studies is done. The slack ratio defined as

$$Slack\quad Ratio = \frac{\Pr ovided\quad slack}{Slack\quad required\quad to\quad preevnt\quad \text{int}eraction} \tag{4.2}$$

is employed to quantify the relative amount of slack. Table 4.2 shows the properties of the interconnecting equipment considered. Their frequencies are in a range of 1 to 4 Hz. TT1 and BUSH3 as mentioned in Chapter 2 are selected as the transformer and bushing elements. An FPS with R = 60 in (T = 2.48 s) is used for isolation. Table 4.3 shows the details of the cases considered.

Table 4.2 Interconnecting Equipment Characteristics for Studies on Effect of Slack Ratio on Interaction

Interconnecting Equipment	Frequency (Hz)	Mass (kips)	Stiffness (kips/in)
INC1	1	6.9	0.70
INC2	2	6.9	2.82
INC3	3	6.9	6.34
INC4	4	6.9	11.28
INC5	1	110.39	11.28
INC6	2	27.6	11.28
INC7	3	12.27	11.28

Table 4.3 The Cases Studied on Interaction of Isolated Transformer-Bushing and Interconnecting Equipment

Case	Interconnecting Equipment	Slack ratio
1	INC1	0%
2	INC1	100%
3	INC2	0%
4	INC2	100%
5	INC3	0%
6	INC3	10%
7	INC3	20%
8	INC3	30%
9	INC3	40%
10	INC3	50%
11	INC3	60%
12	INC3	70%
13	INC3	80%
14	INC3	90%
15	INC3	100%
16	INC4	0%
17	INC4	10%
18	INC4	20%
19	INC4	30%
20	INC4	40%
21	INC4	50%
22	INC4	60%
23	INC4	70%
24	INC4	80%
25	INC4	90%
26	INC4	100%
27	INC5	0%
28	INC5	100%
29	INC6	0%
30	INC6	100%
31	INC7	0%
32	INC7	100%

Table 4.4 presents a summary of the maximum responses for different cases. Positive or negative displacement in the cable refers to sign of the change in distance between two ends of the cable. These results are analyzed and interpreted in what follows in this section.

Table 4.4 Maximum Results of Interaction of Isolated Transformer-Bushing and Interconnecting Equipment

Case	FPS disp. (in)	Transformer rel. disp. (in)	Bushing rel. disp. (in)	Cable Positive disp. (in)	Cable Negative disp. (in)	INC disp. (in)	Support Reaction (kips)	Cable Force (kips)
1	20.2245	0.01128	4.0300	0.51214	20.9221	15.059	30.0448	102.4
2	16.6104	0.00910	0.0421	23.1742	32.9504	19.633	26.1955	0
3	20.0731	0.01228	3.2601	0.39096	23.6968	6.7474	29.8834	78.2
4	16.6104	0.00910	0.0421	12.2273	21.1082	6.1061	26.1955	0
5	19.0661	0.01341	3.9301	0.26034	20.3512	4.9766	28.8109	52.1
6	18.8475	0.01127	3.4058	1.40077	20.1751	4.2425	28.5782	51.2
7	18.9372	0.01082	3.1309	2.5451	20.4563	4.0805	28.6736	51.1
8	18.984	0.01162	3.1766	3.75319	20.818	4.1000	28.7235	63.8
9	19.3753	0.01041	2.9281	4.90446	20.8794	3.7259	29.1402	65.1
10	18.9364	0.00830	2.5742	6.06171	19.6243	3.3038	28.6728	67.6
11	18.8232	0.00882	2.2288	7.1513	18.9974	2.9528	28.5522	56.5
12	18.2283	0.01114	1.7570	8.25529	18.2711	3.1461	27.9187	48.4
13	17.5538	0.01061	1.5311	9.35923	18.7403	3.8158	27.2002	40.2
14	17.0109	0.00908	0.9077	10.4433	18.2871	3.2158	26.6221	28.0
15	16.6104	0.00910	0.0421	11.4479	17.6464	2.6602	26.1955	0
16	17.7541	0.01340	5.1598	0.35217	18.3789	4.0241	27.4137	70.4
17	17.2213	0.01262	4.7445	1.35111	17.8197	3.6984	26.8462	64.3
18	17.2329	0.01266	3.8012	2.31585	17.861	2.8808	26.8585	51.4
19	17.6664	0.01138	3.2796	3.33503	18.4742	2.4601	27.3202	49.3
20	18.1494	0.01029	2.7989	4.3724	19.0852	2.2138	27.8346	50.9
21	18.5737	0.00882	2.3890	5.37586	19.3991	2.0956	28.2865	45.7
22	18.522	0.00882	2.0169	6.40017	19.104	2.0956	28.2315	44.7
23	18.2543	0.00980	1.5359	7.39779	18.7094	2.0956	27.9463	38.3
24	17.9605	0.00978	1.1381	8.36973	18.6216	2.0956	27.6335	26.8
25	17.3962	0.00902	0.7821	9.3572	18.4387	2.0956	27.0324	18.4
26	16.6104	0.00910	0.0421	10.2947	17.7833	2.0956	26.1955	0
27	25.8523	0.03148	10.8418	0.77531	41.2927	17.301	36.0386	155.1
28	16.6104	0.00910	0.0421	23.1742	32.9504	19.633	26.1955	0
29	20.1582	0.02241	8.4990	0.56748	26.3809	8.3451	29.9741	113.5
30	16.6104	0.00910	0.0421	12.2273	21.1082	6.1061	26.1955	0
31	17.7752	0.01577	5.4031	0.36604	18.6194	3.9436	27.4361	73.2
32	16.6104	0.00910	0.0421	11.4479	17.6464	2.6602	26.1955	0

Figure 4.9 shows a time history of the displacement of FPS and interconnecting equipment and relative displacement of bushing when no slack is provided (Case 1). As observed in this figure, the heavy weight of transformer carried on FPS tends to dominate the responses. Hence, when FPS has negative displacement (moving away from interconnecting equipment) it pulls the interconnecting equipment with it. This will put

bushing under an enormous force due to pulling by FPS and resistance by the interconnecting equipment. Therefore, it is observed that bushing experiences large peaks in its response when FPS has negative displacement. In other times, bushing has much smaller response that is free from influence of the interconnecting equipment.

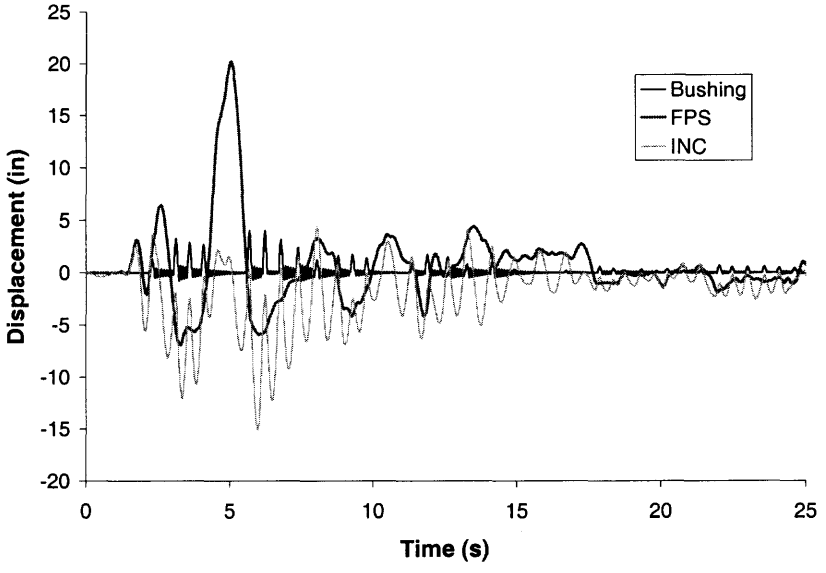

Figure 4.9 Time history responses in simplified model, Case 1.

Figures 4.10 and 4.11 compare the relative displacement in the cable and displacement of FPS in the presence or absence of sufficient slack.

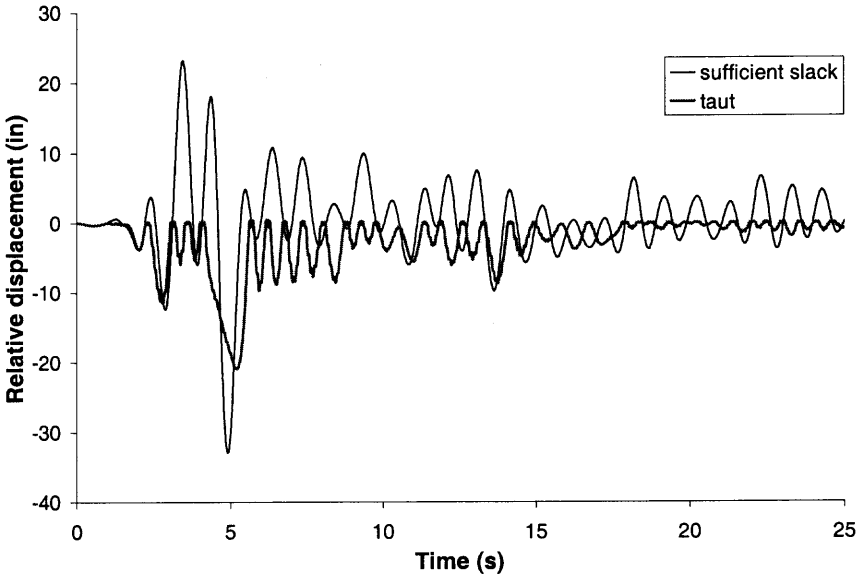

Figure 4.10 Relative displacement of the cable in simplified model, Case 1.

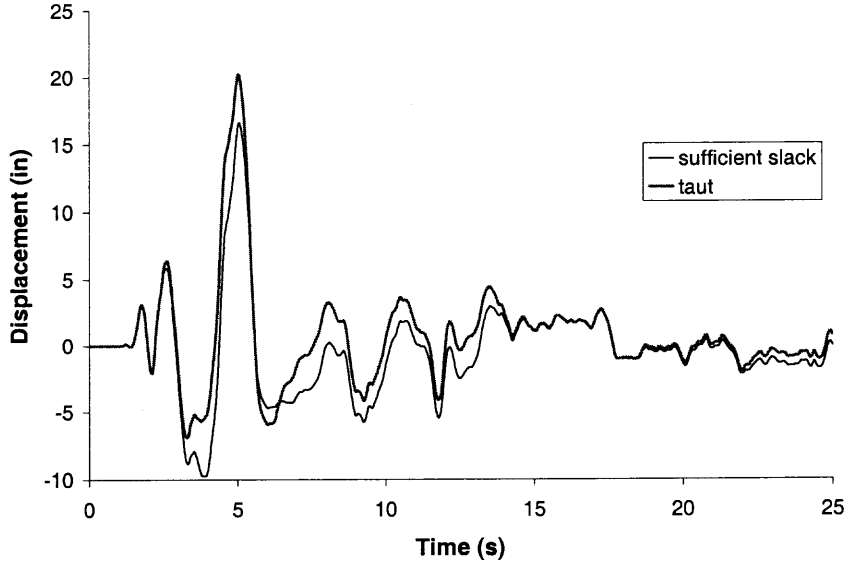

Figure 4.11 FPS displacement in simplified model, Case 1.

To see how much partial slackness of the cable can help reduce the adverse interaction effects, the analyses for INC3 and INC4 are done for different slack

percentages compared to the slack required to prevent interaction. The slack ratio in these analyses is the inverse of the factor β used in other studies [Hong, 2001]. Those results are presented for values of β as high as 2, that are equivalent to slack ratios of 50%~100% in our graphs. For β<1, there will be no interaction in our model.

Figure 4.12 shows the relative displacement of bushing. As obviously observed, even small tautness of the cable will amplify the response of bushing considerably. For slack ratio of 90%, interaction with INC3 causes a relative displacement of 0.91 in the bushing that is more than 21 times that of the sufficient slack case. This ratio is 18 when interaction is with INC4. These values are much higher than the allowable displacement in the bushing that is of order of 0.3 in for a 230 kV bushing [Gilani, 1999(a)]. This suggests that any interaction should be prevented to ensure that bushing does not undergo excessive displacements and sustain large forces. Even the slightest interaction has the potential of damaging the bushing. As expected, it is seen that as the slack is reduced, the bushing response is increased.

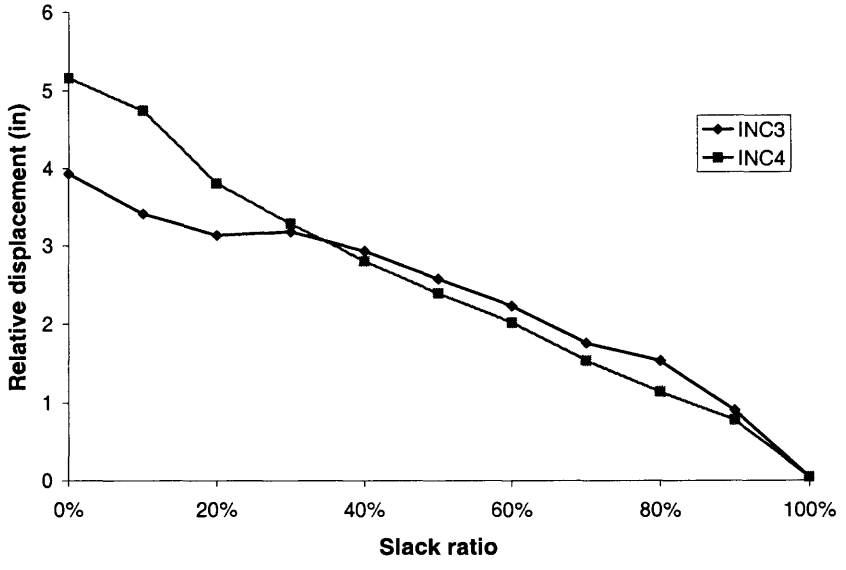

Figure 4.12 Relative displacement of bushing versus slack ratio.

Figure 4.13 shows the interconnecting equipment displacements. Here too, the decrease in slack usually has the effect of amplifying the interconnecting equipment response. However, the amplifications are much more modest compared to those of bushing. The amplification for INC3 and INC 4 are about 1.9 for completely taut cable.

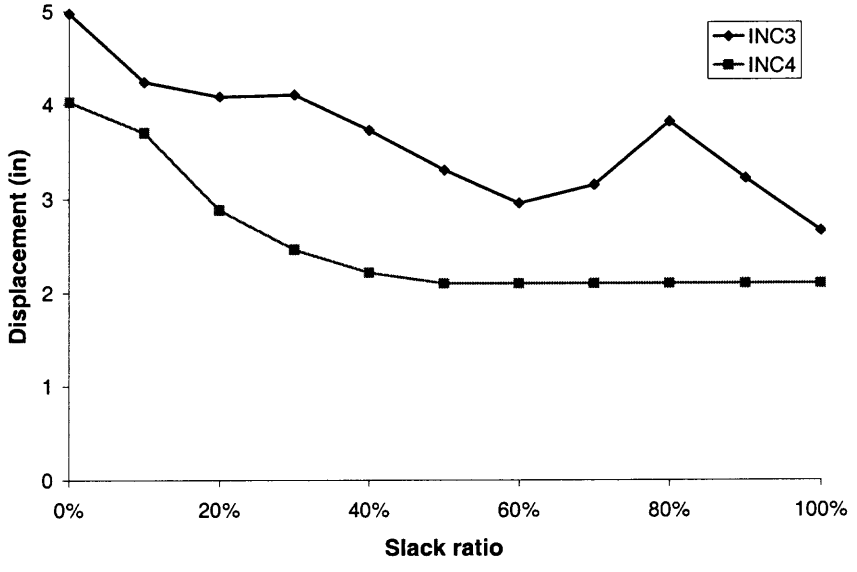

Figure 4.13 Interconnecting equipment displacement versus slack ratio.

Figure 4.14 shows the cable force as a percentage of the transformer weight. This force has a general rising tendency with a decrease in slack. However, this tendency is not always true and sometimes less slack might actually mean slight decrease in cable force due to nonlinear nature of interaction.

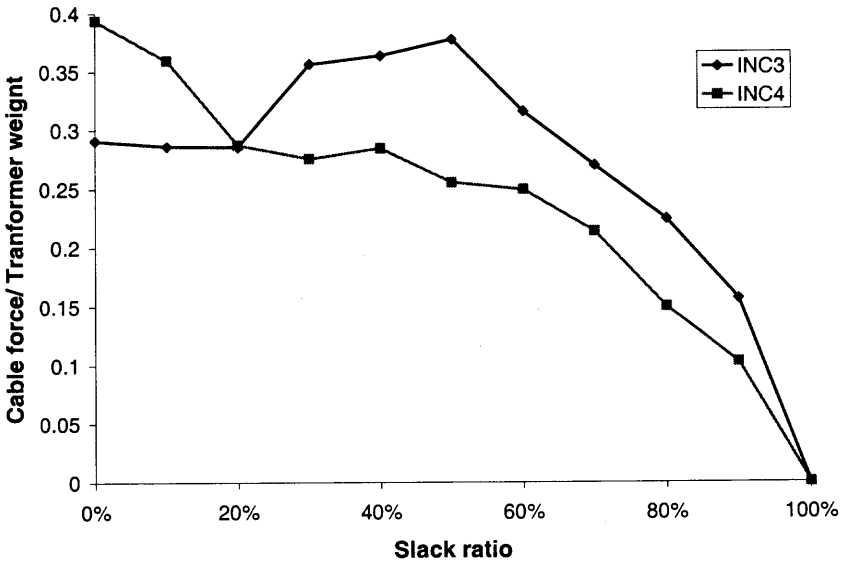

Figure 4.14 Cable force versus slack ratio.

Figure 4.15 shows FPS displacements. It can be seen that although the interaction effect generally increases with a decrease in slack, this relation does not hold very tightly. It should be mentioned here that interaction tends to increase the displacement of FPS toward the interconnecting equipment. Therefore, if the maximum displacement of FPS were in the direction away from the interconnecting equipment, a decrease in this displacement would be observed in the presence of interaction.

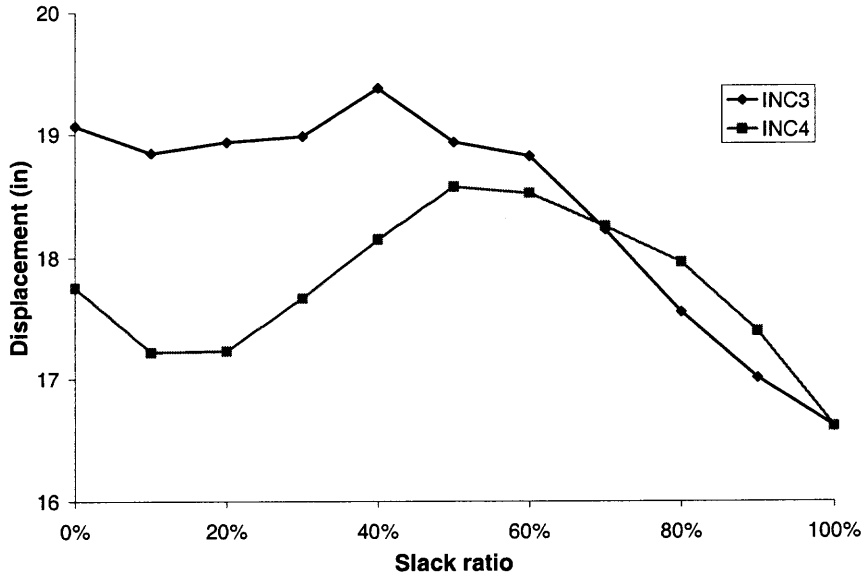

Figure 4.15 FPS displacement versus slack ratio.

Finally, Figure 4.16 shows the transformer force. Transformer response is not affected by the interaction dramatically and despite the increase in its forces, these forces remain very low. Even for certain slack ratios, interaction might reduce the transformer response.

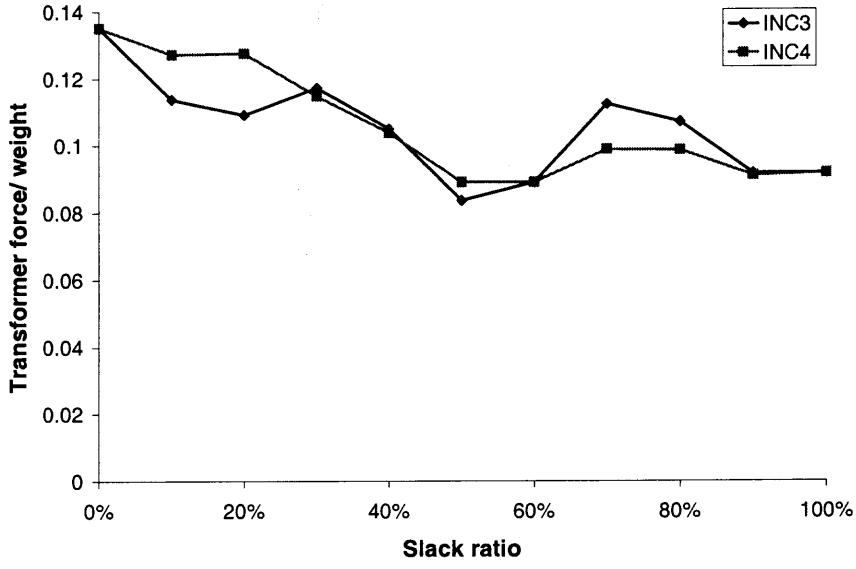

Figure 4.16 Transformer force versus slack ratio.

It should be noted that these are based on limited data, which does not allow conclusive observation on the effect of frequency. For more conclusive interpretations, the results mentioned at the beginning of this chapter should be used. Figures 4.17 through 4.21 shows the effect of interconnecting equipment stiffness and mass, using taut cable connection. For the line with fixed stiffness, decrease in frequency means increase in mass of the interconnecting equipment. For the line with constant mass, this translates into reduction in stiffness. Hence, for any frequency (Except 4 Hz), the point on the line with fixed mass has lower mass and stiffness compared to the other line. Figure 4.17 shows the interaction effects on bushing relative displacement. The response of bushing without interaction is not shown since it is of two lower orders of magnitude. It can be seen that increase in mass and stiffness of interconnecting equipment can exacerbate the

bushing response amplification. However the changes are more pronounced when mass is changing rather than stiffness, suggesting that mass has a more prominent role.

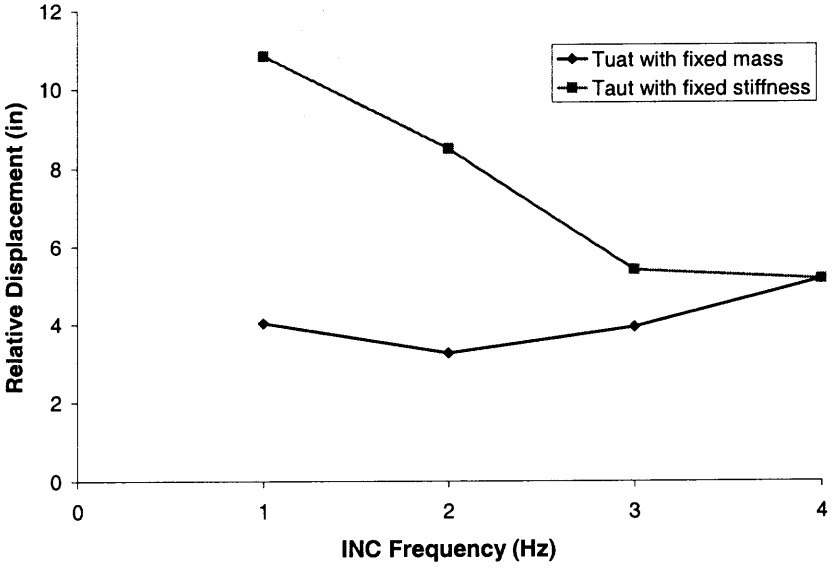

Figure 4.17 Bushing relative displacement versus INC frequency.

Figure 4.18 shows the interconnecting equipment displacement. Presence of interaction might increase or decrease this response. Hence, while interaction can easily increase the bushing response by 2 orders of magnitude, its effect on interconnecting equipment is more limited and can even be positive in some cases.

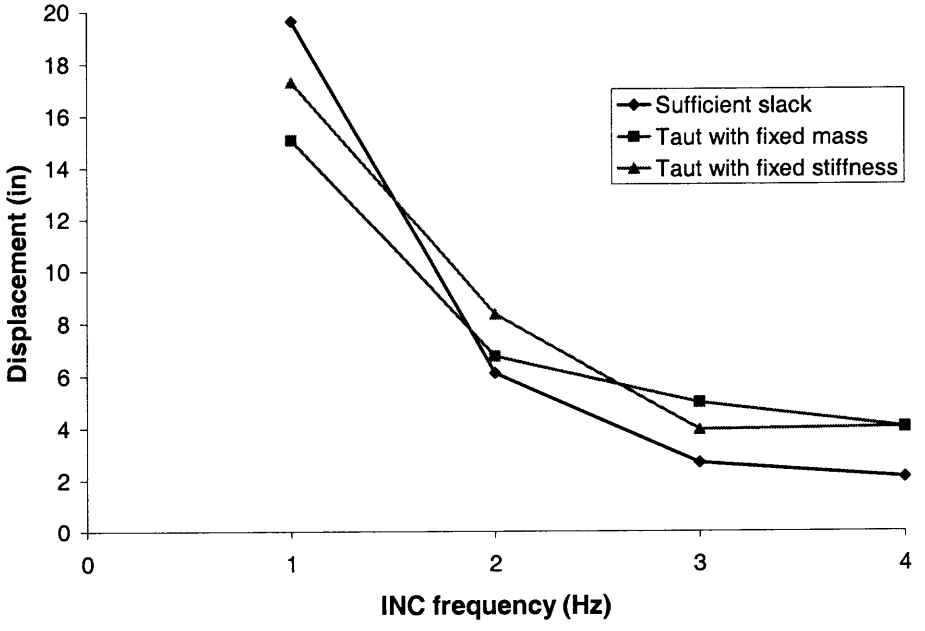

Figure 4.18 Interconnecting equipment displacement versus INC frequency.

Figure 4.19 shows relative displacement in transformer. Interaction always has adverse effect on transformer response. This effect is limited when the INC mass is constant, but is increased considerably with an increase in INC mass.

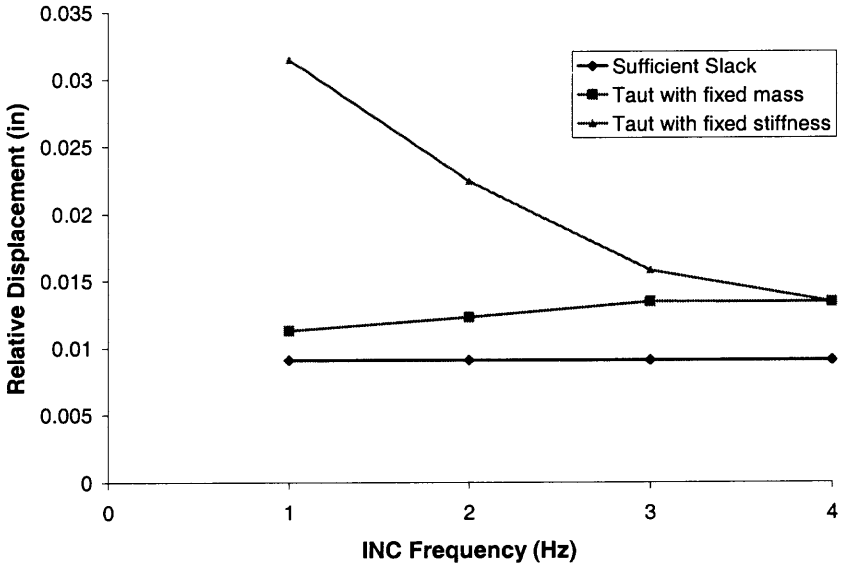

Figure 4.19 Transformer relative displacement versus INC frequency.

Figure 4.20 shows FPS displacement. As mentioned before, interaction tends to pull FPS toward the INC. Hence, it is possible that FPS response is reduced by interaction depending in position of interconnecting equipment relative to FPS and the earthquake record used. Here cases with lower frequencies show a slightly stronger effect on FPS response.

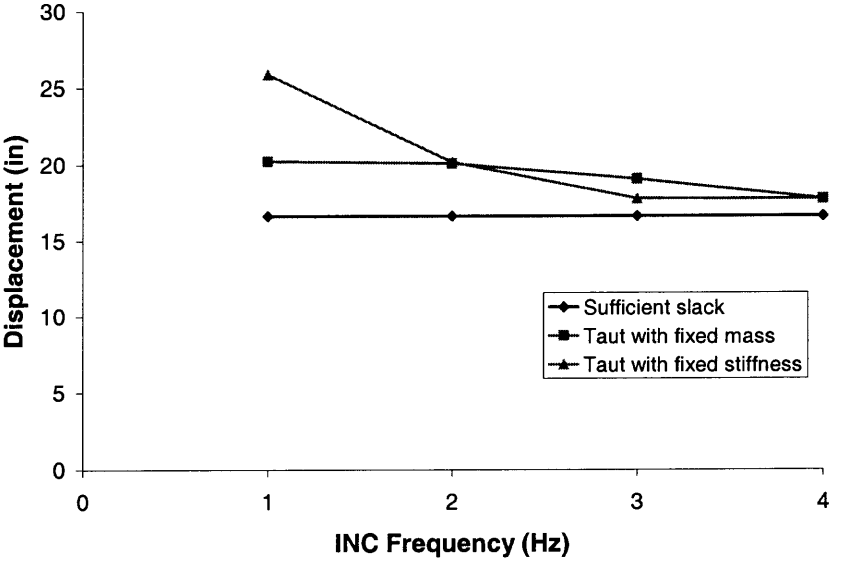

Figure 4.20 FPS displacement versus INC frequency.

Finally, Figure 4.21 shows cable force in presence of interaction. In general, this force tends to increase with a decrease in INC frequency, probably because they would have higher displacements if left alone.

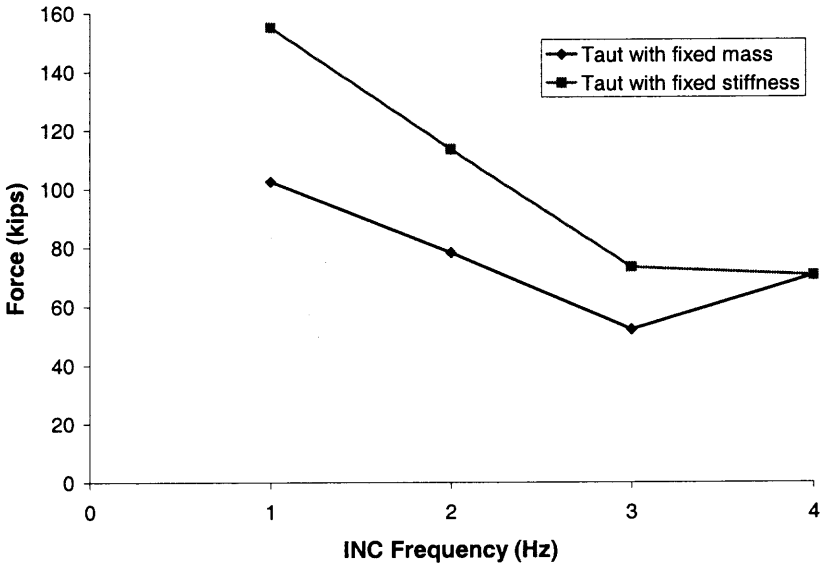

Figure 4.21 Cable force versus INC frequency.

Summing up the analyses results, interaction has the most severe affect on bushing response. The amplifications due to interaction are so high, even for small tautness, that any occurrence of them means failure of bushing. If the FPS is to be used for seismic isolation of transformer, enough slack should be provided in the connecting cable to prevent any interaction between transformer-bushing and interconnecting equipment. One way to be sure that this interaction dos not happen is to provide the slack equal to sum of the maximum absolute value of displacement of FPS and the interconnecting equipment [Ersoy, 2001]. Although this might be too conservative in some cases, the adverse effect of the slightest interaction justifies such conservatism. The relative displacements of bushing and transformer are negligible compared to that of FPS. The next chapter provides the suggested values to be used for FPS response.

Another observation worth consideration is the existence of differences in trends observed in interaction of fixed equipment, and those observed when there is isolation.

For instance, the interaction tends to amplify the response of both of the equipment connected by a cable, particularly that of the higher frequency equipment when both are fixed [Hong, 2001]. However, FPS being the low frequency and interconnecting equipment being the high frequency component in this study, a different trend is observed. The response of the engaged interconnecting equipment may be below its stand-alone response. On the other hand, the FPS is pulled more toward the interconnecting equipment, whether this means a decrease or increase in its maximum response.

4.3 FPS Graphs to Select FPS Radius and Cable Slack

For the same bearing material, the radius of FPS bearing is the only parameter that can be changed to get a different isolation behavior. Changes in this radius will change the natural frequency, FPS displacement, and inertial forces applied to the structure. To be able to choose the proper radius, numerous analyses are performed for different FPS radii and earthquake excitations and effects of radius and peak ground excitation on displacement and inertia response are determined. The results can be used to pick the proper radius to get the desired inertia reduction for the specified soil condition and peak ground acceleration. Once the radius is chosen, the maximum displacement of FPS can also be determined. Consequently, one can determine the amount of slack that should be provided in the connecting cable to prevent interaction between transformer-bushing and interconnecting equipment. Table 4.5 lists the earthquakes used to develop these graphs. These earthquakes are obtained from the PEER strong motion database [PEER, 2002].

Table 4.5 Earthquake Records Used

Case	Earthquake	Station	Ground
1	San Fernando 1971/02/09 14:00	126 Lake Hughes #4	Rock
2	Loma Prieta 1989/10/18 00:05	1161 APEEL 9 - Crystal Springs	Rock
3	Kern County 1952/07/21 11:53	1095 Taft Lincoln School	Rock
4	Kobe 1995/01/16 20:46	0 KJMA	Rock
5	Parkfield 1966/06/28 04:26	1438 Temblor pre-1969	Rock
6	Imperial Valley 1940/05/19 04:37	117 El Centro Array #9	Soil
7	Kern County 1952/07/21 11:53	135 LA - Hollywood Stor FF	Soil
8	Northridge 1994/01/17 12:31	75 Sylmar - Converter Sta East	Soil
9	Parkfield 1966/06/28 04:26	1014 Cholame #5	Soil
10	Mt. Lewis 1986/03/31 11:55	57191 Halls Valley	Soil

Figures 4.22 and 4.23 show the average displacement response and inertia reduction for FPS bearings under a horizontal excitation with a vertical excitation whose peak is set equal to 80% of the horizontal peak according to IEEE [IEEE, 1998]. As can be seen, with increase in radius, the change in displacement will decrease since the surface tends towards a flat surface. The displacements and their differences are higher in higher PGAs as expected, since friction happens more frequently in higher PGAs. Inertia reduction is higher for high radii, and a change in radius usually has more effect on inertia reduction compared to displacement. While the inertia reduction increases with increasing PGA, it tends to flatten in PGAs higher than about 0.5g. In case of R = 30 in, this inertia reduction starts decreasing after a certain PGA. This is because large displacements mean that the slider is in a rather steep position meaning it is under a large re-centering force. Choice of the radius should be based on a balance between displacement, inertia reduction, and bearing cost. The cost increases with increasing radius; Therefore, the bearing with lowest radius that satisfies the structural requirements should be chosen. Based on the graphs, a radius of 30~60 inch seems proper. Higher radii will provide little benefit in terms of higher inertia reductions, have higher displacements, and have much higher costs. Also, looking at benefits for different PGAs, it can be said

that for structures in places with PGA <0.2g, cost is the only important factor and R = 30 in is suggested. For 0.2g < PGA < 0.6g, cost and inertia reduction are the factors to be balanced. For PGA > 0.6g, all the factors should be considered.

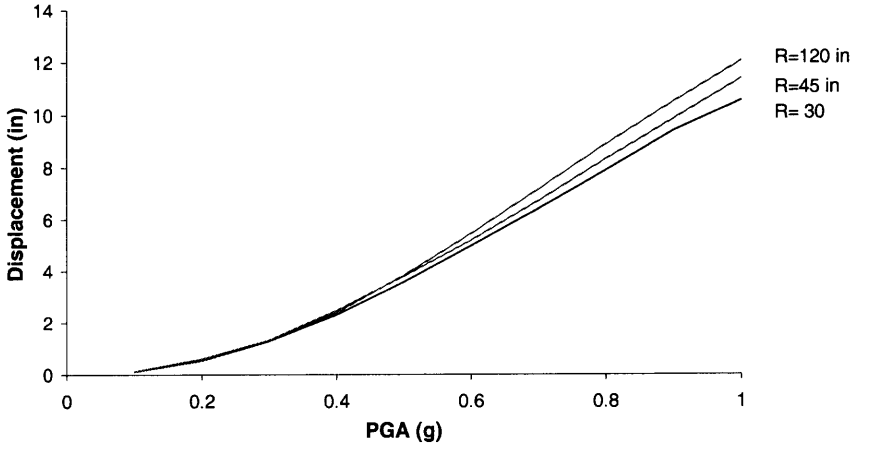

Figure 4.22 Average FPS displacement versus FPS radius.

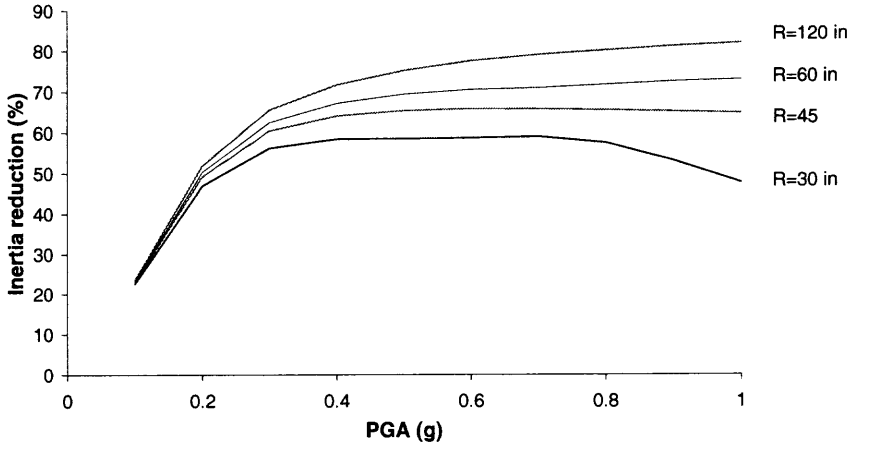

Figure 4.23 Average inertia reduction versus FPS radius.

Figures 4.24 through 4.27 show the same results for rock and soil earthquake records. It can be seen that for rock records, the displacement for R = 45 is slightly higher

and the other radii have very close displacements. This suggests that for the records on rock, the radius of FPS does not have much effect on the displacement responses. Hence, displacement is not among the factors used to determine the desired radius. The inertia reductions are however much different from one radius to another. Therefore, the inertia reduction plays a more prominent role in selecting the proper radius. The decrease in efficiency of FPS in higher PGAs is more pronounced for rock records compared to the average. This is especially more obvious for PGA> 0.7g and for R = 30 in. In soil records, the displacement for R = 30 in is visibly less than the others. The rest of radii have almost the same displacement response. The inertia reductions for soil are less affected by radius compared to rock records. Also, the decrease in efficiency in higher PGAs is not observed in soil records. In general, it can be said that it is easier justified for rock ground conditions to pick higher FPS radii compared to soil conditions due to the higher gain in terms of inertia reduction. For the practical range of radii considered, it can be said that in all cases displacement is of lower prominence. R = 45 in seems to be the choice that combines most of the benefits in general. R = 60 in may be preferred if the gain in terms of inertia reduction can balance the increased FPS cost. R = 30 in may be chosen in cases where the normal structural design can sustain the increased inertial forces with little or no reinforcement.

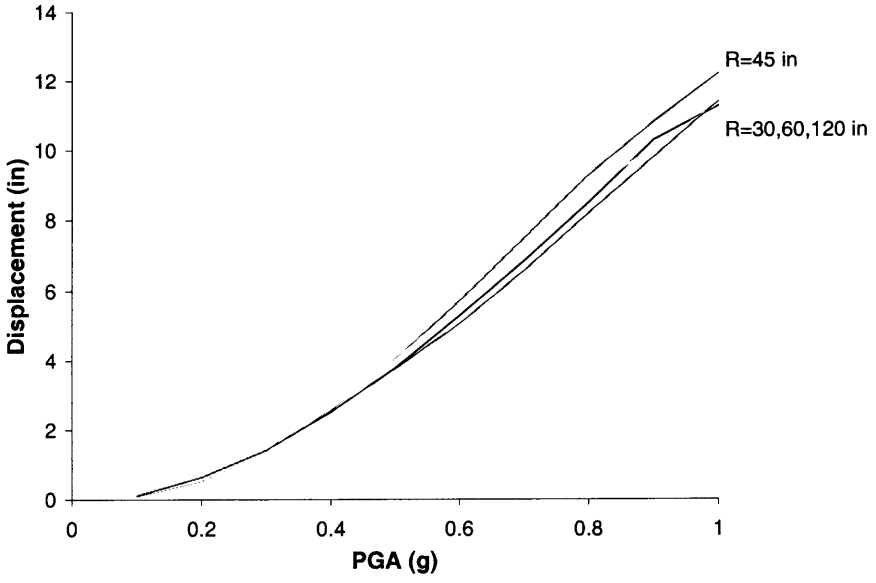

Figure 4.24 Average FPS displacement versus FPS radius for rock.

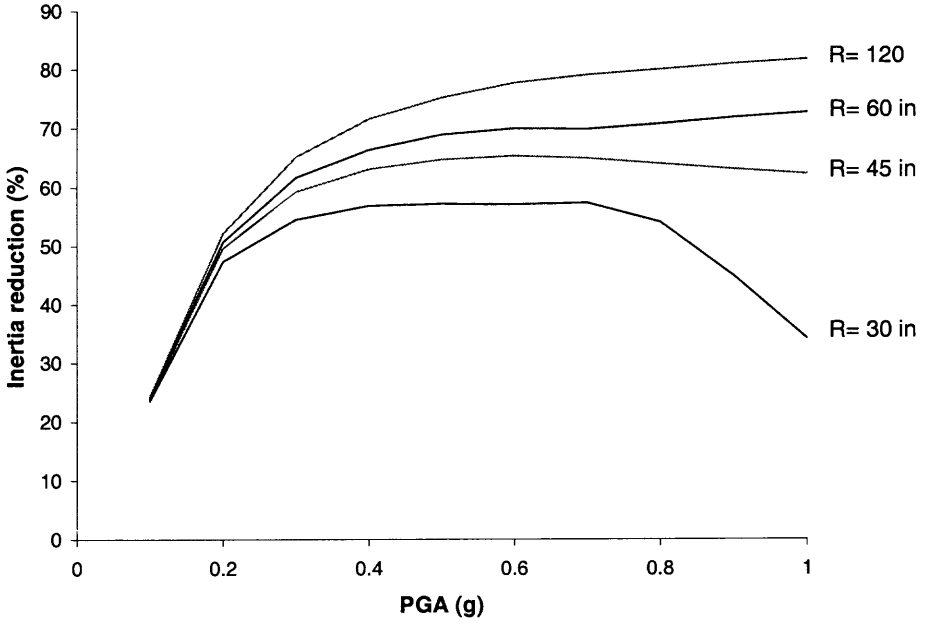

Figure 4.25 Average inertia reduction versus FPS radius for rock.

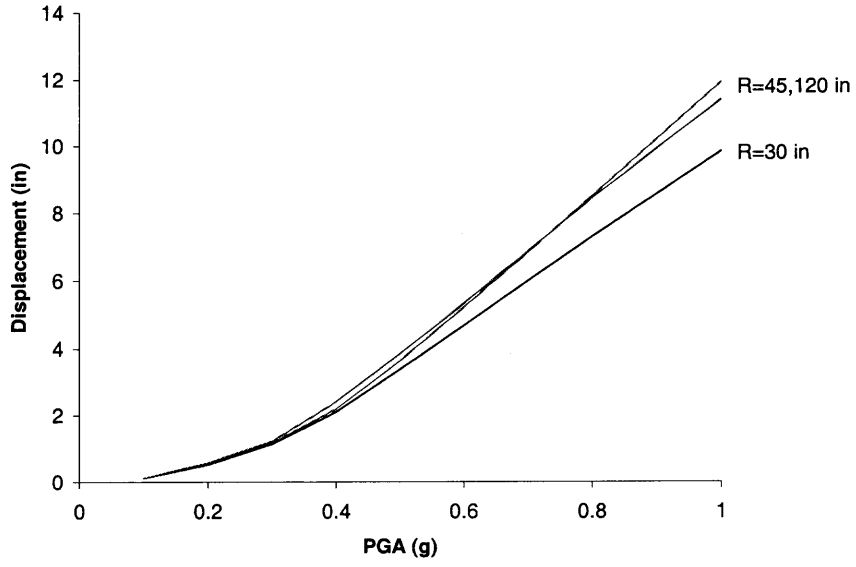

Figure 4.26 Average FPS displacement versus FPS radius for soil.

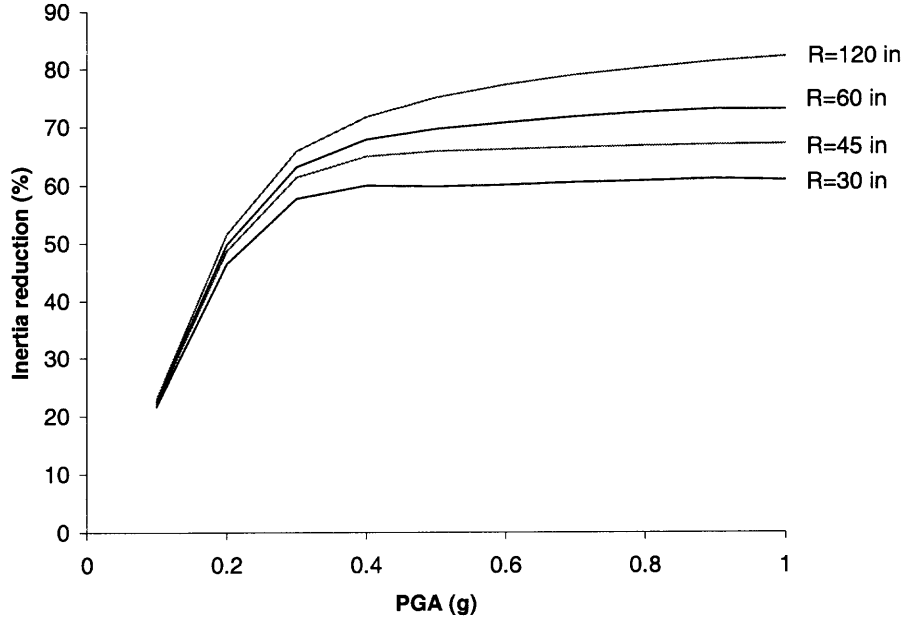

Figure 4.27 Average inertia reduction versus FPS radius for soil.

The displacement from these graphs can be used to determine the slack provided in the connection from bushing to the interconnecting equipment. This value should be

added to the peak displacement response of the interconnecting equipment. Although not considered in this study, it is recommended based on other studies that the cable connect the top of bushing to the point with the same elevation in the interconnecting equipment [Hong, 2001].

CHAPTER 5

INTERNAL COMPONENTS OF HIGH-POWER CORE-FORM ELECTRICAL TRANSFORMERS

Transformers are critical devices, which change or transform voltage levels between two circuits. Current values are also changed in the process. However, the power transferred between the circuits is unchanged, except for a typically small loss. This operation is based on principle of induction discovered by Faraday and works only in presence of alternating or transient current. The induced voltage is proportional to the number of turns linked by the changing flux [Del Vecchio, 2002].

The efficiency of transferring electrical power over long distances increases as the voltage levels rise. This can be seen for the transfer of the electrical power P = V.I noting that

$$Loss = \frac{\rho L P^2}{A V^2} \tag{5.1}$$

$$Voltagedrop = \frac{\rho L P}{A V} \tag{5.2}$$

In these relations, A is the area of the conductor, L is its length, ρ is electrical resistivity, and V and I are the electric potential and current. Since P, L, ρ are given, the loss and voltage drop can be made as small as desired by increasing the voltage V. However, there are other limits to this increase in voltage, such as the availability of adequate and safe insulation structures and the increase of corona losses. Also, a balance

should be achieved between the extra cost of material due to increase in A and the gained loss reduction.

In practice, voltages in the range of 100-500 kV and more recently as high as 765 kV are used for long distance power transmission. These voltages are, however, incompatible with much lower voltages safe for households use. In addition, due to reasons of cost and efficiency generators are designed to produce electrical power at voltage levels of 10 to 40 kV. Hence, there is a need for power transformers to boost the voltage at the generation end and to decrease it at the receiving end. The task of decreasing the voltage is usually done in more than one step.

There is often a need for adjustments in voltage to compensate for the voltage loss in the lines and other equipment. These voltage drops depend on the current level and vary throughout the day. This is accomplished by equipping transformers with tap changers, that are devices adding or subtracting turns from a winding, thus altering its voltage. Load or no-load tap changers are used to perform this task under load conditions or with the power disconnected from transformer, respectively.

Transformers are fairly passive devices containing very few moving parts. These include tap changers and cooling fans, which are needed on most units and sometimes pumps that are used on oil-filled transformers to improve cooling. Transformers are expected to have a long life of 25-50 yeas with little need for maintenance. There are a few routine maintenances. The oil quality must be checked periodically and filtered or replaced if necessary in the oil-filled transformers to protect them against electrical breakdown. Other key transformer parameters such as oil and winding temperatures,

voltages, currents, and oil quality as reflected in gas evolution are monitored continuously in many power systems [Del Vecchio, 2002].

5.1 Components of the Internal Structure

5.1.1 Core

The core is made of thin layers or laminations of dielectric steel especially developed for its good magnetic properties. The magnetic properties are best in the rolling direction. Therefore, in a good core design this is the direction the flux should naturally want to take. The lamination can be wrapped around the cores or stacked. Wrapped or wound cores have few, if any, joints so they have the ability to carry the flux nearly uninterrupted by gaps. However, the stacked cores have gaps at the corners where the core steel changes direction. This results in poorer magnetic characteristics compared to wound cores. Stacked cores are much more common in larger power transformers. The laminations for both types of cores are coated with an insulating coating to prevent development of large eddy current paths, which could lead to high losses.

In stacked cores for core-form transformers, the coils are circular cylinders that surround the core. Hence the preferred cross section shape of circle is chosen for the core since this will maximize the flux carrying area. In practice, the core is built in steps that approximate a circular cross section. The space between the core and the innermost coil is needed to provide insulation clearance for the voltage difference between the winding and the core, which is at ground potential and is also used for structural elements [Del Vecchio].

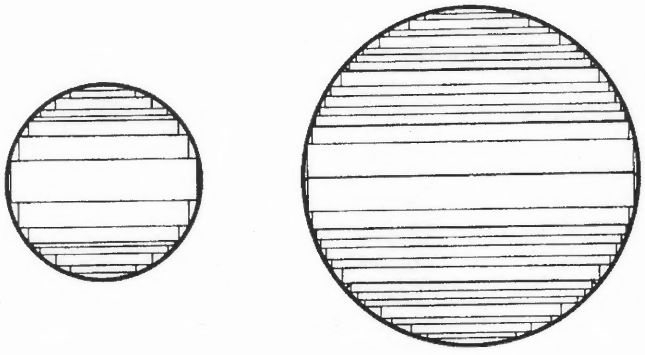

Figure 5.1 Core sections, 7-step taped (left); and 14-step banded (right) [Del Vecchio, 2002].

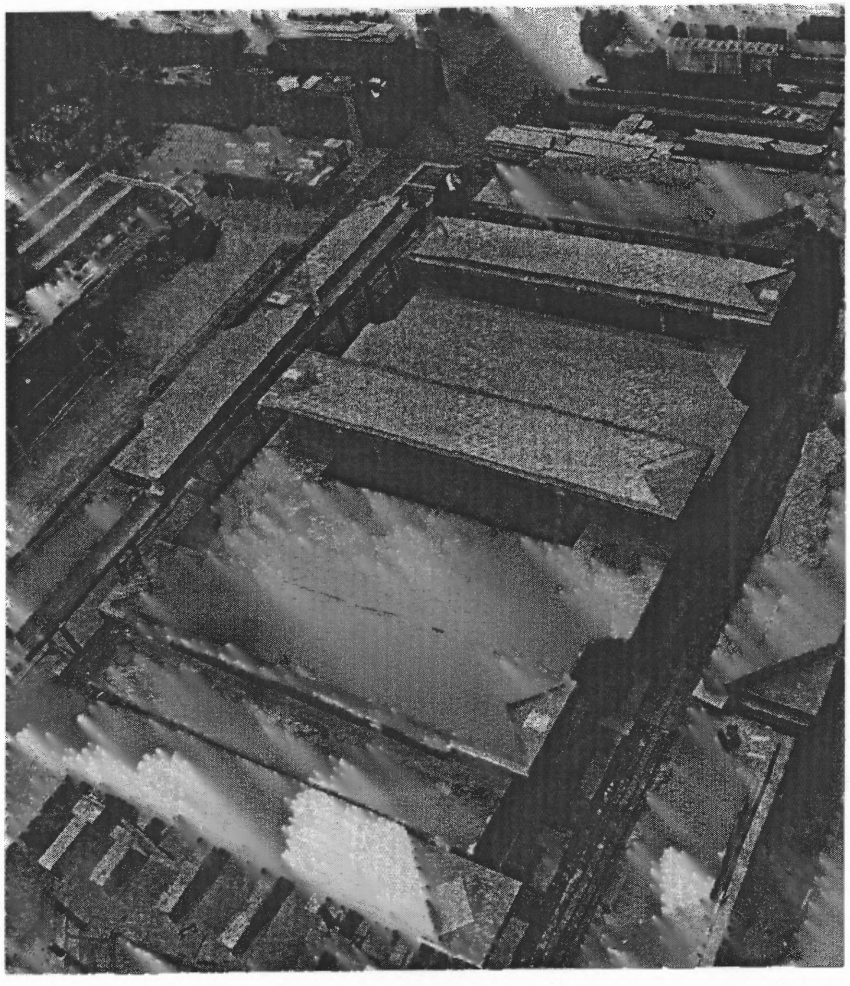

Figure 5.2 Four-limb core in course of building (GEC Alsthom) [Del Vecchio, 2002].

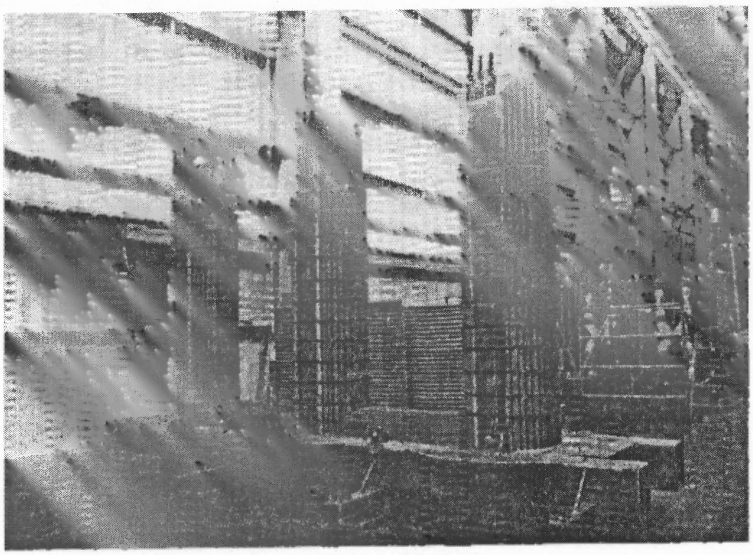

Figure 5.3 Three-phase stepped core for a core-form transformer without the top yoke [Heathcote, 1998].

5.1.2 Transformer Cooling

Electric resistance, changing flux in the electrical steel, and stray time-varying flux in metallic tank walls and other metallic structures result in losses inside a transformer. These losses lead to temperature rises that must be controlled by cooling. The primary cooling media for transformers are oil and air. In oil cooled transformers, the coils and core are immersed in an oil-filled tank. Radiators or other types of heat exchangers are usually used to circulate the oil so that the ultimate cooling medium is the surrounding air or possibly water for some types of heat exchangers.

The cooling medium in contact with coils and core must provide adequate dielectric strength to prevent electrical breakdown or discharge between components at different electric potentials. Oil immersion is more common in higher voltage transformers because of its higher breakdown strength compared to air. One can often

rely on natural convection of oil through the windings driven by buoyancy effects, to provide adequate cooling so that pumping is not necessary. Air is a more efficient means of cooling when it is blown by fans through windings for air-cooled units. Oil is the preferred medium for units not restricted by limitations like weight, mobility and fire hazard for indoor transformers. There are other cooling media for special case like reduction of fire hazard such as hexaflouride gas or silicone oil.

5.1.3 Windings

There are two main methods of winding the coils for core-form power transformers. Both are cylindrical coils, having an overall rectangular cross section. In a disk coil, the turns are arranged in horizontal layers called disks, which are wound alternately out-in, in-out. The winding is usually continuous and the last inner or outer turn gradually transitions between the adjacent layers. If the disks have only one turn, the winding is called a helical winding. The total number of turns usually dictates whether the winding is a disk or helical winding. The turns within a disk are usually touching and a double layer of insulation separates the metallic conductors. There is open space between the disks except for structural separators called key spacers. This allows room for cooling fluid to flow between the disks, in addition to providing clearance for bearing the voltage difference between them [Del Vecchio, 2002].

In a layer coil, the coils are wound in vertical layers, top-bottom, bottom-top, etc. The turns are typically wound in contact with each other in layers that are separated by means of spacers so that cooling fluid can flow between them. These coils are also usually continuous with the last bottom or top turn transitioning between the layers.

Both types of windings are used in practice and one or the other can be more efficient in certain applications. Generally, they can both be designed to function well in terms of ease of cooling, ability to withstand high voltage surges, and mechanical strength under short-circuit conditions.

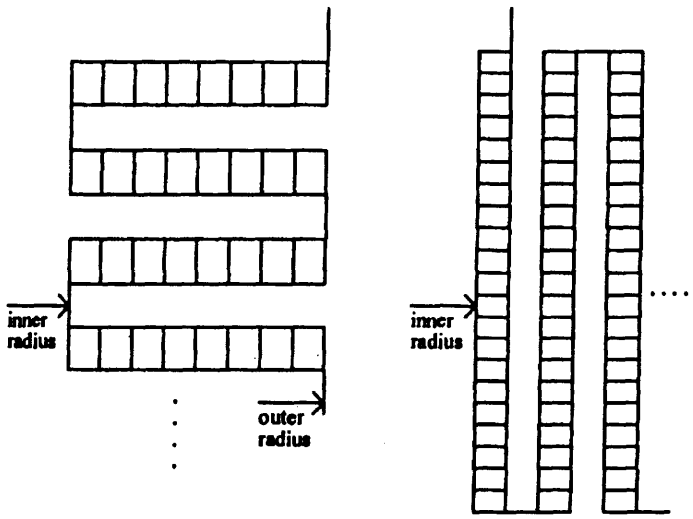

a) Disk coil b) Layer coil

Figure 5.4 Two major types of coil construction for core-form power transformers [Heathcote, 1998].

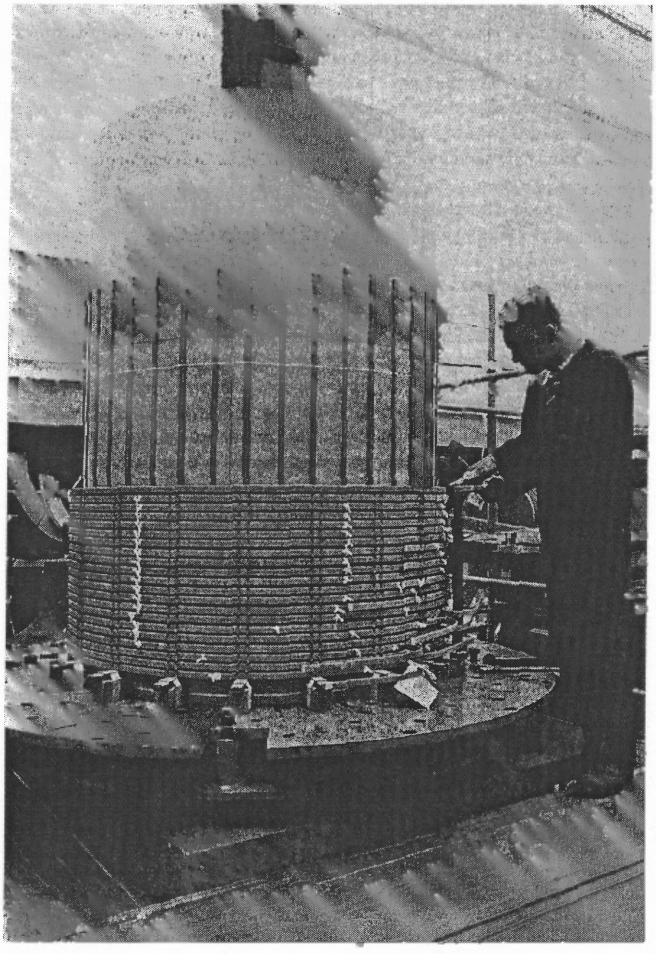

Figure 5.5 Winding in progress [Heathcote, 1998].

When the coils are wound with more than one wire or cable in parallel, transposition or cross-overs must be inserted which interchange the positions of cables at various positions along the winding. This will cancel loop voltages induced by stray flux that would otherwise drive currents around the loops formed when the parallel turns are joined at either end of the winding, and hence create extra losses.

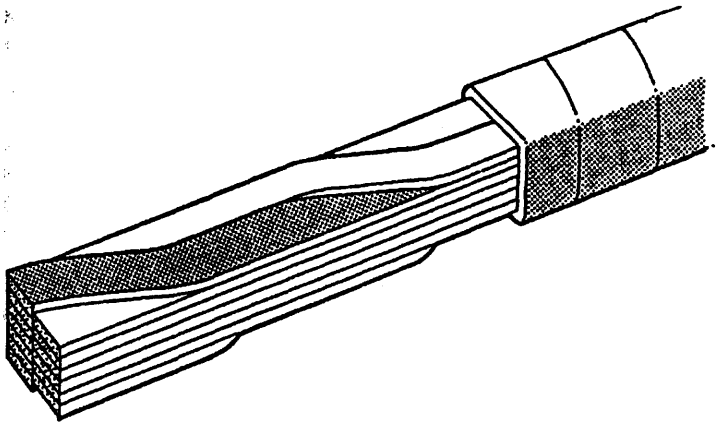

Figure 5.6 Continuously transposed conductor [Heathcote, 1998].

The stray flux also causes localized eddy currents in the conducting wire whose magnitude depends on dimensions of the wire cross-section. Subdividing the wire into strands of smaller cross-sectional dimensions can reduce these eddy currents and their associated losses. However, these strands are then in parallel and must therefore be transposed to reduce the loop voltages and currents. This is done during the winding process when the parallel strands are wound individually. Wire of this type, called magnet wire, consists of strands covered with an insulating paper wrap. The transposition can also be built into the wire to make what is called the continuously transposed wire, generally consisting of a bundle of 5-83 strands, each covered with a thin enamel coating. Strands are transposed one at a time along the cable so that all the strands are eventually transposed approximately every 10-12 inches along the length of the cable. The overall bundle is then sheathed in paper wrap [Del Vecchio, 2002].

5.1.4 Insulating Structure

Transformer windings and leads operate at high voltages relative to the core, tank, and structural elements. Also, different windings and even different parts of the same winding have different voltages. This requires providing some form of insulation between these various parts to prevent voltage breakdown or corona discharges. The surrounding oil or air that provide cooling has some insulating value. This oil has a special composition and must be purified to remove small particles and moisture. The type of oil most commonly used is called transformer oil. Further insulation is provided by paper covering over the wire or cables. This paper has a high insulation value when saturated with oil. Other types of wire covering are sometimes used for specialty applications. Pressboard is another insulation structure that is generally available in sheet form, often made in cylindrical shape. This is a material of cellulose fibers compacted together into a fairly dense and rigid matrix. Key spacers, blocking material, pressure rings, and lead support structures are also commonly made of pressboard.

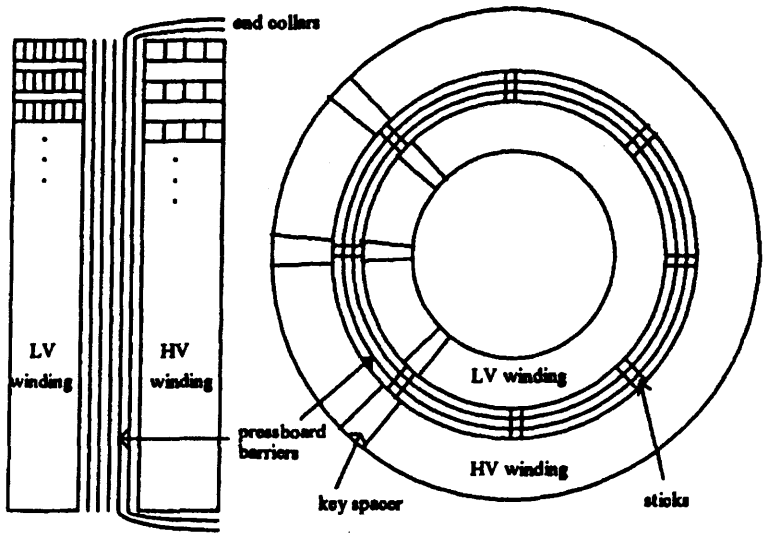

a) Side show b) Top view

Figure 5.7 Major insulation structure consisting of multiple barriers between windings. Not all the key spacers or sticks are shown [Del Vecchio, 2002].

Although normal operating voltages are quite high, 10-500 kV, the transformer must be designed to withstand even higher voltages that can occur if lightning strikes the electrical system or when power is suddenly switched on or off in some part of the system. However infrequently these happen, unless the insulation is designed to withstand them they could permanently damage the insulation, disabling the unit. These events usually have short durations. There is a time dependency on how insulation breaks down. A combination of oil and pressboard barriers can bear higher voltages for shorter periods of time. Therefore, a high-voltage short-duration impulse is no more likely to cause breakdown than a long-duration low-voltage pulse. This means that the same insulation that is used to withstand normal operating voltages that are continuously present can also withstand the high voltages briefly present when lightning strikes or

during switching operation. Lightning or surge arrestors are used to limit these abnormal voltages to insure that they do not exceed the breakdown limits determined by their expected duration. These arrestors thus guarantee that the voltages will not go above a certain value so that breakdown will not occur, provided their durations remain within the expected range.

Due to the different dielectric constants of oil or air and paper, the electric stresses are unequally divided between them. Because the oil dielectric constant is half of that of paper, and that of air is even a smaller fraction of paper's, the electric stresses are generally higher in oil or air than in the paper insulation. Unfortunately, oil or air has a lower breakdown stress than paper. For oil, it has been found that subdividing the oil gaps by mean of thin insulating barriers, usually made of pressboard, can raise the breakdown stress in oil. Thus, large oil gaps between the windings are usually subdivided by multiple pressboard barriers, referred to as the major insulating structure. Long vertical narrow sticks glued around the circumference of the cylindrical pressboard barriers maintain these oil gap thicknesses. The barriers are often extended by means of end collars curving around the ends of the winding to provide subdivided oil gaps at either end of the winding and strengthen these end oil gaps against voltage breakdown

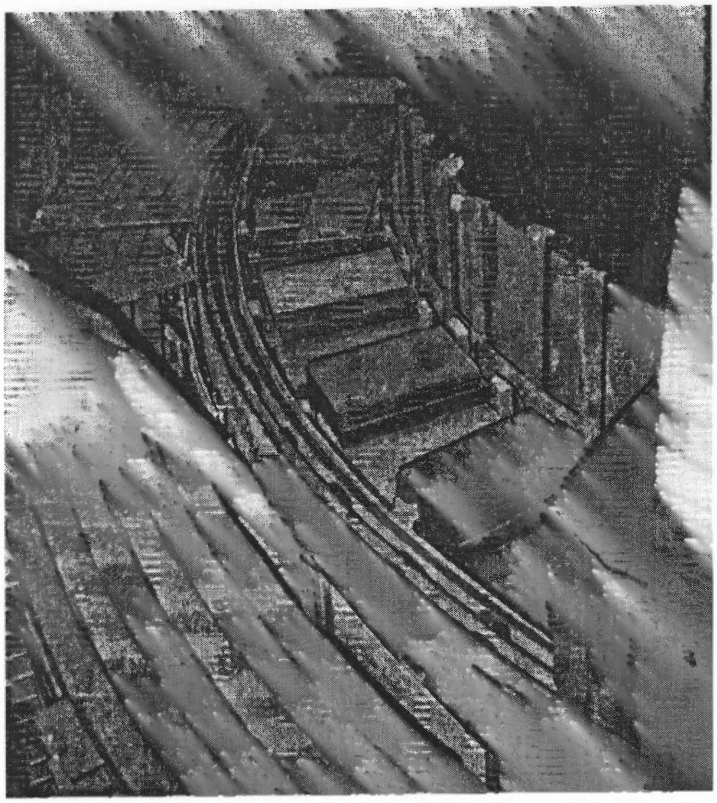

Figure 5.8 Top view of two windings showing the major insulation structure, key spacers, and sticks [Del Vecchio, 2002].

The minor insulation structure consists of the smaller oil gaps separating the disks and maintained by key spacers. Key spacers are narrow insulators, usually made of pressboard, that are spaced radially around the disk's circumference. Usually these oil gaps are small enough that subdivision is not required. Also the turn-to-turn insulation, usually made of paper, can be considered as part of the minor insulation structure.

The leads which connect the windings to bushings or tap changers or to other windings are also at high voltage and pass close to tank wall or structural supports which are grounded and must be properly insulated. They may also pass close to other leads at

different voltages. Additional insulation may be required at bends in the leads, particularly if they are sharp, since high voltages can be developed in these areas.

In addition to voltage breakdown in oil that can be resisted by means of barrier subdivisions, there is another breakdown process, which has to be guarded against. This is breakdown due to creep that occurs along the surface of the insulation. It requires sufficiently high electric stresses directed along the surface present over sufficiently long uninterrupted paths. Thus, the barriers themselves, sticks, key spacers, and lead supports can be a source of this breakdown. It is desired to position these insulation structures so that their surfaces conform to voltage equipotential surfaces to which the electrical field is perpendicular, thus eliminating any electric field directed along the surfaces. This, however, is not always possible and a compromise must be made.

The major and minor insulation designs, such as overall winding to winding and the number of barriers as well as disk to disk separation and paper covering thickness, are often determined by design rules based on extensive experiments. However, it is often desirable in cases of newer or unusual designs to do a field analysis using a finite element program or other numerical procedure. This can be especially helpful when potential of creep breakdown exists. However, it should be added that the breakdown process is not completely understood and deciding what level of electrical stress is acceptable usually involves some judgment [Del Vecchio, 2002].

5.1.5 Structural Elements

Under normal operating conditions, the transformer windings are under quite modest electromagnetic forces. However, the winding currents can increase 10-30 fold in a short-

circuit fault, resulting in forces of 100-900 times normal since the forces increase proportional to the square of electric currents. The windings and supporting structure must be designed to withstand these fault current forces without any permanent distortion or damage. The current protection devices that are usually installed will interrupt the fault currents after a few cycles. Fault currents can be caused by rare events like a falling tree on transmission lines that provides a direct current path to ground, or by animals or birds bridging across two lines belonging to different phases. However, the probability of such accidents over a long life of up to 50 years is credible enough to justify design for such forces.

The coils are usually supported by thick boards of pressboard or other material covering the winding ends, which are called pressure rings. They have a center opening that allows the core to pass through. The rings are in the range of 1-4 inches for large power transformers. Since all the windings are not of the same height, some blocking made of pressboard or wood is required between the top of the windings and the rings. In order to provide some clearance between the high winding voltages and the grounded core and clamp, additional blocking is usually provided between the ring and the top yoke and clamping structure [Del Vecchio, 2002].

Vertical tie-plates that pass along the sides of the core join the top and bottom clamps. These tie plates have threaded ends that are used to pull the top and bottom clamps together by means of tightening bolts, compressing the windings. These compressive forces are transmitted along the windings via the key spacers strong enough in compression to accommodate these forces. The clamps and tie plates are made of steel. Axial forces that tend to elongate the windings when a fault occurs will have to pull the

tie plates in tension. Also since the coils and core are lifted as a unit through lifting hooks attached to the clamps, the tie-plates must be strong enough to carry the gravitational load. The tie plates are usually about 1 cm (3/8 in) thick. They are of varying width depending on the expected short circuit forces and transformer weight, and are often subdivided in width to reduce eddy current losses [Del Vecchio, 2002].

The radial fault forces are countered inwardly by means of the sticks separating the oil barriers, and through additional support next to the core. The windings themselves, particularly the innermost one, provide additional resistance to inward radial forces. The radial force applied to the outermost winding is usually outward and puts the wires or cables in tension. Since there is no supporting structure on the outside to counter these forces, the material itself must be strong enough to resist these tensile forces. A measure of the material's strength is its proof stress that is the stress required to produce a permanent elongation of 0.2% (sometimes 0.1%). Copper of specified proof stress can be ordered from the wire or cable company.

There are also extra loads acting upon leads during a fault that are produced by the stray flux from the coils or from the nearby lead interacting with the lead's current. Therefore, braces made of wood or pressboards that extend from the clamps are used to support the leads. This lead support structure can be quite complicated, especially if there are many leads and interconnections and is usually costume made for each unit.

The assembled coil, core, clamps, and lead structure are placed in a transformer tank. The tank serves many functions including containment of the oil for an oil-filled unit, protection of the coils and other transformer structures and also protecting personnel from the high voltages present. It keeps stray flux from getting outside the tank if it is

made of soft (magnetic) steel. The tank is also usually made airtight to prevent air from entering and oxidizing the oil.

There are also numerous attachments to the tank such bushings for getting the electrical power into and out of the unit, and transferring sensor information to remote processors and receiving control signals, and radiators with or without fans to provide cooling. There is a separate tank compartment on certain units for tap changing equipment. Also attached to some of the tanks over the top of the radiators are conservators. They are large, usually cylindrical, structures that contain oil in communication with the main tank oil. A conservator also has an air space, which is separated from the oil by a sealed diaphragm. Thus, the flexible diaphragm accommodates the changes in the tank oil volume due to temperature changes, while maintaining a sealed oil environment [Del Vecchio, 2002].

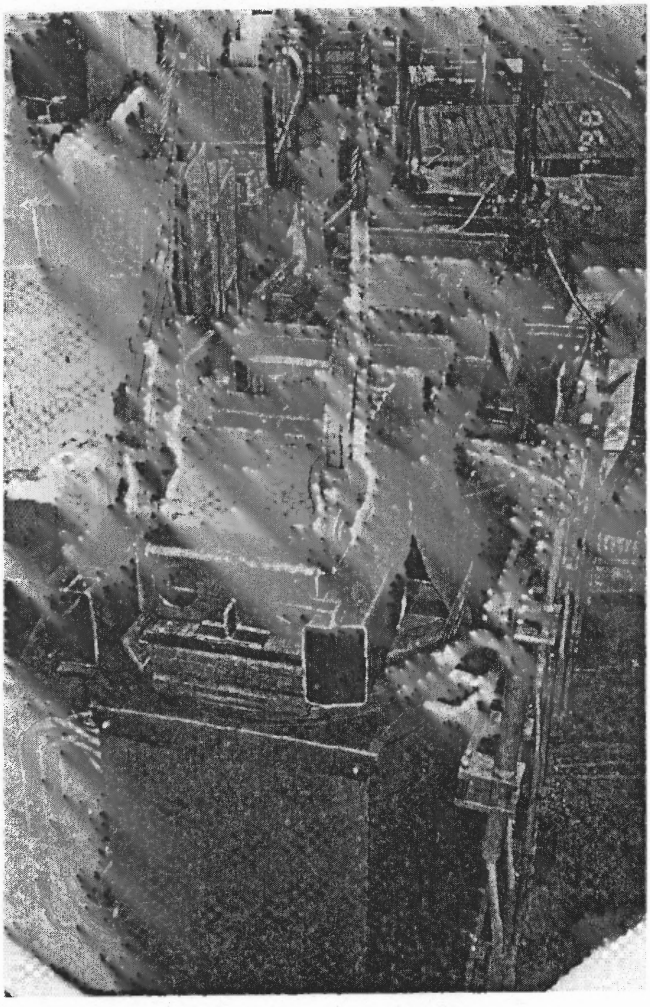

Figure 5.9 Top view of clamping structure for a 3-phase transformer [Del Vecchio, 2002].

5.2 Mechanical Design of Internal Components

Transformers undergo large forces during fault conditions and must be designed to withstand them. These fault currents must be calculated for the standard fault types such as single line to ground, double line to ground, line to line, and all three lines to ground. The data in this section on mechanical design of internal components are based on Del Vecchio [Del Vecchio, 2002] unless otherwise mentioned.

The force density (force/unit volume), f, generated in the windings by the magnetic induction, B, is determined by Lorentz force law

$$f = J \times B \tag{5.3}$$

where J is the current density and SI units are used. An electrical finite element analysis is performed to determine the values of magnetic induction, and hence f, inside the transformer. These force densities are used to determine differences in forces and stresses. To allow for a transient overshoot, the currents are multiplied by an asymmetry factor. This procedure can still be considered static since it does not take the effects dynamic effects of the sudden application of load such as excitations into account. W here these dynamic effects are important, the results of a few studies on these dynamic effects are used to adopt an appropriate enhancement factor [Del Vecchio, 2002].

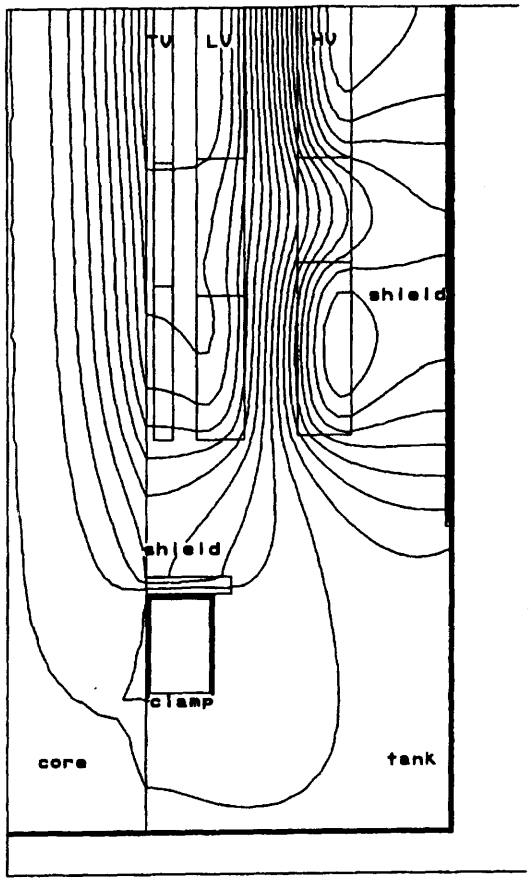

Figure 5.10 Plot of transformer leakage flux. Only the bottom half is shown and the figure is assumed to be cylindrically symmetrical about the core center line [Del Vecchio, 2002].

5.2.1 Force Calculations

As mentioned, the force density throughout the winding is determined through use of finite element analysis. For radial pressure, the radial stresses at each level are integrated to give the pressure at that level and the worst case is used for stress analysis. It should be noted that vector integration of all these force densities results in a total force of zero. Likewise, the axial force density at each level is integrated and the worst case is used for stress analysis. The axial forces are also summed, starting at the bottom of the coil and

their sum is a net upward or downward force that is countered by an equal and opposite force by the pressure ring. Depending on the direction of the force, the ring exerting this force will be the top or bottom ring. The gravitational forces are ignored compared to electromagnetic forces. Starting from bottom or top accordingly, sum of the forces is maximum at a point. This force is called the maximum compressive force and is a worst-case force used in the stress analysis. The sum of axial loads in all the windings should be zero [Del Vecchio, 2002].

The pressure rings are sized based on the net upward or downward axial force due to all the windings, called the total end thrust. If the windings are symmetric about a horizontal center plane, the total axial force on each winding is almost zero and no end thrust is present. However, when one or more windings are even slightly offset vertically from the others, net axial forces develop on each winding that push some windings up and some down. To take into account possible misalignment in the transformer's construction, it is a good practice to include some offset, say ¼ to ½ in, in the calculations [Del Vecchio, 2002].

5.2.2 Stress Analysis

Stresses should be calculated from the resulting forces. Due to the complexity of the structure of windings and the dissimilar materials used and the many openings for the cooling oil, suitable approximations should be made to simplify the complicated stress analysis.

In practice, the windings on different levels of the winding are connected to each other to maintain electrical continuity. However, the coil is assumed to have distinct horizontal sections that are closed on themselves forming rings [Del Vecchio, 2002].

Another approximation is made for the cables that comprise the windings. While magnet wires consist of a single strand of copper surrounded by paper covering and are treated almost without approximation, transposed cables consist of multiple enamel coated copper strands arranged in a nearly rectangular pattern. There is some rigidity in the collection of strands because of transpositions. In addition, bonded cable is often used in which all strands are bonded together by means of epoxy coating over the enamel that is subjected to a heat treatment. The cable can be treated as a rigid structure in this case, though there are questions on how to assess its material properties. Without bonding, the cable is assumed to have a radial thickness equivalent to 2 radial strands for radial force considerations. If there is bonding, a radial thickness equivalent to 80% of the actual radial thickness is assumed [Del Vecchio, 2002].

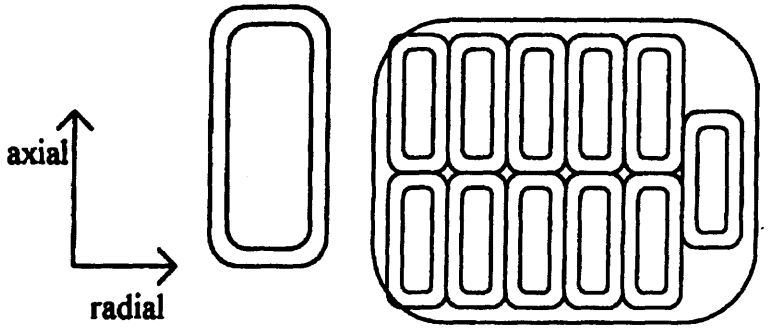

a) Magnet wire b) Transposed cable

Figure 5.11 Types of wire or cable used in transformer coils [Del Vecchio, 2002].

5.2.2.1 Compressive Stress in Key Spacers. The maximum axial compressive force F_c is used for the purpose of obtaining the key spacer compressive stress σ_{ks}, according to

$$\sigma_{ks} = \frac{F_c}{N_{ks} W_{ks} B} \tag{5.4}$$

where N_{ks} is the number of key spacers around the section, W_{ks} is the width of a key spacer, and B is the radial build of the coil. Key spacers with maximum compressive stresses as high as 310 MPA (45,000 psi) are used [Del Vecchio, 2002].

5.2.2.2 Axial Bending Stress per Strand. The maximum axial force F_a over the vertical subdivisions is calculated for each coil. The number of strands in the entire coil, N_s, is given by [Del Vecchio, 2002]

$$N_s = N_t N_h N_w N_{st} \tag{5.5}$$

where N_t is the number of turns/leg, N_h is the number of cables/turn high (radially), N_w is the number of cables/turn wide (axially), and N_{st} is the number of strands/cable. For the coils consisting of two separate center fed windings stacked axially with each of them having electrical turns, the winding is divided into N_p sections for this analysis, and the maximum force/unit length on a single strand, q_{st}, is given by

$$q_{st} = \frac{N_p F_a}{N_s \pi D_m} \tag{5.6}$$

where D_m is the average diameter of the coil.

This problem can be analyzed analogous to a uniformly loaded rectangular beam with built-in ends. The moment is calculated as [Del Vecchio, 2002]

$$M(x) = \frac{q}{2}[x(L-x) - \frac{L^2}{6}] \tag{5.7}$$

and the maximum stress will be

$$\sigma_{x,\max} = \frac{q}{2t}(\frac{L}{h})^2 \tag{5.8}$$

Introducing the actual load into this equation, the maximum axial bending stress can be calculated as

$$\sigma_{x,\max} = \frac{N_p F_a}{2N_s \pi D_m t}(\frac{L}{h})^2 \tag{5.9}$$

The span length, L, can be calculated as

$$L = \frac{\pi D_m}{N_{ks}} - W_{ks} \tag{5.10}$$

The strand height h and thickness t apply to a single strand, whether in a cable having many strands or as a single strand in a magnet wire. For bonded cables, the maximum axial bending stress is divided by 3 to take into account the greater rigidity of bonded cable [Del Vecchio, 2002].

5.2.2.3 Tilting Strength. If large enough, the axial compressive force that is applied to the key spacers can cause tilting in the individual strands of the conductors that are pressed between the key spacers

Considering a small section in the azimuthal direction of length $\Delta\ell$, the pressure exerts a torque, τ_c, given by [Del Vecchio, 2002]

$$\tau_c = P_c(t\Delta\ell)h\sin\theta \tag{5.11}$$

where t is the radial thickness of the strand and where $t\Delta\ell$ is the area on which the pressure P_c acts. The axial height of the strand is h and θ is the tilting angle from the vertical, assumed to be small. Due to tilting, the material of the ring will stretch above its axial center and compress below it. This produces stresses in the ring that cause the opposing torque. y being the distance above the axial center of the strand, it follows that

$$\sigma = E\varepsilon = \frac{Ey\tan\theta}{R} \tag{5.12}$$

$$F_r = \sigma(t\Delta y)\Delta\varphi = \sigma(t\Delta y)\frac{\Delta\ell}{R} \tag{5.13}$$

where E is the Young's modulus, and F_r is an inward force.

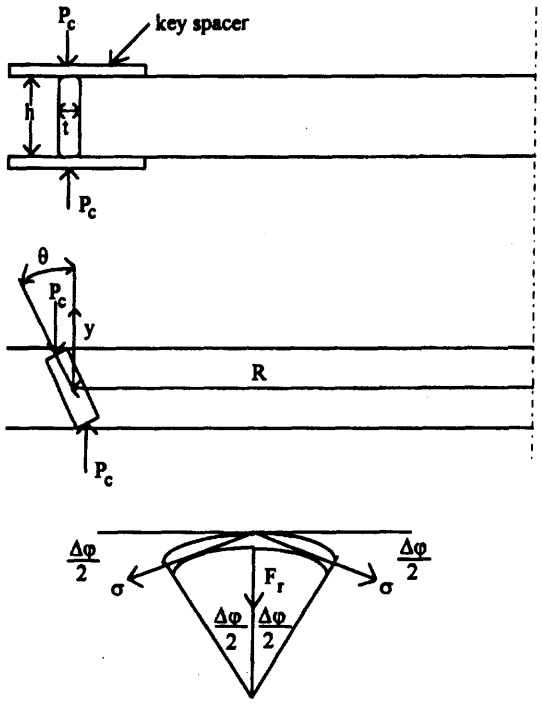

Figure 5.12 Geometry of strand tilting due to axial compressive force [Del Vecchio, 2002].

The resisting torque produced by this force can be calculated as

$$\Delta\tau = F_r y = \frac{\sigma t \Delta\ell y \Delta y}{R} = \frac{Et\Delta\ell \tan\theta y^{2\Delta y}}{R^2} \tag{5.14}$$

$$\tau = \frac{Et\Delta\ell \tan\theta h^3}{12R^2} \tag{5.15}$$

Equating this counter torque with the applied torque and assuming small θ, we get

$$P_c = \frac{E}{12}(\frac{h}{R})^2 \tag{5.16}$$

When the conductor strand has squared ends, there is an additional resistance to tilting because of the ends digging into the key spacers or paper. This results in a tilting pressure of

$$P_c = \frac{E}{12}(\frac{h}{R})^2 + C\frac{N_{ks}W_{ks}t^2}{6h^2(2\pi R)} \tag{5.17}$$

For a strand with rounded corners of radius R_c, t in the above formula is reduced by $2R_c$ so that only its flat portion is considered. The resulting critical axial pressure is therefore

$$P_c = \frac{E}{12}(\frac{h}{R})^2 + C\frac{N_{ks}W_{ks}}{6(2\pi R)}(\frac{t-2R_c}{h})^2 \tag{5.18}$$

C in the above formula is a constant depending on the spacer material. A value of $C = 6.21\times10^4 MPA\ (9\times10^6\ psi)$ can be used here.

To compare this with the applied maximum axial compressive force, this stress is multiplied by the radial surface area of the strands in one horizontal layer, A_{layer}, that is

$$A_{layer} = \pi D_m t N_d N_h(\frac{N_{st}-1}{2}) \tag{5.19}$$

where N_d is the number of turns in a disk. The term $(\frac{N_{st}-1}{2})$ yields the number of radial strands that are part of the double layer. For magnet wire, the expression in parentheses is assumed to be 1. Hence, the critical axial force for unbonded cable is

$$F_{cr} = P_c A_{layer} \tag{5.20}$$

For bonded cable, it is assumed that tilting cannot happen. For a viable design, we should have $F_{cr}/F_c > 1$.

In the above process, it was assumed that the compressive force was applied uniformly around the strand ring, whereas in reality it is only applied to the portions of the ring that are in contact with the key spacers. Therefore, the uniformly applied pressure represents an averaging process over the entire ring that is a reasonable approximation [Del Vecchio, 2002].

5.2.2.4 Stress in Tie-Plates. The tie-bars or tie-plates are used to join the upper and lower clamping structures that keep the coils under compression. These are generally long rectangular bars of steel placed along both sides of the core legs. Tie-plates are under mild tension during normal transformer operation. However, the tensile stresses can increase considerably during short circuit. Also, the tie bars support the entire weight of the coils and core when the transformer is lifted [Del Vecchio, 2002].

The short circuit stress in the tie bars is a result of the total end thrust produced by all the coils. This is the sum of all the upward or downward forces acting on the coils and is an output of the force calculation program. Since this output refers to a single leg, the tie bars carrying this force should only be the ones associated with a single leg. If there is a three-phase fault, all the bars are affected equally. However, if there is a single line to ground fault where the forces are much higher on one leg than the other two, the tie bars along the leg having the greater force will probably sustain the greatest stress. Therefore, as a worst-case scenario, it is assumed that the legs act independently at least for the short duration of the fault [Del Vecchio, 2002].

The total end thrust is calculated from a static force analysis. To account for the dynamic effects, enhancement factors are used based on numerical studies. A force of 1.8 times the end thrust is used if it is larger than 0.8 times the maximum compressive force over all the windings. Else, 0.8 times the maximum compressive force over all the windings is used. However, because the tie bars must support the weight of the core and coils during lifting, the stresses produced in tie bars by lifting are checked. During lifting, it is assumed that only the tie bars go under stress that are associated with the outer legs where the lifting hooks are positioned. Both the short circuit dynamic stresses and the lifting stresses must be within the allowable stress limit. The maximum allowable stress is taken to be 620 MPA (60,000 psi) if a stainless steel used for the tie bar material [Del Vecchio, 2002].

5.2.2.5 Stress in Pressure Rings. The total end thrust of the windings is received by the pressure rings. These ring covers the radial build of the windings with a little overhang. During a fault, it must support the entire dynamic end thrust of the windings, which is the larger of 1.8 times the end thrust and 0.8 times the maximum compressive force in all the windings. The ring is supported on radial blocks and space is provided in between for the leads. Hence, there is an unsupported span of a certain length L_u. This is analogous to the axial bending of a strand discussed before and the same equations can be used with $L = L_u$, $t = 0.5(D_{ring,out} - D_{ring,in})$ the radial build of the ring, $h = h_{ring}$ the ring's thickness, and $q = P_{ring} t$ the force/unit length along the unsupported span. Hence

$$\sigma_{x,\max} = \frac{P_{ring}}{2}\left(\frac{L_u}{h_{ring}}\right)^2 = \frac{F_{ring}}{2A_{ring}}\left(\frac{L_u}{h_{ring}}\right)^2 \tag{5.21}$$

$$F_{ring,\max} = \sigma_{bend}(\pi/2)(D^2_{ring,out} - D^2_{ring,in})(\frac{h_{ring}}{L_u})^2 \tag{5.22}$$

For pressboard, $\sigma_{x,\max} = 103MPA$ (15,000 psi) is a reasonable maximum allowable bending stress [Del Vecchio, 2002].

5.2.2.6 Hoop Stress. The radial pressure acting on the winding creates a hoop stress in the winding conductor. The hoop stress can be tensile or compressive, depending on whether the pressure acts radially outward or inward respectively. The winding will be treated as an ideal cylinder or ring under radial pressure P_r. R_m being the mean radius of the cylinder, H its axial height, and B the radial dimension of the cylinder, it can be shown that

$$\sigma_{hoop} = \frac{F}{A} = \frac{P_r HR_m}{A} = \frac{P_r R_m}{B} \tag{5.23}$$

In this formula, it is assumed that the winding is built of homogeneous material. Since this force is primarily supported by the conductor, A should equal the cross sectional area of all the conductors in the winding that is $A = A_t N_t$, where A_t is the cross-sectional area of a turn and N_t is the total number of turns in the winding. This stress shall not exceed the proof stress of the winding material [Del Vecchio, 2002].

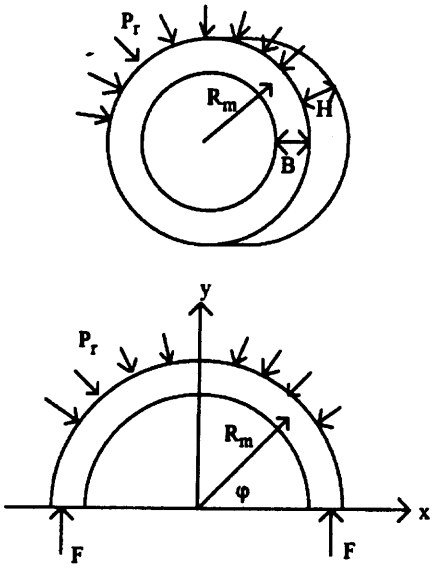

Figure 5.13 Geometry for determining the hoop stress in a cylinder acted on by a radially inward pressure [Del Vecchio, 2002].

When the radial pressure acts inward, the winding may buckle before reaching its proof stress. It has been suggested based on limited experimental test that this compressive stress not exceed some fraction of the proof stress, varying from 0.4 to 0.7 depending on the type of cable used and whether it is bonded [Del Vecchio, 2002].

The hoop stress is an average over the disk. However, in reality, the axial magnetic field varies from nearly zero on the inside of the winding to close to its maximum value at the outer radius of the winding for the innermost winding. Because of uniformity of the current density, the force density also varies in the same fashion as the magnetic field. Thus, it is reasonable to expect higher hoop stresses in the outermost turns as compared with the inner turns. Nonetheless, because of the layered structure with paper insulation between turns, the stress tends to be shared more equally by all the turns [Del Vecchio, 2002].

5.2.2.7 Radial Bending Stress. There are inner radial supports for windings such as sticks made of pressboard, which are spaced uniformly along their circumference and extend the height of the winding. In presence of an inward radial pressure acting on the winding, the sections of the winding between supports act like a curved beam subjected to a uniform load. This is similar to the case of a rotating flywheel with radial spokes that has been analyzed by Timoshenko. Performing an extensive parallel analysis results in

$$\sigma_{\max} = \sigma_{hoop}\left[\left(\frac{\cos\alpha}{2\sin\alpha}+\frac{3R}{h}(\cos\alpha-\frac{\sin\alpha}{a})(\frac{1}{\sin\alpha})\right)\left(f_1(\alpha)+12(\frac{R}{h})^2 f_2(\alpha)+\frac{EA}{E_{eq}A_{stick}}\right)^{-1}-1\right] \quad (5.24)$$

where

$$f_1(\alpha)=\frac{1}{4\sin^2\alpha}(\alpha+\frac{\sin 2\alpha}{2}) \quad (5.25)$$

$$f_2(\alpha)=\frac{1}{4\sin^2\alpha}(\alpha+\frac{\sin 2\alpha}{2})-\frac{1}{2\alpha} \quad (5.26)$$

$$E_{eq}=\frac{L}{\frac{L_w}{E_w}+\frac{L_s}{E_s}+\frac{L_c}{E_c}} \quad (5.27)$$

α is half the angle between the consecutive supports, L_w is the length of the winding portion and E_w its Young's modulus, and the subtitles s and c referring to stick and core parameters. $L = L_w + L_s + L_c$. The innermost winding is not part of the supporting system [Del Vecchio, 2002].

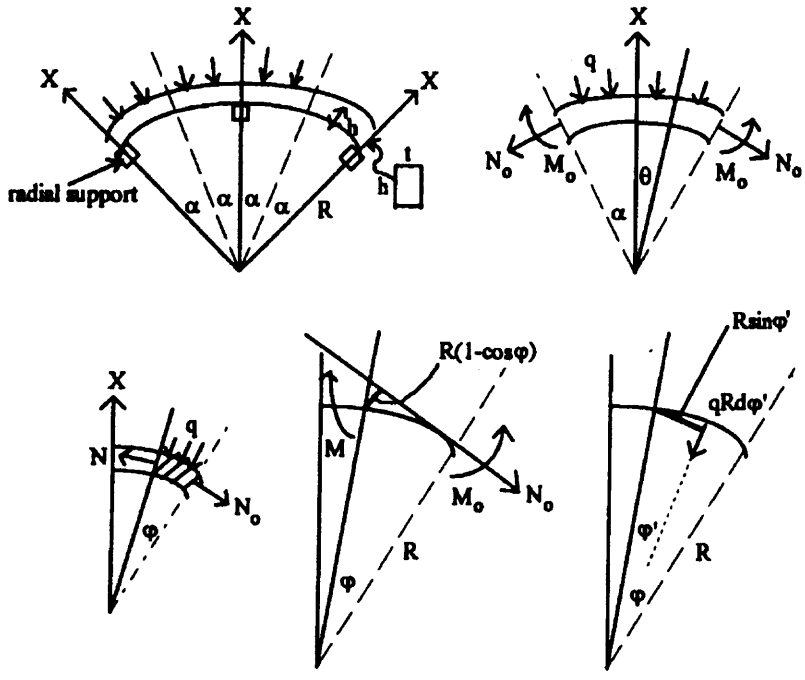

Figure 5.14 Geometry for determining the radial bending stresses [Del Vecchio, 2002].

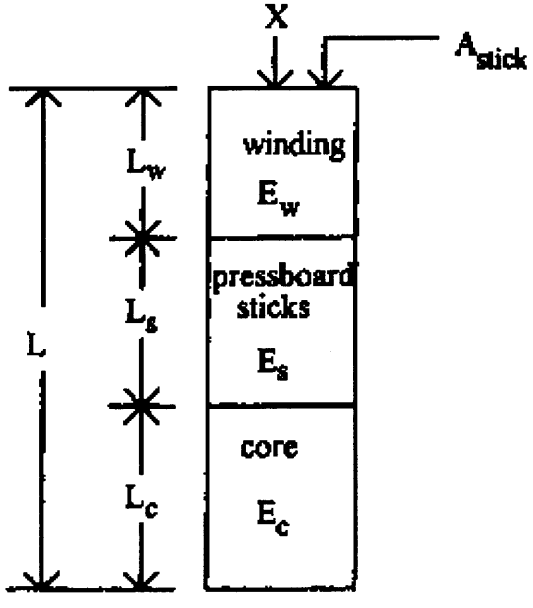

Figure 5.15 Radial support structure [Del Vecchio, 2002].

This stress is negative and occurs at the support. These analyses consider a ring that is under a hoop stress. A coil is usually not a monolithic structure, but consists of a number of cables distributed radially. The paper insulation tends to equalize the average hoop stress in the winding in all the cables. The radial thickness h refers to a single cable. For a magnet wire, the radial thickness should be used. In multi-stranded transposed cables, a number less than the radial thickness should be used due to its non-homogeneousness. For unbonded cables, twice the thickness of an individual strand is used as the effective radial build. If bonded, this value will be 80% of the actual radial thickness [Del Vecchio, 2002].

5.2.3 Radial Buckling Strength

To study the possible buckling of a winding under an inward radial pressure, an individual cable is treated as a closed loop like before, since the cables are not bonded to each other [Del Vecchio, 2002]. In a free buckling analysis, the inner supports can be ignored due to the argument that they are loose enough to have no effect on the onset of the buckling. These effects could be taken into account after the onset of buckling in a forced or constrained buckling analysis. For free buckling

$$q_{crit} = \frac{3EI}{R^3} \tag{5.28}$$

$$\sigma_{crit} = \frac{qR}{A} = \frac{3EI}{AR^2} = \frac{1}{4}E\left(\frac{h}{R}\right)^2 \tag{5.29}$$

Therefore, the critical hoop stress is only geometrically dependent on the ratio of the radial build to the radius of the ring. The tangent modulus should be used in these equations.

When the supports (sticks) are engaged in the buckling process, there is forced or constrained buckling. Because of some looseness in the supports due to the building tolerance, it is regarded as a hinged type of attachment for calculation purposes. The lowest-order buckling mode for this case is shown. The corresponding critical force/unit length, q_{crit}, is

$$q_{crit} = \frac{3EI}{R^3}[(\frac{2\pi}{\beta})^2 - 1] \tag{5.30}$$

where β is the angle between the supports. Hence, the critical hoop stress is

$$\sigma_{crit} = \frac{E_t}{12}\left(\frac{h}{R}\right)^2\left[\left(\frac{2\pi}{\beta}\right)^2 - 1\right] \tag{5.31}$$

where h is the radial build of the arch. This will exceed the free buckling critical stress if $\beta \leq \pi$, i.e. for only two diametrical supports. However, usually $\beta << \pi$, and the constrained buckling stress will be much larger than the free buckling stress. B is taken as the angle between three consecutive inner supports. Arched buckling with this value seems to yield a more realistic value of buckling strength in practice compared to the totally free unsupported buckling [Del Vecchio, 2002].

5.2.4 Points About the Mechanical Design

During a short circuit, the higher fault current in the leads and busbars interact with the higher leakage flux from the main windings and from nearby leads. Hence, the leads

must be braced to prevent deformation or large movement during a fault. Although these extra forces could be determined through finite element analysis, past experience has shown that braces usually have sufficient margin so that the extensive analysis will be necessary only for unusual or novel designs [Del Vecchio, 2002].

The weight was neglected except for design of the tie bars. These forces affect the compressive force on the key spacers and the downward end thrust acting on the bottom pressure ring. Similarly, the pre-stressing axial force applying stress in key spacers, the top and bottom thrust on the pressure rings, and the tension in tie bars should be considered. The change in compressive forces acting on the key spacers will also affect the design against conductor tilting [Del Vecchio, 2002].

In addition, the axial and radial stress calculations were done separately whereas in reality there is biaxial stress condition. The combination of the two stresses is what has to be checked at each point along the winding to account for the worst-case situation. However, as long as the materials remain linear, the approach to look at the worst case stresses caused by axial and radial forces separately and apply a failure criterion to each is probably a good approximation to the reality, particularly because the worst case axial and radial forces typically occur at different places along the winding. The radial forces are a result of axial flux that is high in the middle of the winding while the axial forces are produced by radial flux that is high at the ends of the winding [Del Vecchio, 2002].

Some studies on dynamic axial response of the windings subjected to a sudden application of short current found that the prestress level is important. For low levels of prestress, namely about 10% of the normal value, the winding literally bounced against the upper support, resulting in a force much higher than expected. The amplification over

the static maximum force was about 4. However, for normal prestress, there was no amplification over the expected maximum force. If sufficient prestress is applied to clamp the windings in axial direction, there should be little or no amplification of the end thrust over the value determined from static analysis of maximum fault currents. Nonetheless, an amplification factor of 1.8 in used in design [Del Vecchio, 2002].

5.3 Behavior of Internal Components Under Earthquakes

5.3.1 Possible Failure Modes of Internal Components

The internal components of transformer are mechanically designed to withstand substantial forces caused by fault currents. These forces include radial forces applied to the inner and outer windings and axial forces applied to the windings. Combination of these forces can have different effects like radial stress in windings, radial forces on sticks, buckling of windings under radial stress, compressive stresses in key spacers, bending of strands under axial force, axial stresses in tie bars and pressure rings, and tilting (in a plane normal to winding) of strands under axial key spacer pressure and deformation or movement of leads. The internal components are designed to withstand these forces that give them a considerable resistance. Hence, the internal components are expected to show a good behavior in resisting the earthquake excitations and transferring the loads to their core and avoiding structural damage.

However, the ability of transformers to function depends on keeping the insulation of different parts of the system with substantial difference in electric potential intact. Any damage to the insulation system or anything that causes different components to get closer than their design values produces the possibility of electrical discharge that

results in malfunctioning of the transformer with immediate or long-term implications. Based on study of the structure and design of internal components, site visits to inspect opened transformers, and discussions with technical staff of Southern California Edison along with limited information from past performance under earthquakes, the following probable failure modes are identified:

- Sliding of key spacers
- Movement or separation of leads
- Decrease or loss of safe clearance between layers of conductors due to seismic excitations
- Loss of close fitting tolerances between limbs and yokes causing long-term electrical loss

Each of these possible failure modes is explained below.

5.3.1.1 Sliding of Key Spacers. The following picture, taken during a site visit to Southern California Edison, shows key spacers between different layers of windings. Note that in this case spacer consists of a stack of thin pressboards.

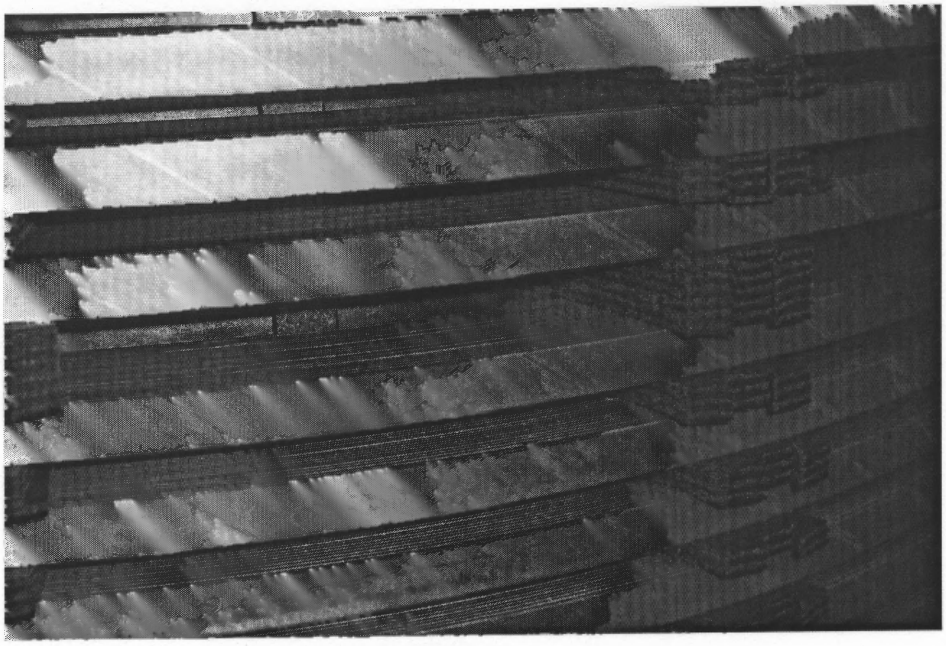

Figure 5.16 Key spacers separating different layers of winding.

Under normal situation, the key spacers are under compressive pressure due to axial pre-stressing of the winding plus weight of the windings. However, ground motion and oil circulation can cause these spacers to slide. That is, vertical excitations can relieve the normal compressive force. Subsequently, two factors, namely the oil circulation between layers of winding and horizontal excitations caused by the earthquake can result in sliding of the key spacers. The oil used inside transformers has two functions, insulation and cooling. Convection is a source of movement of the oil inside the tank. In large transformers pumping of the oil through transformer might accelerate oil circulation. Hence, it is reasonable to assume that when pre-stressing is relieved, oil movement and/or horizontal vibrations can cause the key spacers to slide.

Loss of key spacers under the above scenario will result in lower spacing between vertically stacked layers of conductors. Closeness or perhaps even attachment of

windings from different layers, which have different electric potentials, will interrupt the insulation design and can cause electric discharge.

Sliding of key spacers is the most probable and critical failure mode of transformer internal elements under earthquakes. It will be the main thrust of this study. A simplified model is developed that will be used to determine the level of forces that can result in loss of prestressing. Linear models are employed to determine the level of ground accelerations that can cause total prestressing loss. In light of scarceness of data on transformer designs and the fact that transformer design is very case specific, there is not enough knowledge on the exact amount of prestressing force and exact geometry of the internal components. However, reasonable assumptions based on technical data gathered from different sources are made. Using the analytical model, the behavior for different geometric configurations, material properties and earthquake inputs is calculated and is used to assess the probability of failure under earthquake and also evaluate the effectiveness of base isolation as a rehab scheme.

Similar to static design of the tie plates, only one limb will be modeled. Due to rigidity of the top and bottom clamps it is reasonable to assume that the limbs behave independently. Since there are tie plates on both sides of each limb, the resisting vertical element for each limb will be its tie plates. The winding and key spacers will be simplified into a few alternate segments with the same properties as the winding and the key spacers. There are also two elements representing top and bottom wooden isolation (pressure rings and wooden blockings) and an element representing the vertical spacers, extending between the pressure rings. Thus, the system will be idealized as shown in Figure 5.17.

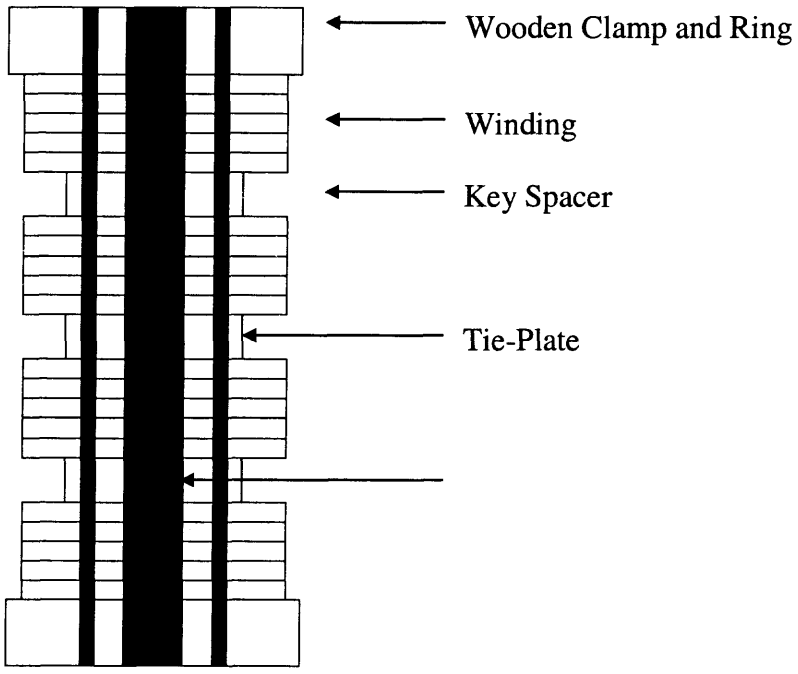

Figure 5.17 The model of internal components used for analysis.

5.3.1.2 Movement or Separation of Leads. Leads coming from different parts of windings each have their own electric potential. They have differences in potential with all the other elements, and with the steel clamps and the tank that are of ground potential. Hence, they are well insulated and designed in a way to keep sufficient distance from all these other elements. To hold them in place, they are attached to a wooden frame built around the coil clamps. This frame is designed to carry their weight and the loads applied to them during fault currents [Del Vecchio, 2002]. If the connections of leads and the frame are compromised in any way resulting in their movement, the insulation design of the system could be jeopardized. Displacement of the wooden frame relative to the core can happen under seismic excitation due to differences in their frequencies. The core is a

relatively stiff structure. The wooden frame, however, is much less stiff and may tend to have excessive displacement, thus, pulling the leads and applying an extra force on the connections.

The following picture shows the leads and their supporting wooden structure.

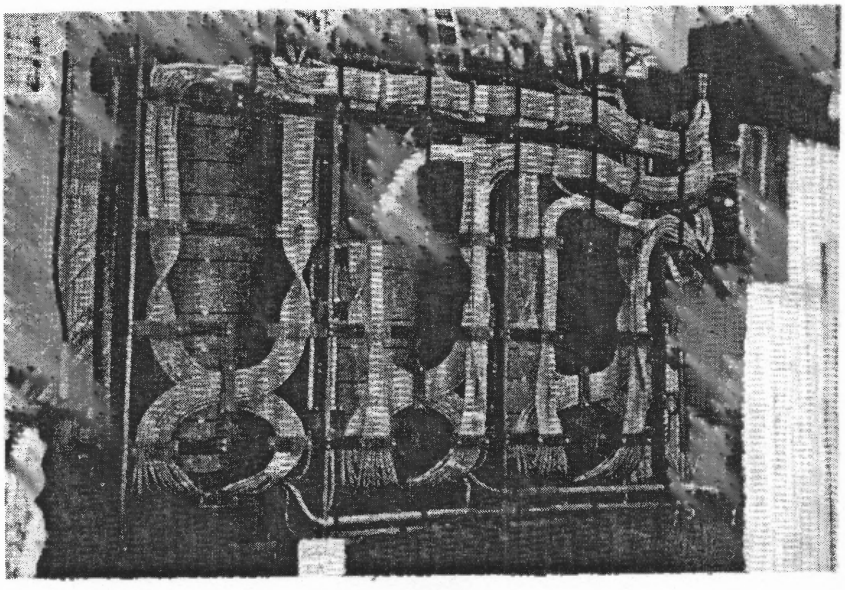

Figure 5.18 The wooden frame designed to support the leads [Del Vecchio, 2002].

Design of the wooden frames and their connections to the leads is very case specific and depends on various components of the system ranging from its size to its structure and its voltage. For this reason and the fact that designers can easily develop a remedy, no further work on this possible mode of failure is envisioned under this study.

5.3.1.3 Decrease or Loss of Safe Clearance between Layers of Conductors Due to Seismic Excitations. Windings at each level form a horizontal plane supported by key spacers where the distance/clearance between two layers is equal to the height of the key

spacers. This clearance can be momentarily reduced due to vertical vibration of the layers of winding behaving as simply supported beams spanning between any two key spacers.

However, for two reasons it is not expected that this mode of possible damage is important. First of all, the winding has the same properties in different layers, except for small differences in the axial and radial electromagnetic forces applied to the winding. Therefore, it can be expected that all windings go through more or less the same response due to seismic excitation, thus, resulting in no relative displacement. The second and more important reason is that unlike the previous cases, even if loss of clearance happens, it is a momentary phenomenon that vanishes after ground motion ceases. It should be noted that the resistance of the insulation system to an electric potential difference is both a function of the magnitude of the potential difference and its duration. Hence, the same insulation that is sufficient for a stationary potential field will also be adequate under a higher potential difference in small fractions of time [Del Vecchio, 2002]. Therefore, it can be expected that the probability of any adverse effect under this situation is non-existent or quite minimal.

5.3.1.4 Loss of Close Fitting Tolerances Between Limbs and Yokes Causing Long-Term Electrical Loss. With advance of time, the efficiency of the transformers has increased dramatically. One of the major sources of loss is the core of the transformer. Grain-oriented core steel has been used to increase the electrical efficiency of core. Any factor that requires the flux to deviate from the grain direction will increase the core loss. With modern steels having a very high degree of grain orientation, the loss penalty for such deviation is higher than ever making manufacturers to go through pains to design cores with minimum discontinuity and change of the direction. The most common

approach in power transformers is to use mitered corners at the connection of yokes and limbs. This is to limit the extent to which the flux path cuts across of the grain direction at the intersection. The core plates at these mitered corners must be overlapped so that the flux can transfer to the adjacent face rather than cross the air gap which is directly in its path. The fitting should be done to a very close tolerance of order of 0.5 mm to insure the efficiency [Heathcote, 1998].

Because no bolts are used in the joint due to the efficiency considerations, the integrity of core is maintained through the clamps. The top clamps contain the top yoke while the tie-plates connecting the top and bottom clamp apply prestressing force to the core and coil [Heathcote, 1998]. During earthquake, it is possible that the prestressing in the core is temporarily lost. Such loss could results in loss of the close fitting clearance at the yoke-limb joint, hence decreasing the long-term efficiency of transformer. Also, oil might penetrate through these momentary gaps, seriously impeding the electrical functioning of the core. Hence loss of prestressing can be regarded as the critical criteria for this mode of damage. The same model used for studying the axial forces in windings will be used to study this failure mode as well.

5.3.2 The Analytical Model

Finding detailed information on mechanical design and properties of internal elements of a transformer is very hard and challenging. However, different pieces of information gathered from multiple sources have been used to make reasonable assumption about these properties. The details of how different geometric and mechanical properties are selected are given before

5.3.2.1 The Geometric and Mechanical Details. The geometric dimensions of the model are chosen from data from several sources mentioned in the text and a site visit to Southern California Edison. The actual dimensions of the components do not have any real effect on the response and it is just the relative dimension of different parts that is important. Two configurations for the cross section of the system and two configurations for its vertical dimensions are chosen. All the geometric ratios selected are based on study of several pictures in different sources or pictures taken from the visit to Southern California Edison. Figure 5.19 shows the dimension of a cross section. A ratio of 1.5 to 1.8 between the outer radius of windings and the radius of the core is proper.

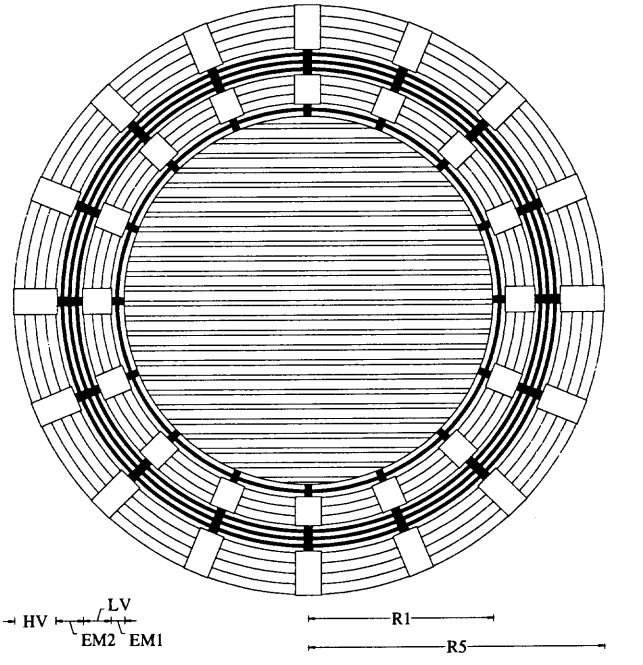

Figure 5.19 Dimensions of a cross-section of the model.

Horizontal Configuration 1:

$$R_5 = 15in$$

$$R_5/R_1 = 1.6$$

$$LV/D = 0.25$$

$$HV/D = 0.375$$

$$EM_1/D = 0.125$$

$$EM_2/D = 0.25$$

Horizontal Configuration 2:

$$R_5 = 15in$$

$$R_5/R_1 = 1.8$$

$$LV/D = 0.25$$

$$HV/D = 0.375$$

$$EM_1/D = 0.125$$

$$EM_2/D = 0.25$$

The ratio of area of key spacers over the winding is assumed to be 24% for the outer winding and 31% and 33% for inner winding of configuration 1 and 2 respectively. The vertical spacers in both configurations are assumed to occupy 25% of the empty area between the windings themselves, and between the windings and the core. In a few cases, the effective area of windings for calculation of stiffness is taken to be equal to that of spacers based on the assumption that not much stress is distributed in it.

For calculating the vertical dimensions, use is made of a reference to a ratio of 40% for the height of the cellulosic material to the height of the winding [Prevost, 2003]. This consists of the wooden pressure rings, blockings, and key spacers. This ratio is used for the vertical configuration 1. The ratio used for vertical configuration 2 is 30%. In both cases, this amount is divided equally between pressure rings and blockings on one hand, and key spacers on the other hand. The height of pressure rings and blockings are also assumed to be equal. However, because the area of blockings is about half of that of the pressure rings, they are both combined into an element having an area equal to 75% of the area of windings. The winding is modeled by four elements between which there are three elements of key spacers. The numerical values of the vertical configurations are as follows:

Vertical Configuration 1:

$Height = 45in$

$Ring = 9in$

$Spacer = 9in$

$Winding = 27in$

Vertical Configuration 2:

$Height = 60in$

$Ring = 9in$

$Spacer = 9in$

$Winding = 42in$

5.3.2.2 The Mechanical Properties of Material. The core consists of Cold Rolled Grain Oriented Silicon Steel (CRGO). The density of this material is $\rho = 7650\,{}^{Kg}/_{m^3} = 477.146\,{}^{lb}/_{ft^3}$ [KRYFS Laminations, 2003] and it has $E = 29000ksi$. The steel for tie-plates has very close properties with the same module of elasticity and a density of $\rho = 7874\,{}^{Kg}/_{m^3} = 491.117\,{}^{lb}/_{ft^3}$.

The winding itself is made of copper (or aluminum in some cases) and Kraft paper wrapped around it. Based on figures of the winding wires [Prevost, 2003], it is assumed that 12/14 of the height of wire consists of wire while the rest is made of Kraft paper. Having $\rho = 8920\,{}^{Kg}/_{m^3} = 556.358\,{}^{lb}/_{ft^3}$ and $E = 18831ksi$ for copper, and $\rho = 1225\,{}^{Kg}/_{m^3} = 76.296\,{}^{lb}/_{ft^3}$ and $E = 1448.6ksi$ for Kraft paper [Gilani, 1999(a)], the equivalent properties of windings are calculated as $\rho = 7820\,{}^{Kg}/_{m^3} = 487.778\,{}^{lb}/_{ft^3}$ and $E = 16348ksi$.

For properties of pressboard, the data from business material data sheets are used [The Gund Company, 2003]. The pressboard type TX is appropriate for use in pressure rings and blockings. For vertical spacers, the HI-LAM pressboard is used. These material respectively have $\rho = 1270\,{}^{Kg}/_{m^3} = 79.212\,{}^{lb}/_{ft^3}$ and $\rho = 970\,{}^{Kg}/_{m^3} = 60.501\,{}^{lb}/_{ft^3}$, and $E = 1600ksi$ and $E = 500ksi$.

The obtained data suggest a wider range of properties for key spacers. It is suggested that pressboard type 994 be used for key spacers with

$\rho = 1150\,{}^{Kg}/_{m^3} = 71.728\,{}^{lb}/_{ft^3}$ and $E = 72.43ksi$ [Dupont, 2002]. However, since it is probable that more stiff material is also used, some analyses with two other sets of properties for key spacers were done as well. In one case, the key spacers are assumed to have the same properties as pressboard TX [The Gund Company, 2003]. In the second set, the intermediate values of $\rho = 1270\,{}^{Kg}/_{m^3} = 79.212\,{}^{lb}/_{ft^3}$ and $E = 200ksi$ are used and it is designated as pressboard type TXX.

5.3.3 The Results

The model for internal components was put under vertical excitations. These excitations include the vertical components of El Centro plus vertical excitations obtained from analyses of primary-secondary systems on FPS. It will be seen that there was no need to use a more extensive collection of earthquake records. All forces including the weight of elements and any prestressing force are excluded from the model and can be added later. Therefore, the results obtained purely show the effect of earthquake. The maximum tensile forces produced in elements in each case are extracted from the results.

Table 5.1 shows the earthquake inputs used. Table 5.2 shows the details of the properties of model and earthquake excitation used for these analyses.

Table 5.1 Characteristics of the Acceleration Time-Histories Used for the Analyses

Case	Input Acceleration	PGA (g)
1	El Centro 05/19/40	0.8
2	Response to Case 1 of isolated Primary system with f = 14 Hz, bearing secondary system with f =10 Hz, R = 60 in	0.8586
3	Response to Case 1 of isolated Primary system with f = 8 Hz, bearing secondary system with f=8 Hz, R=60 in	0.8518
4	Response to Case 1 of isolated Primary system with f = 8 Hz, bearing secondary system with f = 11 Hz, R = 60 in	0.8481
5	Response to Case 1 of isolated Primary system with f =11.7 Hz, bearing secondary system with f = 7 Hz, R = 60 in	0.8816

Table 5.2 Specifications of the Models Used for Each Analysis

Case	Horizontal Configuration	Vertical Configuration	Key Spacer Material	Input Acceleration
1	1	1	994	1
2	1,LA	1	994	1
3	1	1	TX	1
4	1,LA	1	TX	1
5	1	1	TXX	1
6	1,LA	1	TXX	1
7	2	1	994	1
8	2,LA	1	994	1
9	1	2	994	1
10	1	1	994	2
11	1	1	994	3
12	1	1	994	4
13	1	1	994	5

Figure 5.20 shows the maximum tensile force in the internal elements due to earthquake.

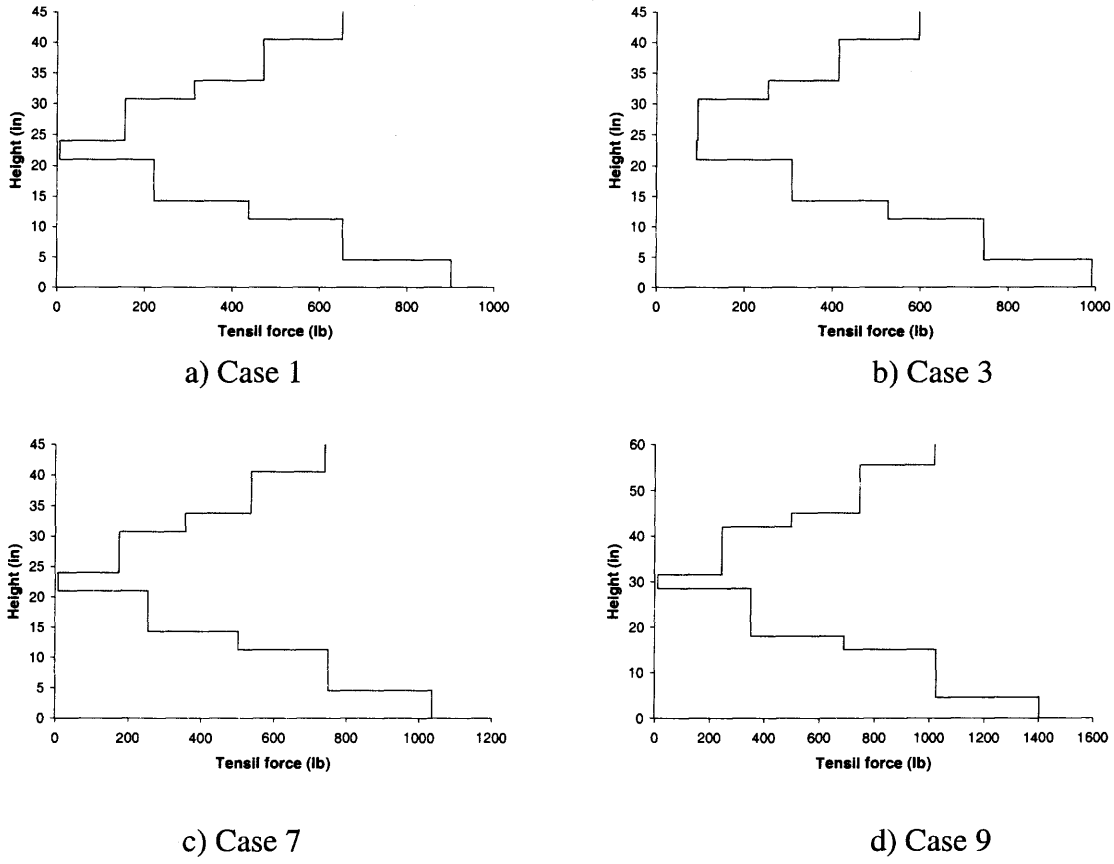

a) Case 1

b) Case 3

c) Case 7

d) Case 9

Figure 5.20 Maximum tensile force in coil due to earthquake.

Figure 5.21 shows the same result when the weight is added to these forces.

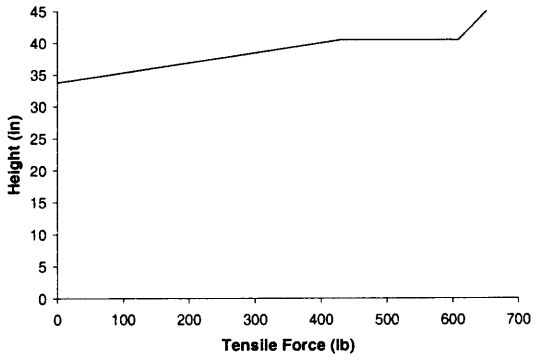

a) Case 1

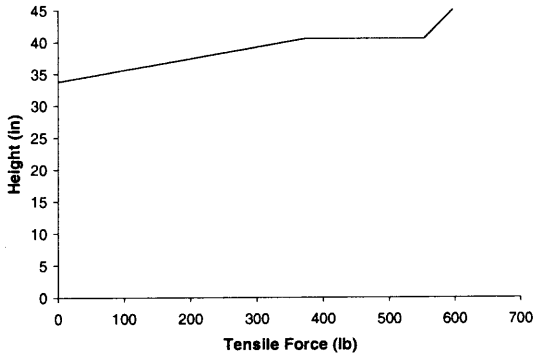

b) Case 3

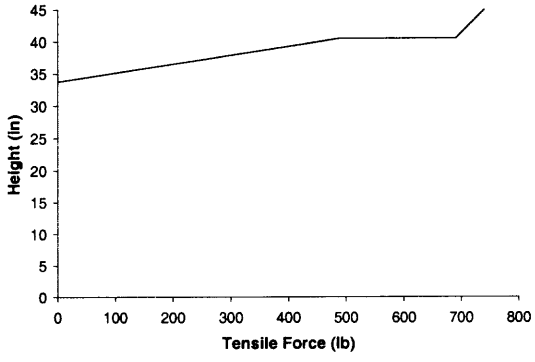

c) Case 7

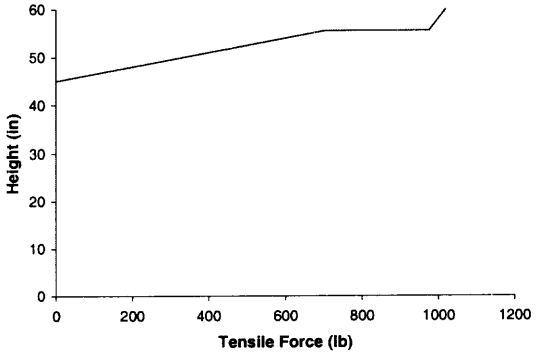

d) Case 9

Figure 5.21 Maximum tensile force in coil due to earthquake and weight.

Figure 5.22 shows the maximum tensile force in the internal elements as a percentile of weight due to earthquake.

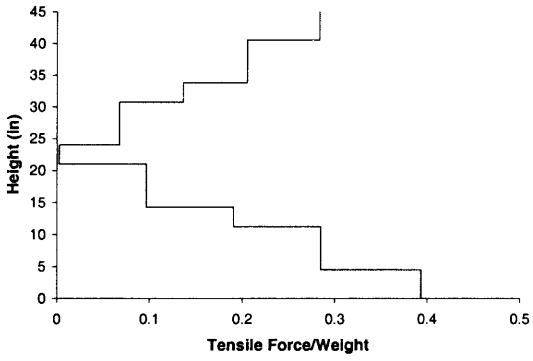

a) Case 1

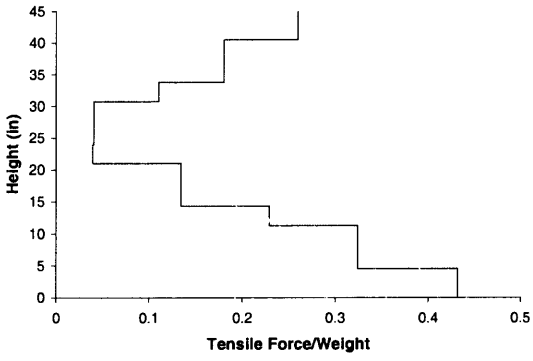

b) Case 3

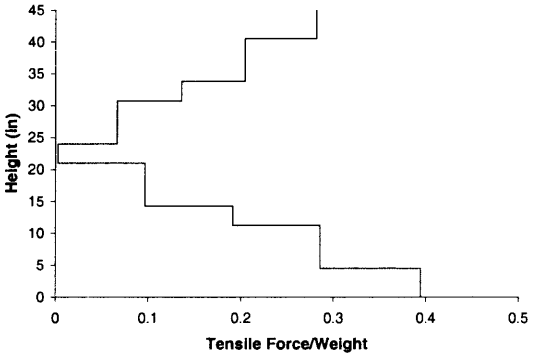

c) Case 7

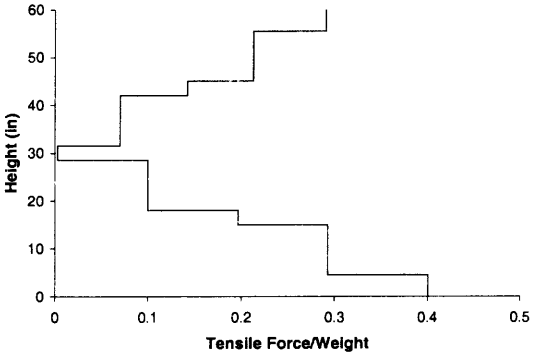

d) Case 9

Figure 5.22 Maximum tensile force in coil due to earthquake as a percentage of weight.

Figure 5.23 shows the same results when the weight is added to the forces.

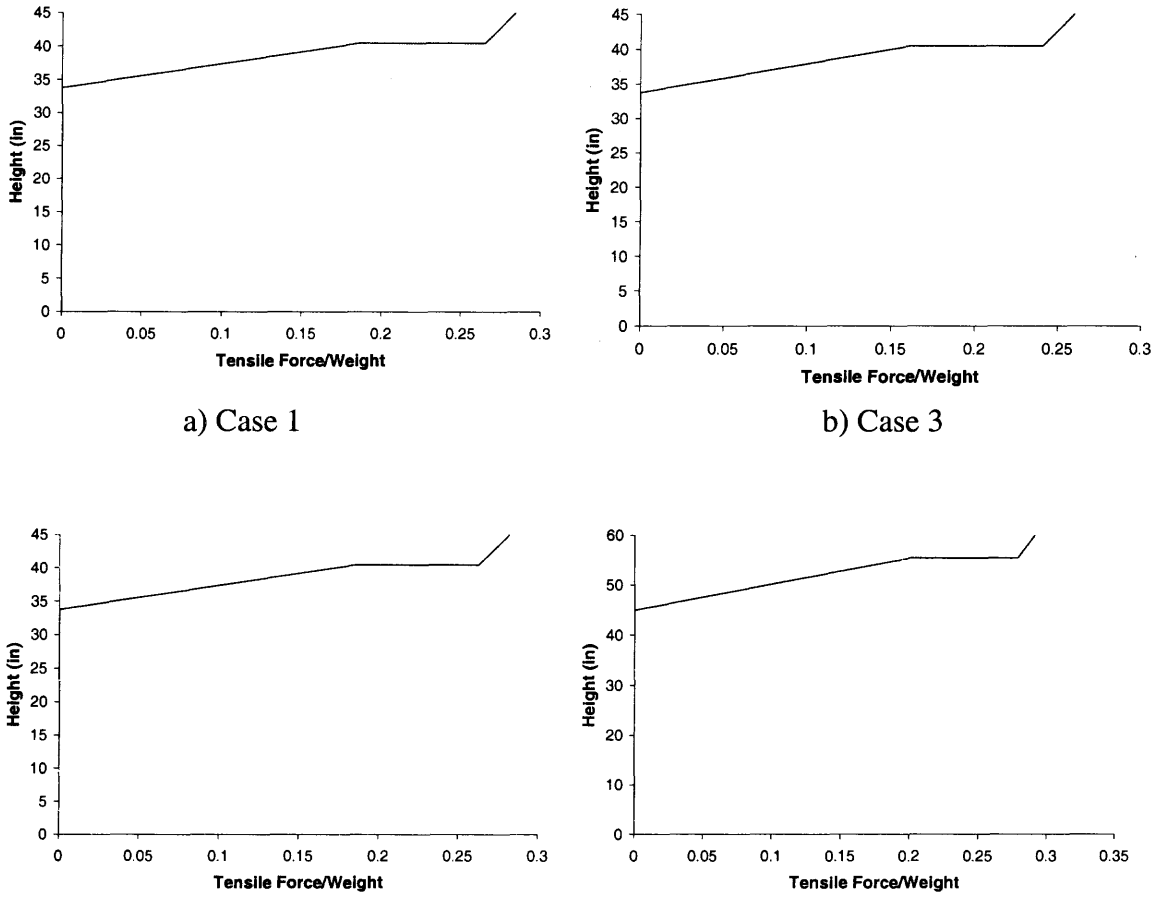

Figure 5.23 Maximum tensile force in coil due to earthquake and weight as a percentage of weight.

The results show a very low sensitivity to the changes in horizontal and vertical configuration of the system. Also, different properties for the key spacers have not had much of an effect on the internal tensile forces. This is due to immense rigidity of the system in vertical direction. In particular, the presence of a big rigid core in the center gives very high frequency to the system. For example, the first vertical frequency for case

1 is 176Hz (142 Hz for case 9). Hence, response of the system is always in the very rigid side of spectrum, making changes in geometric and mechanical properties almost immaterial. Considering the effect of weight, most of the height of the winding is free from any tensile force during the earthquake, which means there is no possibility of slipping of the key spacers in this region. The maximum net tensile force will be about 30% of the weight of internal elements minus the weight of core and tie-plates. This is a modest force that can be provided through prestressing.

Figure 5.24 shows the same results for an earthquake input equal to the vertical acceleration response of a primary-secondary system on FPS. The input is chosen from analyses of four different models with different primary and secondary system properties. The responses are all close, so the one set of results shown can be representative of the response of isolated internal elements in general. These responses are slightly higher compared to the fixed case. This is due to the fact that FPS is primarily a horizontal isolation mechanism, not a vertical one. It is only when the slider in FPS is sliding enough that some effects on vertical direction can be observed; and these effects are not necessarily positive.

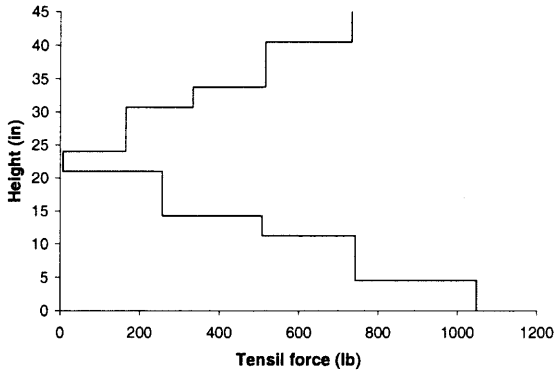

a) Tensile force excluding weight

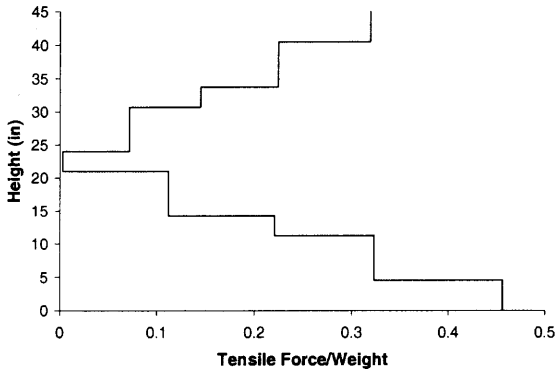

b) Tensile force excluding weight as a percentage of coil weight

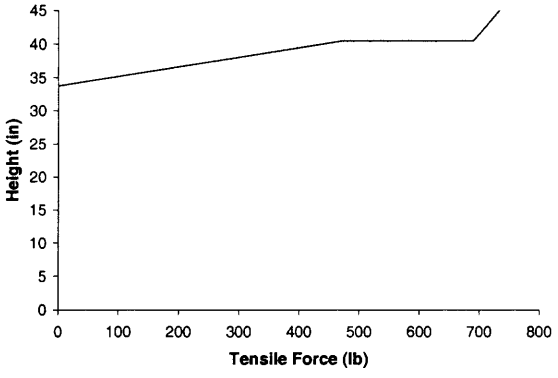

c) Tensile force including weight

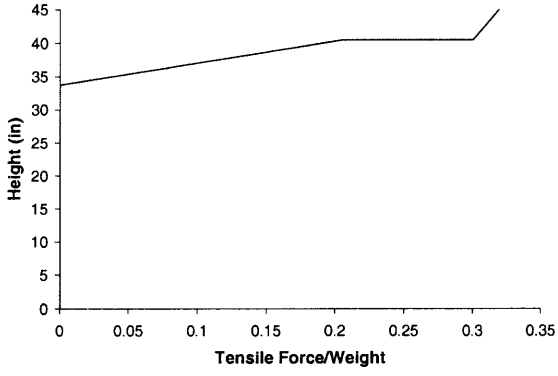

d) Tensile force including weight as a percentage of coil weight

Figure 5.24 Maximum tensile force in coil under earthquake for case 10.

Table 5.3 shows the tensile force caused in core and tie-plates for different cases. As seen, most of the force is tolerated by core, because of its high stiffness. These tensile forces are undesirable and will cause loss of close fitting in the yoke to limb joint. Prestressing should be applied to prohibit development of such tensile forces in the core.

Table 5.3 Maximum Tensile Forces in the Core and Tie-Plates for Different Analyses

Case	Core Force (lb)	Core Force/ Core Weight	Tie-plate Force (lb)	Tie-plate Force/ Core Weight
1	1767.30	0.5422	20.2122	0.006201
2	1766.06	0.5418	20.1981	0.006197
3	1698.75	0.5212	19.4282	0.005961
4	1686.50	0.5174	19.2881	0.005918
5	1758.61	0.5396	20.1128	0.006171
6	1760.87	0.5402	20.1387	0.006179
7	1701.59	0.6607	24.6300	0.009564
8	1701.42	0.6607	24.6275	0.009563
9	2532.83	0.5828	28.9675	0.006666
10	2006.99	0.6158	22.9535	0.007042
11	1958.67	0.6009	22.4009	0.006873
12	2101.75	0.6448	24.0373	0.007375
13	1956.81	0.6004	22.3796	0.006866

Table 5.4 shows the maximum tensile force in coil for different cases. It is seen that the force is almost the same in all cases and does not go over 30% of the weight excluding core and tie-plates for fixed cases. In the cases where the response of FPS is considered as the input earthquake, this force is increased to less than 35%. These are very modest forces.

Table 5.4 Maximum Tensile Forces in the Coil for Different Analyses

Case	Maximum Tensile Force in Coil Excluding Weight (lb)	Maximum Tensile Force /Coil Weight	Maximum Tensile Force in Coil Including Weight (lb)	Maximum Tensile Force /Coil Weight
1	902.88	0.3932	651.58	0.2837
2	904.93	0.3941	653.49	0.2846
3	993.70	0.4322	596.85	0.2596
4	983.16	0.4276	607.79	0.2643
5	919.60	0.3999	657.21	0.2858
6	918.90	0.3996	659.26	0.2867
7	1035.91	0.3941	740.31	0.2816
8	1038.18	0.3949	741.21	0.2820
9	1403.35	0.4007	1018.66	0.2909
10	1047.19	0.4560	733.16	0.3193
11	1046.86	0.45587	775.65	0.3378
12	1116.60	0.4862	798.14	0.3476
13	1052.39	0.4583	777.54	0.3386

The proper method used for applying the prestressing force poses an intriguing question. There are two ways to apply the prestressing. It was learned through the visit to the Southern California Edison that one method of prestressing is through fitting in the wooden blockings that have dimensions larger than the available space. This will require using jacks to increase the available space and then letting the blockings in and letting them to bear the additional load. This will produce tensile forces in tie-plates and core and compressive force in winding. Most of this force is absorbed by core rather than the tie-bar. The second method is to apply the prestressing force through tightening the bolts of the tie-plates [Del Vecchio, 2002]. This will produce compressive forces in both the winding and the core. However, most of this force is absorbed by the core.

The first method has the advantage that it is very effective in the sense that not much force is applied to the tie-bars. The force in winding is almost equal to that in the core. However, it has the effect that it produces tensile forces in core and is counter-productive. Also, this method is practically very hard to apply. The second method has the advantage of simultaneously applying compressive force to both the core and the winding. However, since core absorbs most of the force, a lot of force must be applied to reach the desired level of force in the winding. Therefore, either a combination of methods one or two or just the second method should be used to produce the required compressive force in both the core and winding.

The amount of force in each element required for achieving the specified prestressing force in coil and core is calculated for the cases 1,7, 9. If all the prestressing is done through the tie-plates, the corresponding force in the tie-plates will be between 80~139 kips. This force will cause a prestressing force of 79~138 kips in the core and the

required force of less than 1 kips in the windings. This is a very inefficient since most of the force is taken to produce a prestressing in the core that is much higher than its required value of 2~3 kips.

A better method is to combine the two methods of prestressing to achieve the predefined goals. Since the force in the core in all cases is comfortably less than 3 times that in the winding, the ratio of the goal prestressing force in core to winding is set equal to 3. This assumption leads to a combination of the prestressing methods that will produce the tensile force of less than 4 kips in the tie-plates.

However, for two reasons, it is suggested that an independent prestressing mechanism is used for prestressing the winding by itself to the level required by seismic considerations. The extra prestressing in the winding and core for other considerations can be applied, as they would otherwise be done. The first reason is that finding the right balance between the amount of prestressing applied through tie-plates and blockings is a hard task and its application is practically very hard. Erring on this will result in an insufficiently prestressed core in one side and in a very inefficient design and immense sizes for tie-plates on the other side. The second reason is that the prestressing in a transformer is compromised through its life due to several reasons. The inelasticity in behavior of the key spacers, and their aging precipitated by the amount of heat produced in transformer will result in loss of prestressing after some time. It is a well-known experience that many transformers have not much prestressing left in them when they are opened after their life-cycle [Prevost, 2003]. Having a separate prestressing mechanism for the windings can help insure that the required amount of prestressing needed for seismic reasons is maintained in the winding throughout its life.

A hint to the amount of prestressing force that is actually applied in a typical transformer is found in one of the studies performed on windings [Prevost, 2003]. It is said that a prestressing pressure of about 5 N/mm² (724.29 psi) is the value for a 550 kV BIL 20MVA transformer at $90^{\circ C}$. Considering the area of key spacers in the different geometric configurations used, this stress translates into a prestressing force of 53~63 kips in the windings. This value is much higher than the amount needed under seismic considerations to prevent the failure modes. Hence, it seems that the probability of seismic excitations to cause failures in internal components due to structural reasons is very slim, unless the prestressing is lost before earthquake happens. This also suggests that more focus should be put on side reasons for an explanation of the occasional internal damage observed in past earthquakes in the form of slipping of key spacers.

CHAPTER 6

CONCLUSIONS

Continuing the work of Ersoy and Saadeghvaziri [Ersoy, 2002], several issues of seismic behavior and rehabilitation for transformers and their internal components, bushings, transformer foundation, interaction among electrical equipment in a substation, and use of FPS for seismic improvement of the electric substation have been studied. Based on the results of these studies, the following conclusions can be made:

1- FPS is very effective in reducing the seismic response of bushings for all frequencies. In the cases studied, the 196 kV bushing is not damaged in any case. Such a determination for other bushings should be made based on the results provided and their allowable displacement.

2- The proximity of the vertical and horizontal frequencies in transformers can reduce the effectiveness of FPS in terms of bushing response and inertia force reduction. However, for the practical range of frequencies, this adverse effect is limited and does not reduce FPS efficiency very much.

3- FPS is very effective in reducing the foundation size and cost. For the cases studied, the use of FPS makes possible the seismic design of foundation without use of piles. Hence, it appears that use of FPS bearings can be even justified on an initial cost basis.

4- The interaction between transformer-bushing and interconnecting equipment has an adverse effect on different responses, particularly bushing response. This

effect exists independent of the relative value of the FPS frequency to that of the interconnecting equipment. This phenomenon is even observed when these frequencies are equal.

5- The FPS response is the predominant factor determining the behavior of the various interacting components. When the FPS displacement is in the direction away from the interconnecting equipment, it pulls the interconnecting equipment. The resistance of the interconnecting equipment to pulling by FPS will put the connecting cable under enormous tension. The displacements of transformers, bushings, and interconnecting equipment in this condition can be described as vibrations about a center point that is the FPS displacement. This is always the case for the transformer and bushing. The displacement of FPS itself is to some extent shifted toward the direction of interconnecting equipment, whether this is an increase in its maximum displacement or not.

6- Even the slightest interaction has significant adverse effects. Therefore, the interaction of the transformer-bushing with the interconnecting equipment must be prevented at any cost. One way to insure this is to provide a slack equal to sum of the maximum absolute values of FPS and interconnecting displacements in the connecting cable. The displacement of FPS can be determined from graphs provided in this study.

7- Some of the trends observed in interaction responses when the transformer is isolated are different from those observed for the interaction of fixed equipment. Hence, it should be emphasized that the results of previous studies on interaction of fixed structures does not automatically hold when base isolation is used.

8- The proper radius of FPS that can offer a desirable balance between cost, displacement, and inertia reduction is in the range of 30~60 inches For records on rock, the difference of FPS displacement for different radii is not large. The difference in inertia reduction is particularly high for PGA > 0.7g where the inertia reduction for R = 30 inches starts to decline. For records on soil, only the displacement for R = 30 inches is visibly lower than others. The choice of radius is mostly based on cost and inertia reduction balance, because they are more sensitive to FPS radius, compared to displacement. The inertia reductions in soil are less affected by radius compared to those of rock. Hence, the use of higher FPS radii is easier to justify for rock ground conditions than soil conditions due to the higher gain in terms of inertia reduction. R = 45 inches seems to be the radius that combines most of the benefits. R = 60 inches may be preferred if the gain in terms of inertia reduction can balance the increased FPS cost. R = 30 inches may be chosen in cases where normal structural design can sustain the increased inertial forces with little or no reinforcement.

9- Among the four modes of damage and failure stipulated for internal components of transformers, the sliding of key spacers and loss of close fitting tolerances between limbs and yokes are investigated with the first mode being the most critical one. Both of these damage modes can be attributed to loss of prestressing. The assessments show that the internal components behave as a rigid body. The tensile forces in windings and core caused by vertical excitation are modest, and are easily offset by the typical prestressing forces. Therefore, it seems that failures of internal components in earthquakes due to structural reasons is very unlikely,

unless the prestressing is lost before earthquake occurs. This also suggests that more focus should be put on other reasons to explain the occasional internal damage observed in past earthquakes in the form of slipping of key spacers.

10- It is suggested that an independent prestressing mechanism be employed for prestressing the winding itself to the level required by seismic considerations. Having such an independent prestressing mechanism for the windings can help ensure that the required amount of prestressing needed for seismic reasons is not compromised throughout the winding life cycle. This will also facilitate the application of the proper prestressing to the winding, without practical application problems or inefficient design.

APPENDIX

IMPLEMENTATION OF AN FPS ELEMENT IN ADINA

The details of calculation of forces in an FPS element in each time step and its implementation in ADINA are presented here. The details of the data about ADINA can be found in the software manuals. ADINA provides a subroutine in Fortran called *CUSERG* that can be used to model a user-supplied element [ADINA, 2001(b)]. The details of the variables used are provided within the subroutine as comments and can be seen in this appendix. This subroutine can be seen in ADINA files under the name *ovl160u.f* [ADINA, 2001(a)]. The calls from ADINA to *CUSERG* are divided into several phases controlled by the integer value KEY and include four cases. At the start of the program, KEY is equal to 1, where ADINA calls the phase one. In this phase, all the initial values and anything that should be defined once at the beginning of the program are defined. KEY = 2 refers to the part of subroutine where the element nodal forces are calculated. KEY = 3 refers to the section where the stiffness matrix is defined. In each time step, the program refers repeatedly to phase two and then three and checks for convergence. After the convergence is achieved, the program will refer to the last section with KEY = 4. Any action that should be done after the convergence is achieved should be done in this phase. For instance, swapping variables between different time steps that is done after convergence belongs to this section.

The subroutine retains the nodal positions at the last time step. It is for the writer of the element to retain any other variable needed from previous time steps in memory. Temperature-independent and -dependent constants can also be defined and used to

describe the behavior of the element. Using these constants and a given nodal position for the element at the next time step, the solution in this time step, including forces and stiffness, should be achieved. The process involves receiving the nodal coordinates at t_{n+1} and calculating forces and stiffness for that displacement. The results are used in time-history analysis and the modified displacement is achieved. This process is repeated until convergence is achieved. Each time step involves the following calculations:

$$dX = X_{n+1} - X_n \tag{A.1}$$

$$\varphi = \tan^{-1}\left(\frac{\sqrt{x_1^{\,2} + x_2^{\,2}}}{R}\right)_{n+1} \tag{A.2}$$

$$\theta = \tan^{-1}\left(\frac{x_2}{x_1}\right)_{n+1} \tag{A.3}$$

$$v_1 = \begin{pmatrix} 1/\sqrt{1+\tan(\phi)^2 * \cos(\theta)^2} \\ 0 \\ \sqrt{1-v_{11}^{\,2}} * sign(\cos(\theta)) \end{pmatrix} \tag{A.4}$$

$$v_3 = \begin{pmatrix} -\sin(\phi) * \cos(\theta) \\ -\sin(\phi) * \sin(\theta) \\ \cos(\theta) \end{pmatrix} \tag{A.5}$$

$$v_2 = v_3 \times v_1 \tag{A.6}$$

$$z_{surf} = \left(R - \sqrt{R^2 - x_1^2 - x_2^2}\right)_{n+1} \tag{A.7}$$

$$z_{normal,n+1} = (x_{3,n+1} - z_{surf})\cos(\phi) \tag{A.8}$$

$$vel_{normal} = \frac{(Z_{normal,n+1} - Z_{normal,n-1})}{2\Delta t} \tag{A.9}$$

$$dX_{v1} = dX \cdot v_1 \tag{A.10}$$

$$dX_{v2} = dX \cdot v_2 \tag{A.11}$$

$$vel = \frac{(X_{n+1} - X_{n-1})}{2\Delta t} \tag{A.12}$$

$$vel_{plane} = \sqrt{|vel|^2 - (vel \cdot v_3)^2} \tag{A.13}$$

$$\mu = \mu_{\max} - \Delta\mu \exp^{-\alpha . vel_{plane}} \tag{A.14}$$

$$\rho = X_{n+1} - C_n \tag{A.15}$$

$$\rho_{v1} = \rho \cdot v_1 \tag{A.16}$$

$$\rho_{v2} = \rho \cdot v_2 \tag{A.17}$$

$$Z_{n+1} = \begin{bmatrix} Z_{1,n+1} \\ Z_{2,n+1} \end{bmatrix} = \begin{bmatrix} \frac{\rho_{v1}}{Y} \\ \frac{\rho_{v2}}{Y} \end{bmatrix} \tag{A.18}$$

$$if \quad |Z_{n+1}| > 1, \quad Z_{n+1} = \frac{Z_{n+1}}{|Z_{n+1}|} \tag{A.19}$$

$$N = -k_{normal} * z_{normal,n+1} - c * vel_{normal} \tag{A.20}$$

$$if \quad N < 0, \quad N = 0 \tag{A.21}$$

$$F_{f1} = -\mu N Z_1 \tag{A.22}$$

$$F_{f2} = -\mu N Z_2 \tag{A.23}$$

$$\begin{pmatrix} F_{x1} \\ F_{x2} \\ F_{x3} \end{pmatrix} = -\overbrace{\begin{Bmatrix} v_1 v_2 v_3 \end{Bmatrix}}^{} \begin{pmatrix} F_{f1} \\ F_{f2} \\ N \end{pmatrix} \tag{A.24}$$

In a model with 12 degrees of freedom, these forces are returned via ADINA subroutine to the main program through

RE(1)= $-F_{x1}$
RE(2)= $-F_{x2}$
RE(3)= $-F_{x3}$
RE(4)= 0._8
RE(5)= 0._8
RE(6)= 0._8
RE(7)= F_{x1}
RE(8)= F_{x2}
RE(9)= F_{x3}
RE(10)= 0._8
RE(11)= 0._8
RE(12)= 0._8

In the next phase, the stiffness related to these forces should be calculated. This stiffness matrix for the FPS element should satisfy the equation

$$K\Delta X = \Delta F \tag{A.25}$$

It is defined as a diagonal matrix as follows:

$$K = \begin{bmatrix} T & 0 & -T & 0 \\ 0 & 0 & 0 & 0 \\ -T & 0 & T & 0 \\ 0 & 0 & 0 & 0 \end{bmatrix} \tag{A.26}$$

$$T = \begin{bmatrix} \Delta F_{x1} / \Delta x_1 & 0 & 0 \\ 0 & \Delta F_{x2} / \Delta x_2 & 0 \\ 0 & 0 & \Delta F_{x3} / \Delta x_3 \end{bmatrix} \tag{A.27}$$

However, to achieve convergence, it might be needed that this is smoothened through use of an average value for forces and displacements over a certain number of cycles of the same time step. For example if the current cycle is number j, Equation A.27 can be written as

$$T = \begin{bmatrix} \sum_{i=j-4}^{j} \Delta F_{x1,i} / \Delta x_{1,i} & 0 & 0 \\ 0 & \sum_{i=j-4}^{j} \Delta F_{x2,i} / \Delta x_{2,i} & 0 \\ 0 & 0 & \sum_{i=j-4}^{j} \Delta F_{x3,i} / \Delta x_{3,i} \end{bmatrix} \tag{A.28}$$

After achieving convergence, all the variables having a time index are scrolled once back and the process of solving for the next time step is started.

The modified subroutine used here for FPS element is shown below:

```
SUBROUTINE CUSERG [DLLEXPORT] (IA,A,NG,NEL,IELD,ND,NOD, &
&            VNI,VNT,IGLOB,THICK, &
&            XYZ,DISP1,DISP2,TEMP1,TEMP2,TREF, &
&            SCP,CTD,CTDD,CTI,ALFA, &
&            TIME,DT,IDEATH,ETIMV,ETIMV2, &
&            NUIPT,NUIT1,NUIT2,NUIT3,XYZIPT, &
&            LGTH1,LGTH2,ARRAY,IARRAY, &
&            RUPLOT,IUPLOT, &
```

```
     &              RE,AS,REBM,KEY)
!*|
!*|  THIS SUBROUTINE IS TO BE SUPPLIED BY THE USER TO CALCULATE
!*|  THE FORCES AND STIFFNESS MATRIX OF A GENERAL ELEMENT
!*|
!*|  THIS SUBROUTINE IS CALLED IN USERG FOR EACH GENERAL ELEMENT
!*|  TO PERFORM THE FOLLOWING OPERATIONS :
!*|
!*|    KEY.EQ.1   INITIALIZE THE WORKING ARRAYS DURING INPUT PHASE
!*|           PROVIDE THE COORDINATES OF INTERIOR POINTS
!*|           XYZIPT OF THE ELEMENT, FOR DISPLAYING CALCULATED
!*|           QUANTITIES
!*|
!*|    KEY.EQ.2   CALCULATE ELEMENT FORCES
!*|
!*|    KEY.EQ.3   CALCULATE THE ELEMENT STIFFNESS
!*|
!*|    KEY.EQ.4   PRINT CALCULATED FORCES AND PROVIDE OTHER
!*|           QUANTITIES (STRESSES, STRAINS, ETC)
!*|           FOR POSTPROCESSING
!*|
!*|
!*|  THE FOLLOWING VARIABLES ARE PROVIDED TO PERFORM THE ABOVE OPERATIO
!*|
!*|    NG              ELEMENT GROUP NUMBER
!*|
!*|    NEL             ELEMENT NUMBER
!*|
!*|    IELD            NUMBER OF NODES IN THE ELEMENT
!*|
!*|    ND              NUMBER OF DEGREES OF FREEDOM
!*|                  IN THE ELEMENT
!*|                  ND=(5+IGLOB(1))+...+(5+IGLOB(IELD))
!*|                    IGLOB() IS EITHER 0 OR 1
!*|
!*|    NOD(IELD)         GLOBAL NODE NUMBERS OF THE ELEMENT
!*|
!*|    VNI(3,IELD)       INITIAL DIRECTOR VECTORS
!*|
!*|    VNT(3,IELD)       DIRECTOR VECTORS AT TIME T
!*|
!*|    IGLOB(IELD)       SHELL NODAL D.O.F. FLAG ;
!*|                  =0, 6 D.O.F. ASSIGNED FOR THIS NODE
!*|                  =1, 5 D.O.F. ASSIGNED FOR THIS NODE
!*|
!*|    THICK(IELD)       THICKNESS FOR EACH NODE
!*|
!*|    XYZ(3,IELD)       ELEMENT NODAL COORDINATES
!*|
!*|    DISP1(ND)         ELEMENT DISPLACEMENTS, AT TIME T
!*|
!*|    DISP2(ND)         ELEMENT DISPLACEMENTS, AT TIME+DT
!*|
!*|    TEMP1(IELD)       ELEMENT TEMPERATURE AT TIME T
!*|
!*|    TEMP2(IELD)       ELEMENT TEMPERATURE AT TIME T+DT
```

```
!*|
!*|    TREF             REFERENCE TEMPERATURE
!*|
!*|    SCP(99)          SOLUTION CONTROL PARAMETERS
!*|                   (MAXIMUM 99)
!*|
!*|    CTD(98,IELD)       TEMPERATURE-DEPENDENT CONSTANTS
!*|                   AT TIME T (MAXIMUM 98),
!*|                   AT EACH ELEMENT NODE
!*|
!*|    CTDD(98,IELD)      TEMPERATURE-DEPENDENT CONSTANTS
!*|                   AT TIME T+DT (MAXIMUM 98),
!*|                   AT EACH ELEMENT NODE
!*|
!*|    CTI(99)          TEMPERATURE-INDEPENDENT CONSTANTS
!*|                   (MAXIMUM 99)
!*|
!*|    ALFA(IELD)         COEFFICIENT OF THERMAL EXPANSION AT
!*|                   EACH NODE AT TIME T
!*|
!*|    TIME             TIME AT CURRENT STEP , T+DT
!*|
!*|    DT               TIME STEP INCREMENT , DT
!*|
!*|    IDEATH             ELEMENT BIRTH/DEATH OPTION
!*|                   EQ.0 OPTION NOT USED
!*|                   EQ.1 ELEMENTS BECOME ACTIVE
!*|                      AT TIME OF BIRTH
!*|                   EQ.2 ELEMENTS BECOME INACTIVE
!*|                      AT TIME OF DEATH
!*|                   EQ.3 ELEMENTS BECOME ACTIVE
!*|                      AT TIME OF BIRTH, THEN
!*|                      INACTIVE AT TIME OF DEATH
!*|
!*|    ETIMV            BIRTH TIME OF THE CURRENT ELEMENT
!*|
!*|    ETIMV2           DEATH TIME OF THE CURRENT ELEMENT
!*|
!*|    NUIPT            NUMBER OF INTERIOR POINTS OF THE ELEMENT,
!*|    (=NUIT1*NUIT2*NUIT3) WHERE THE QUANTITIES TO BE CACLULATED FOR
!*|                   DISPLAY, INPUT FROM THE ADINA-IN COMMAND
!*|                   MATRIX USER-SUPPLIED
!*|
!*|    NUIT1            NUMBER OF INTEGRATION POINTS IN THE
!*|                   FIRST LOCAL AXIS DIRECTION
!*|                   DEFAULT: NUIT1=1
!*|
!*|    NUIT2            NUMBER OF INTEGRATION POINTS IN THE
!*|                   SECOND LOCAL AXIS DIRECTION
!*|                   DEFAULT: NUIT1=1
!*|
!*|    NUIT3            NUMBER OF INTEGRATION POINTS IN THE
!*|                   THIRD LOCAL AXIS DIRECTION
!*|                   DEFAULT: NUIT3=1
!*|
!*|    LGTH1            LENGTH OF REAL WORKING ARRAY AT EACH
```

```
!*|                IPT LOCATION
!*|
!*|   LGTH2          LENGTH OF INTEGER WORKING ARRAY AT
!*|                EACH IPT LOCATION
!*|
!*| THE FOLLOWING VARIABLES ARE TO BE CALCULATED BY THE USER:
!*|
!*|   ARRAY(LGTH1,NUIPT)  VARIABLE LENGTH WORKING ARRAY (REAL)
!*|                RECEIVED AT TIME T AND UPDATED BY
!*|                USER-SUPPLIED CODING TO CORRESPOND TO
!*|                TIME T+DT, STORED FOR IPT LOCATIONS
!*|                (CF. "AUI" MATERIAL INPUT: LENGTH1)
!*|
!*|   IARRAY(LGTH2,NUIPT)  VARIABLE LENGTH WORKING ARRAY (INTEGER)
!*|                RECEIVED AT TIME T AND UPDATED BY
!*|                USER-SUPPLIED CODING TO CORRESPOND TO
!*|                TIME T+DT, STORED FOR IPT LOCATIONS
!*|                (CF. "AUI" MATERIAL INPUT: LENGTH2)
!*|
!*|   XYZIPT(3,NUIPT)    COORDINATES OF IPT LOCATIONS
!*|
!*|   RUPLOT(100,NUIPT)   USER-CALCULATED REAL QUANTITIES AT IPT
!*|                AND MUST BE PLACED IN THE FOLLOWING
!*|                ORDER TO BE PROCESSED IN THE ADINA-PLOT,
!*|
!*|                RUPLOT(1,IPT) :STRESS-XX(-RR)
!*|                RUPLOT(2,IPT) :STRESS-YY(-SS)
!*|                RUPLOT(3,IPT) :STRESS-ZZ(-TT)
!*|                RUPLOT(4,IPT) :STRESS-XY(-RS)
!*|                RUPLOT(5,IPT) :STRESS-XZ(-RT)
!*|                RUPLOT(6,IPT) :STRESS-YZ
!*|                RUPLOT(7,IPT) :STRAIN-XX(-RR)
!*|                RUPLOT(8,IPT) :STRAIN-YY(-SS)
!*|                RUPLOT(9,IPT) :STRAIN-ZZ(-TT)
!*|                RUPLOT(10,IPT):STRAIN-XY(-RS)
!*|                RUPLOT(11,IPT):STRAIN-XZ(-RT)
!*|                RUPLOT(12,IPT):STRAIN-YZ
!*|                RUPLOT(13,IPT):PLASTIC_STRAIN-XX(-RR)
!*|                RUPLOT(14,IPT):PLASTIC_STRAIN-YY(-SS)
!*|                RUPLOT(15,IPT):PLASTIC_STRAIN-ZZ(-TT)
!*|                RUPLOT(16,IPT):PLASTIC_STRAIN-XY(-RS)
!*|                RUPLOT(17,IPT):PLASTIC_STRAIN-XZ(-RT)
!*|                RUPLOT(18,IPT):PLASTIC_STRAIN-YZ
!*|                RUPLOT(19,IPT):CREEP_STRAIN-XX(-RR)
!*|                RUPLOT(20,IPT):CREEP_STRAIN-YY(-SS)
!*|                RUPLOT(21,IPT):CREEP_STRAIN-ZZ(-TT)
!*|                RUPLOT(22,IPT):CREEP_STRAIN-XY(-RS)
!*|                RUPLOT(23,IPT):CREEP_STRAIN-XZ(-RT)
!*|                RUPLOT(24,IPT):CREEP_STRAIN-YZ
!*|                RUPLOT(25,IPT):THERMAL_STRAIN-XX(-RR)
!*|                RUPLOT(26,IPT):THERMAL_STRAIN-YY(-SS)
!*|                RUPLOT(27,IPT):THERMAL_STRAIN-ZZ(-TT)
!*|                RUPLOT(28,IPT):THERMAL_STRAIN-XY(-RS)
!*|                RUPLOT(29,IPT):THERMAL_STRAIN-XZ(-RT)
!*|                RUPLOT(30,IPT):THERMAL_STRAIN-YZ
!*|                RUPLOT(31,IPT):TEMPERATURE
```

```
!*I                  RUPLOT(32,IPT):ACCUM_EFF_PLASTIC_STRAIN
!*I                  RUPLOT(33,IPT):YIELD STRESS
!*I
!*I     IUPLOT(50,NUIPT)     USER-CALCULATED INTEGER QUANTITIES
!*I                  AT IPT POINT
!*I                  IUPLOT(1,IPT) :STRESS STATE
!*I
!*I     RE(ND)          ELEMENT NODAL FORCES, TO BE CALCULATED
!*I                  BY USER-SUPPLIED CODING
!*I
!*I     AS(ND,ND)          ELEMENT STIFFNESS MATRIX, TO BE
!*I                  CALCULATED BY USER-SUPPLIED CODING
!*I
!*I     REBM(ND)          BEAM-SUBTYPE ELEMENT NODAL FORCES IN
!*I                  LOCAL SYSTEM, TO BE CALCULATED
!*I                  BY USER-SUPPLIED CODING
!*I
CCCCCCCCCCCCCCCCCCCCCCCCCCCCCCCCCCCCCCCCCCCCCCCCCCCCCC
CCCCCCC
!*I !                                              !
!*I !  THIS SUBROUTINE IS PROVIDED FOR NONLINEAR ANALYSIS.          !
!*I !  IF THIS NONLINEAR GENERAL ELEMENT IS TO BE USED              !
!*I !  AS A LINEAR ELEMENT, THEN SET RE=0.0 AND USE                 !
!*I !  THE OPTION OF NO EQUILIBRIUM ITERATION IN THE ADINA EXECUTION.!
!*I !  E.G.  USE AUI COMMANDS: ITERATION METHOD=MODIFIED-NEWTON      !
!*I !                   EQUILIBRIUM-STEPS / @CLEAR          !
!*I !                   STIFFNESS-STEPS   / @CLEAR          !
!*I !                                              !
!*I
CCCCCCCCCCCCCCCCCCCCCCCCCCCCCCCCCCCCCCCCCCCCCCCCCCCCCC
CCCCCCC
!*I
implicit none
!    IMPLICIT DOUBLE PRECISION ( A-H,O-Z )
!

double precision  :: x(3,1)=0._8,x1(3,1)=0._8
double precision  :: normal_force,normal_force1,R, rigid_slide, all_normal_forces
double precision  :: kk(3)=0._8, stiff1(3,3),norm_dx,norm_ro, ro(3,1)= 0._8
double precision  :: fb(2,1)=0._8,fb1(2,1)=0._8, norm_fb1, mu= 0.1_8, d_x(3,1), center(3,1)= 0._8
double precision  :: z(2,1)=0._8, z1(2,1)=0._8, norm_z1,w,w1
double     precision     ::     real_x3,     real_xn1,     real_xn=0._8,     old_real_xn=0._8,
k_vertical,phi=0._8,teta=0._8
double precision  :: vector_X(3,1),vector_Y(3,1),normal_direction(3,1)
double precision  :: norm_temp,the_sign
double precision  :: initial_normal_force
integer :: time_step=0, inside_2=0, inside_3=0
double     precision     ::     mu_max=0.095_8,     delta_mu=0.045_8,     alpha=     0.9_8,
old_x(3,1),vel(3,1),vel_plane, vel_normal
double precision  :: dx_plane(3,1), norm_dx_plane, ro_plane(3,1), norm_ro_plane
integer,parameter :: N_smooth=5
double precision  :: damping, sum_dx(3), sum_df(3), all_dx(N_smooth,3), all_dforce(N_smooth,3)


    DIMENSION IA(*),A(*)
    REAL A
```

```
integer IA
integer Ield,nuipt,lgth1,lgth2,nd
integer NOD(IELD), IARRAY(LGTH2,NUIPT), IUPLOT(50,NUIPT),IGLOB(*)
double precision SCP(99), CTI(99), CTD(98,IELD), CTDD(98,IELD)
double precision DISP1(ND), DISP2(ND) !, NOD(IELD)
double precision TEMP1(IELD), TEMP2(IELD)
double precision ARRAY(LGTH1,NUIPT) !, IARRAY(LGTH2,NUIPT)
double precision AS(ND,ND), RE(ND), REBM(ND)
double precision XYZIPT(3,NUIPT), XYZ(3,*), ALFA(IELD)
double precision RUPLOT(100,NUIPT) !, IUPLOT(50,NUIPT)
double precision VNI(3,*),VNT(3,*),THICK(*) !,IGLOB(*)
!
double precision xdis1, xdis2, atemp, tref, time, dt, etimv, etimv2, my_stiffness
integer  IIN,key,i,j,m,nel,ipt,k,l,ng,ideath,NUIT1,NUIT2,NUIT3
integer IOUT
integer my_integer


          IIN=50
 IOUT=46
          R= CTI(1)
          k_vertical= CTI(2)
          mu_max= CTI(3)
          delta_mu= CTI(4)
          alpha= CTI(5)
          damping=CTI(6)


    GO TO (1,2,3,4), KEY
!*I
!*I
!*I   K E Y  =  1
!*I
!*I   INITIALIZE COMPONENTS OF REAL AND INTEGER WORKING ARRAYS
!*I   ( INITIALIZE ARRAY(LGTH1,NUIPT) AND IARRAY(LGTH2,NUIPT) )
!*I   PROVIDE XYZIPT(3,NUIPT) COORDINATES IF CALCULATED QUANTITIES
!*I   TO BE DISPLAYED INSIDE THE ELEMENT
!*I
   1 CONTINUE

rigid_slide= 0.005_8
initial_normal_force= 0._8
normal_force= initial_normal_force
normal_force1= initial_normal_force
w=-normal_force
w1=-normal_force1
kk(1)= (mu+rigid_slide/R)*normal_force1/rigid_slide
kk(2)= normal_force1/R
kk(3)= normal_force1/2._8/R
stiff1=0._8
stiff1(1,1)=kk(1)
stiff1(2,2)=kk(1)
stiff1(3,3)= normal_force1/2._8/R


IELD= 2
```

```
ND= 12
Ideath=0
nuipt= 1
nuit1=1
nuit2=1
nuit3=1
my_stiffness =10000._8

!*I
!*I  ***  INSERT  USER-SUPPLIED  CODING
!*I
     DO 11 I=1,LGTH1
     DO 11 J=1,NUIPT
  11 ARRAY(I,J)=FLOAT(I)*FLOAT(J)*FLOAT(NEL)
     DO 12 I=1,LGTH2
     DO 12 J=1,NUIPT
  12 IARRAY(I,J)=I*J*NEL
!
     DO 13 IPT=1,NUIPT
     DO 13 L=1,3
  13 XYZIPT(L,IPT)=0.0D0
!
     DO 14 K=1,IELD
     DO 14 L=1,3
     XYZIPT(L,1)=XYZIPT(L,1)+XYZ(L,K)
  14 CONTINUE
!
     DO 15 M=1,3
  15 XYZIPT(M,1)=XYZIPT(M,1)/IELD
!
     IF (NUIPT.LT.2) GO TO 19
     DO 16 IPT=2,NUIPT
     DO 16 J=1,3
  16 XYZIPT(J,IPT)=XYZIPT(J,1)
  19 CONTINUE
     RETURN
!*I
!*I
!*I  K E Y = 2
!*I
!*I  CALCULATIONS OF ELEMENT FORCES, STRESSES, STRAINS
!*I
   2 CONTINUE
     DO 21 I=1,ND
     DO 21 J=1,ND
  21 AS(I,J)=0.0D0
     AS(1,1)=CTDD(1,1)
     AS(1,5)=-CTDD(2,1)
     AS(1,7)=-CTDD(1,1)
     AS(1,11)=-CTDD(2,1)
!
     AS(2,2)=CTDD(1,1)
     AS(2,4)=CTDD(2,1)
     AS(2,8)=-CTDD(1,1)
     AS(2,10)=CTDD(2,1)
!
```

```
      AS(3,3)=CTDD(3,1)
      AS(3,9)=-CTDD(3,1)
!
      AS(4,2)=AS(2,4)
      AS(4,4)=CTDD(4,1)/3.0D0
      AS(4,8)=-CTDD(2,1)
      AS(4,10)=CTDD(5,1)/3.0D0
!
      AS(5,1)=AS(1,5)
      AS(5,5)=CTDD(4,1)/3.0D0
      AS(5,7)=CTDD(2,1)
      AS(5,11)=CTDD(5,1)/3.0D0
!
      AS(6,6)=CTDD(6,1)/27.0D0
      AS(6,12)=-CTDD(6,1)/27.0D0
!
      AS(7,1)=AS(1,7)
      AS(7,5)=AS(5,7)
      AS(7,7)=CTDD(1,1)
      AS(7,11)=CTDD(2,1)
!
      AS(8,2)=AS(2,8)
      AS(8,4)=AS(4,8)
      AS(8,8)=CTDD(1,1)
      AS(8,10)=-CTDD(2,1)
!
      AS(9,3)=AS(3,9)
      AS(9,9)=CTDD(3,1)
!
      AS(10,2)=AS(2,10)
      AS(10,4)=AS(4,10)
      AS(10,8)=AS(8,10)
      AS(10,10)=CTDD(4,1)/3.0D0
!
      AS(11,1)=AS(1,11)
      AS(11,5)=AS(5,11)
      AS(11,7)=AS(7,11)
      AS(11,11)=CTDD(4,1)/3.0D0
!
      AS(12,6)=AS(6,12)
      AS(12,12)=CTDD(6,1)/27.0D0
!
      DO 22 I=1,ND
      DO 22 J=I,ND
   22 AS(J,I)=AS(I,J)
!
      ATEMP=0.0D0
      DO 295 I=1,IELD
  295 ATEMP=ATEMP+TEMP2(I)/IELD
      DO 296 I=1,ND
      RE(I)=0.0D0
      REBM(I)=0.0D0
      DO 296 J=1,ND
  296 RE(I)=RE(I)+AS(I,J)*DISP2(J)
      REBM(1)=RE(3)
      REBM(7)=RE(9)
```

```
      XDIS1=DISP2(2)
      XDIS2=DISP2(7)
!
      DO 298 IPT=1,NUIPT
      RUPLOT(7,IPT)=(XDIS1-XDIS2)
      RUPLOT(1,IPT)=CTI(1)*RUPLOT(7,IPT)
      IUPLOT(1,IPT)=2
      RUPLOT(27,IPT)=ALFA(1)*(ATEMP-TREF)
      RUPLOT(3,IPT)=CTI(1)*RUPLOT(27,IPT)
      RUPLOT(31,IPT)=ATEMP
      RUPLOT(33,IPT)=RUPLOT(1,IPT)
  298 CONTINUE
!
      DO 299 IPT=1,NUIPT
      IARRAY(1,IPT)=IUPLOT(1,IPT)
      DO 299 J=1,33
      ARRAY(J,IPT)=RUPLOT(J,IPT)
  299 CONTINUE
!*|
!*|  ***  INSERT  USER-SUPPLIED  CODING
!*|
!*|


inside_2= inside_2 + 1

x1(1:3,1)= DISP2(7:9)- DISP2(1:3)
x(1:3,1)= DISP1(7:9)- DISP1(1:3)
d_x= x1-x

phi= datan2(dsqrt(x1(1,1)**2 + x1(2,1)**2),R)
if ((dabs(x1(1,1)) < 1.d-14) .and. (dabs(x1(2,1)) < 1.d-14)) then
        teta = 0._8
else
        if (x1(2,1) >= 0._8) then
                teta= datan2(x1(2,1),x1(1,1))
        else
                teta= datan2(x1(2,1),x1(1,1)) !+ 3.141592654_8
        end if
end if

! normal_direction always has a positive z component
normal_direction(1,1)= -dsin(phi)*dcos(teta)
normal_direction(2,1)= -dsin(phi)*dsin(teta)
normal_direction(3,1)= dcos(phi)
! vector_X is the tangent vector with no y- component and with always positive x component
vector_X(1,1)= 1._8/dsqrt(1._8+ dtan(phi)**2*dcos(teta)**2)
vector_X(2,1)= 0._8
vector_X(3,1)= dsign(dsqrt(1._8- vector_X(1,1)**2),dcos(teta))
! vector_Y is the other tangent vector and is equal to normal_direction*x1 and always has positive
y component
vector_Y(1,1)= normal_direction(2,1)* vector_X(3,1) - normal_direction(3,1)* vector_X(2,1)
vector_Y(2,1)= normal_direction(3,1)* vector_X(1,1) - normal_direction(1,1)* vector_X(3,1)
vector_Y(3,1)= normal_direction(1,1)* vector_X(2,1) - normal_direction(2,1)* vector_X(1,1)
!
!
```

```
real_x3= R- dsqrt(R**2-x1(1,1)**2- x1(2,1)**2) !(x1(1,1)**2 + x1(2,1)**2)/R
real_xn1= (x1(3,1)-real_x3)*dcos(phi)
vel_normal= (real_xn1-old_real_xn)/2._8/dt

dx_plane(1,1)=d_x(1,1)*vector_X(1,1)+ d_x(2,1)*vector_X(2,1)+ d_x(3,1)*vector_X(3,1)
dx_plane(2,1)=d_x(1,1)*vector_Y(1,1)+ d_x(2,1)*vector_Y(2,1)+ d_x(3,1)*vector_Y(3,1)
dx_plane(3,1)=0._8
norm_dx_plane=dsqrt(dx_plane(1,1)**2 +dx_plane(2,1)**2)

vel=(x1-old_x)/2._8/dt
vel_plane= dsqrt(vel(1,1)**2 + vel(2,1)**2 + vel(3,1)**2 -(vel(1,1)*normal_direction(1,1) +
vel(2,1)*normal_direction(2,1) + vel(3,1)*normal_direction(3,1))**2 )
mu= mu_max- delta_mu*dexp(-alpha*vel_plane)

ro= x1-center
ro_plane(1,1)=ro(1,1)*vector_X(1,1)+ ro(2,1)*vector_X(2,1)+ ro(3,1)*vector_X(3,1)
ro_plane(2,1)=ro(1,1)*vector_Y(1,1)+ ro(2,1)*vector_Y(2,1)+ ro(3,1)*vector_Y(3,1)
norm_ro_plane=dsqrt(ro_plane(1,1)**2 +ro_plane(2,1)**2)

ro_plane(3,1)=0._8
norm_dx= dsqrt(d_x(1,1)**2 + d_x(2,1)**2 + d_x(3,1)**2)

z1=ro_plane(1:2,1:1)/rigid_slide

norm_z1= dsqrt(z1(1,1)**2 + z1(2,1)**2)

if (norm_z1 > 1._8) then
        z1=z1/norm_z1
        norm_z1= dsqrt(z1(1,1)**2 + z1(2,1)**2)
end if

normal_force1=      -(k_vertical*(x1(3,1)-real_x3)*dcos(phi)      -      initial_normal_force)      -
damping*vel_normal
if (normal_force1 < 0._8) normal_force1=0._8
all_normal_forces= normal_force1
fb1(1,1)=      all_normal_forces*      -normal_direction(1,1)      +      normal_force1*      (
mu*z1(1,1)*dabs(vector_X(1,1)) + mu*z1(2,1)*vector_Y(1,1))
fb1(2,1)=      all_normal_forces*      -normal_direction(2,1)      +      normal_force1*      (
mu*z1(2,1)*dabs(vector_Y(2,1)))
w1= normal_force1* (mu*z1(1,1)*vector_X(3,1) + mu*z1(2,1)*vector_Y(3,1)) + all_normal_forces*
-normal_direction(3,1)



        RE(7)= fb1(1,1)
        RE(8)= fb1(2,1)
        RE(9)= w1
        RE(10)= 0._8
        RE(11)= 0._8
        RE(12)= 0._8
        RE(1)= -fb1(1,1) !RE(7)
        RE(2)= -fb1(2,1) !RE(8)
        RE(3)= -w1 !RE(9)
        RE(4)= 0._8
        RE(5)= 0._8
        RE(6)= 0._8
```

```
      RETURN
!*I
!*I  K E Y = 3
!*I
!*I  FORM GENERAL ELEMENT STIFFNESS
!*I  ( CALCULATE AS(ND,ND) )
!*I
    3 CONTINUE
      DO 31 I=1,ND
      DO 31 J=1,ND
   31 AS(I,J)=0.0D0
      AS(1,1)=CTDD(1,1)
      AS(1,5)=-CTDD(2,1)
      AS(1,7)=-CTDD(1,1)
      AS(1,11)=-CTDD(2,1)
!
      AS(2,2)=CTDD(1,1)
      AS(2,4)=CTDD(2,1)
      AS(2,8)=-CTDD(1,1)
      AS(2,10)=CTDD(2,1)
!
      AS(3,3)=CTDD(3,1)
      AS(3,9)=-CTDD(3,1)
!
      AS(4,2)=AS(2,4)
      AS(4,4)=CTDD(4,1)/3.0D0
      AS(4,8)=-CTDD(2,1)
      AS(4,10)=CTDD(5,1)/3.0D0
!
      AS(5,1)=AS(1,5)
      AS(5,5)=CTDD(4,1)/3.0D0
      AS(5,7)=CTDD(2,1)
      AS(5,11)=CTDD(5,1)/3.0D0
!
      AS(6,6)=CTDD(6,1)/27.0D0
      AS(6,12)=-CTDD(6,1)/27.0D0
!
      AS(7,1)=AS(1,7)
      AS(7,5)=AS(5,7)
      AS(7,7)=CTDD(1,1)
      AS(7,11)=CTDD(2,1)
!
      AS(8,2)=AS(2,8)
      AS(8,4)=AS(4,8)
      AS(8,8)=CTDD(1,1)
      AS(8,10)=-CTDD(2,1)
!
      AS(9,3)=AS(3,9)
      AS(9,9)=CTDD(3,1)
!
      AS(10,2)=AS(2,10)
      AS(10,4)=AS(4,10)
      AS(10,8)=AS(8,10)
      AS(10,10)=CTDD(4,1)/3.0D0
```

```
!
    AS(11,1)=AS(1,11)
    AS(11,5)=AS(5,11)
    AS(11,7)=AS(7,11)
    AS(11,11)=CTDD(4,1)/3.0D0
!
    AS(12,6)=AS(6,12)
    AS(12,12)=CTDD(6,1)/27.0D0
!*|
!*|  * * *  I N S E R T   U S E R - S U P P L I E D   C O D I N G
!*|
! assigning the stiffnesses

inside_3= inside_3 + 1

do j=1,N_smooth-1
        forall (i=1:3) all_dx(j,i)=all_dx(j+1,i)
        forall (i=1:3) all_dforce(j,i)=all_dforce(j+1,i)
end do
forall (i=1:3) all_dx(N_smooth,i)=d_x(i,1)
forall (i=1:2) all_dforce(N_smooth,i)=fb1(i,1)-fb(i,1)
all_dforce(N_smooth,3)=w1-w
sum_dx=0._8
sum_df=0._8

do j=1,N_smooth
        do i=1,3
                sum_dx(i)= sum_dx(i)+ all_dx(j,i)
                sum_df(i)= sum_df(i)+ all_dforce(j,i)
        end do
end do


if (inside_3<20) then

        if(dabs(d_x(3,1)) > 1.d-14) then
                kk(3)= (w1-w)/ d_x(3,1)
        end if
        !if (time_step <4)          kk(3)= k_vertical

        do j=1,2
                if (dabs(d_x(j,1)) > 1.d-14 ) then
                        kk(j)=(fb1(j,1)- fb(j,1))/ d_x(j,1)
                end if
        end do

else
        forall (j=1:3) kk(j)=sum_dx(j)/sum_df(j)
end if

do j=1,3
        stiff1(j,j)=kk(j)
end do


AS(1:3,1:3)= stiff1
```

```
AS(1:3,7:9)= -stiff1
AS(7:9,7:9)= AS(1:3,1:3)
AS(7:9,1:3)= AS(1:3,7:9)
AS(4:6,1:12)= 0._8
AS(10:12,1:12)= 0._8
AS(1:12,4:6)= 0._8
AS(1:12,10:12)= 0._8

!

    DO 32 I=1,ND
    DO 32 J=I,ND
  32 AS(J,I)=AS(I,J)
    RETURN
!*|
!*|
!*|  K E Y = 4
!*|
!*|  PRINTING OF ELEMENT RESPONSE
!*|  ( PRINT FORCES, STRESSES, STRAINS )
!*|
   4 CONTINUE
    IF (NEL.EQ.1) WRITE (IOUT,9000)
    DO 499 IPT=1,NUIPT
    IF (IPT.EQ.1) WRITE (IOUT,9002) NEL
    WRITE (IOUT,9003) IPT,(RUPLOT(I,IPT),I=1,12)
 499 CONTINUE
!
!*|
!*|  * * *  I N S E R T  U S E R - S U P P L I E D  C O D I N G
!*|
time_step=time_step+1
inside_2= 0
inside_3= 0
if (norm_ro_plane > rigid_slide) then
        center(1:3,1) = DISP2(7:9)- DISP2(1:3) - rigid_slide* ro(1:3,1)/ norm_ro_plane
end if

normal_force=normal_force1
w=w1
fb=fb1
old_x=x
x=x1
z=z1
old_real_xn=real_xn
real_xn=real_xn1
!*|
    RETURN
 9000 FORMAT (//,4X,3HNEL,2X,3HIPT,6X,9HSTRESS-RR,6X,          &
   &      9HSTRESS-SS,6X,9HSTRESS-TT,6X,9HSTRESS-RS,6X,      &
   &      9HSTRESS-RT,6X,9HSTRESS-ST, /, 20X,9HSTRAIN-RR,6X, &
   &      9HSTRAIN-SS,6X,9HSTRAIN-TT,6X,9HSTRAIN-RS,6X,      &
   &      9HSTRAIN-RT,6X,9HSTRAIN-ST, /)
 9002 FORMAT (/ I7 /)
 9003 FORMAT (7X,I5,8(2X,E13.6)/102X,2(2X,E13.6)/             &
   &       14X,8(2X,E13.6)/102X,2(2X,E13.6))
```

```
!*FILE END
    END subroutine cuserg
```

This subroutine should be compiled and linked to other subroutines of ADINA existing under the same directory. The steps required are [ADINA, 2002]:

1- Run *dfvars.bat* from the compiler you use to make its compiler the active compiler

2- Put the compiled version of the subroutine that is *ovl160u.obj* where the original file *ovl160u.f* is installed.

3- Run NMAKE (type NMAKE) in that directory.

There are also steps that should be taken to put the relevant information about the model to be analyzed in the ADINA input file. This is achieved through insertion of the commands defining the user-supplied material group, its associated mass, damping and stiffness matrices, and the element group in the input file (that will have *.in* extension).

The command `MATERIAL USER-SUPPLIED` defines a material group that will be used for the element [ADINA, 2001(b)]. The characteristics of FPS bearings can be provided here. In this command, $CTI1 = R$, the bearing radius, $CTI2 = k_{normal}$, $CTI3 = \mu_{\max}$, $CTI4 = \Delta\mu$, $CTI5 = \alpha$, and $CTI6 = c$, the damping associated with k_{normal}. All these symbols are the same as those defined in Chapter 2. Dummy values for CTI7~CTI10 and SCP1 ~SCP5 are provided in case that more constants will be required to represent additional parameters. The command `EGROUP` defines the element group with the specified set of characteristics determined using `MATRIXSE=1` [ADINA, 2001(b)]. The command `MATRIX USER-SUPP` is used to define the element type. Mass, stress, and damping matrices are defined next. There is no internal mass considered for the element

and there is no need for any stress calculation inside it. The damping is also taken care of directly inside the subroutine and through the coefficient CTI6. However, these dummy matrices with zero elements should be defined since they are required in the command MATRIXSET that defines the set of characteristics related to the defined element group. The following is an example of this part of the input file. If the bearings have different characteristics, they can be defined under more than one element group.

```
*
MATERIAL USER-SUPPLIED NAME=1 INTEG=FORWARD NSUBD=10,
   TREF=0.00000000000000 DENSITY=0.00000000000000 LENGTH1=65,
   LENGTH2=5 OPTION=NONE NCTI=10 NSCP=5 NCTD=0,
   CTI1=60.0000000000000 CTI2=1.17050000000000E+07,
   CTI3=0.0950000000000000 CTI4=0.0450000000000000,
   CTI5=0.900000000000000 CTI6=41914.7000000000,
   CTI7=-5.00000000000000E+07 CTI8=1.00000000000000E+08,
   CTI9=-5.00000000000000E+07 CTI10=1.00000000000000E+08,
   SCP1=2.00000000000000E+09 SCP2=100000.000000000,
   SCP3=10000.0000000000 SCP4=1000.00000000000,
   SCP5=100.000000000000
*
EGROUP GENERAL NAME=1 MATRIXSE=1 RESULTS=FORCES SKEWSYST=NO,
   USER-SUP=YES
*
MATRIX USER-SUPP NAME=1 ELEMENT-=THREEDSOLID ELNDOF=6 MATERIAL=1,
   NUIPT=1 NUIT1=1 NUIT2=1 NUIT3=1
*
MATRIX MASS NAME=2 ND=12
@CLEAR
1 0.00000000000000
2 0.00000000000000
3 0.00000000000000
4 0.00000000000000
5 0.00000000000000
6 0.00000000000000
7 0.00000000000000
8 0.00000000000000
9 0.00000000000000
10 0.00000000000000
11 0.00000000000000
12 0.00000000000000
@
*
MATRIX DAMPING NAME=4 ND=12
@CLEAR
1 0.00000000000000 0.00000000000000 0.00000000000000 0.00000000000000,
   0.00000000000000 0.00000000000000 0.00000000000000,
```

```
    0.00000000000000 0.00000000000000 0.00000000000000,
    0.00000000000000 0.00000000000000
2 0.00000000000000 0.00000000000000 0.00000000000000 0.00000000000000,
    0.00000000000000 0.00000000000000 0.00000000000000,
    0.00000000000000 0.00000000000000 0.00000000000000,
    0.00000000000000 0.00000000000000
3 0.00000000000000 0.00000000000000 0.00000000000000 0.00000000000000,
    0.00000000000000 0.00000000000000 0.00000000000000,
    0.00000000000000 0.00000000000000 0.00000000000000,
    0.00000000000000 0.00000000000000
4 0.00000000000000 0.00000000000000 0.00000000000000 0.00000000000000,
    0.00000000000000 0.00000000000000 0.00000000000000,
    0.00000000000000 0.00000000000000 0.00000000000000,
    0.00000000000000 0.00000000000000
5 0.00000000000000 0.00000000000000 0.00000000000000 0.00000000000000,
    0.00000000000000 0.00000000000000 0.00000000000000,
    0.00000000000000 0.00000000000000 0.00000000000000,
    0.00000000000000 0.00000000000000
6 0.00000000000000 0.00000000000000 0.00000000000000 0.00000000000000,
    0.00000000000000 0.00000000000000 0.00000000000000,
    0.00000000000000 0.00000000000000 0.00000000000000,
    0.00000000000000 0.00000000000000
7 0.00000000000000 0.00000000000000 0.00000000000000 0.00000000000000,
    0.00000000000000 0.00000000000000 0.00000000000000,
    0.00000000000000 0.00000000000000 0.00000000000000,
    0.00000000000000 0.00000000000000
8 0.00000000000000 0.00000000000000 0.00000000000000 0.00000000000000,
    0.00000000000000 0.00000000000000 0.00000000000000,
    0.00000000000000 0.00000000000000 0.00000000000000,
    0.00000000000000 0.00000000000000
9 0.00000000000000 0.00000000000000 0.00000000000000 0.00000000000000,
    0.00000000000000 0.00000000000000 0.00000000000000,
    0.00000000000000 0.00000000000000 0.00000000000000,
    0.00000000000000 0.00000000000000
10 0.00000000000000 0.00000000000000 0.00000000000000,
    0.00000000000000 0.00000000000000 0.00000000000000,
    0.00000000000000 0.00000000000000 0.00000000000000,
    0.00000000000000 0.00000000000000 0.00000000000000
11 0.00000000000000 0.00000000000000 0.00000000000000,
    0.00000000000000 0.00000000000000 0.00000000000000,
    0.00000000000000 0.00000000000000 0.00000000000000,
    0.00000000000000 0.00000000000000 0.00000000000000
12 0.00000000000000 0.00000000000000 0.00000000000000,
    0.00000000000000 0.00000000000000 0.00000000000000,
    0.00000000000000 0.00000000000000 0.00000000000000,
    0.00000000000000 0.00000000000000 0.00000000000000
@
*
MATRIX STRESS NAME=3 NS=12 ND=12
@CLEAR
1 1.00000000000000 0.00000000000000 0.00000000000000 0.00000000000000,
    0.00000000000000 0.00000000000000 0.00000000000000,
    0.00000000000000 0.00000000000000 0.00000000000000,
    0.00000000000000 0.00000000000000
2 0.00000000000000 1.00000000000000 0.00000000000000 0.00000000000000,
    0.00000000000000 0.00000000000000 0.00000000000000,
```

```
    0.00000000000000 0.00000000000000 0.00000000000000,
    0.00000000000000 0.00000000000000
3 0.00000000000000 0.00000000000000 1.00000000000000 0.00000000000000,
    0.00000000000000 0.00000000000000 0.00000000000000,
    0.00000000000000 0.00000000000000 0.00000000000000,
    0.00000000000000 0.00000000000000
4 0.00000000000000 0.00000000000000 0.00000000000000 1.00000000000000,
    0.00000000000000 0.00000000000000 0.00000000000000,
    0.00000000000000 0.00000000000000 0.00000000000000,
    0.00000000000000 0.00000000000000
5 0.00000000000000 0.00000000000000 0.00000000000000 0.00000000000000,
    1.00000000000000 0.00000000000000 0.00000000000000,
    0.00000000000000 0.00000000000000 0.00000000000000,
    0.00000000000000 0.00000000000000
6 0.00000000000000 0.00000000000000 0.00000000000000 0.00000000000000,
    0.00000000000000 1.00000000000000 0.00000000000000,
    0.00000000000000 0.00000000000000 0.00000000000000,
    0.00000000000000 0.00000000000000
7 0.00000000000000 0.00000000000000 0.00000000000000 0.00000000000000,
    0.00000000000000 0.00000000000000 1.00000000000000,
    0.00000000000000 0.00000000000000 0.00000000000000,
    0.00000000000000 0.00000000000000
8 0.00000000000000 0.00000000000000 0.00000000000000 0.00000000000000,
    0.00000000000000 0.00000000000000 0.00000000000000,
    1.00000000000000 0.00000000000000 0.00000000000000,
    0.00000000000000 0.00000000000000
9 0.00000000000000 0.00000000000000 0.00000000000000 0.00000000000000,
    0.00000000000000 0.00000000000000 0.00000000000000,
    0.00000000000000 1.00000000000000 0.00000000000000,
    0.00000000000000 0.00000000000000
10 0.00000000000000 0.00000000000000 0.00000000000000,
    0.00000000000000 0.00000000000000 0.00000000000000,
    0.00000000000000 0.00000000000000 0.00000000000000,
    1.00000000000000 0.00000000000000 0.00000000000000
11 0.00000000000000 0.00000000000000 0.00000000000000,
    0.00000000000000 0.00000000000000 0.00000000000000,
    0.00000000000000 0.00000000000000 0.00000000000000,
    0.00000000000000 1.00000000000000 0.00000000000000
12 0.00000000000000 0.00000000000000 0.00000000000000,
    0.00000000000000 0.00000000000000 0.00000000000000,
    0.00000000000000 0.00000000000000 0.00000000000000,
    0.00000000000000 0.00000000000000 1.00000000000000
@
*
MATRIXSET NAME=1 STIFFNE=1 MASS=2 DAMPING=4 STRESS=3
*
```

The following points regarding the proper choice of values should be considered for the element to work:

1- This is a highly nonlinear element. For the simplest cases use of $\Delta t > 0.001s$ is not recommended and for bigger and more complex models, convergence may require $\Delta t = 0.0002s$ or smaller.

2- The choice of dimensions and vertical spring constants used for the model should be such that it does not jeopardize accuracy or prevent convergence. The spring used should have stiffness high enough to act rigidly. This may require a frequency of at least 50Hz. The corresponding damping should be high as well to prevent any excessive excitation in this spring so that the value of normal force calculated remains accurate. These considerations mean high values for the stiffness and damping. However, the tolerance chosen for the convergence of the model cannot be outside a certain range. A bigger tolerance will mean loss of accuracy and smaller tolerance will require very large number of cycles that will exceed ADINA limits. The stiffness should be of dimensions that combined with this tolerance describe the behavior with enough accuracy. A Proper choice of dimension units will require some experiments by the user.

REFERENCES

ADINA, ADINA Theory and Modeling Guide, Volume I: ADINA, Report ARD 01-7, ADINA R & D, Inc., June, 2001.

ADINA, ADINA User Interface Command Reference Material, Volume I: ADINA Model Definition, Report ARD 01-2, ADINA R & D, Inc., June, 2001.

ADINA, from http://www.adina.com/faq/qg001.shtml, Retrieved November, 2002.

Al-Hussaini, T. M., Zayas, V. A., and Constantinou, M. C., "Seismic Isolation of Multi-Story Frame Structures with Friction Pendulum Isolators", Technical Report NCEER 94-007, National Center for Earthquake Engineering Research, State University of New York, Buffalo, 1994.

Almazan, Jose L., and De la Llera, Juan C., "Analytical Model of Structures with Frictional Pendulum Isolators", Earthquake Engineering and Structural Dynamics, vol. 31, no. 2, pp. 305-332, February, 2002.

Almazan, J. L., De la Llera, J. C., and Inaudi, J. A., "Modeling Aspects of Structures Isolated with the Frictional Pendulum System", Earthquake Engineering and Structural Dynamics, vol. 27, no. 8, pp. 845-867, August, 1998.

Constantinou, M. C., Tsopelas, P., Kim, Y-S., and Okamoto, S., "NCEER-Taisei Corporation Research Program on Sliding Isolation Systems for Bridges: Experimental and Analytical Study of Friction Pendulum System (FPS)", Technical Report NCEER 93-0020, National Center for Earthquake Engineering Research, State University of New York, Buffalo, November, 1993.

Das, Braja M., Principles of Foundation Engineering, PWS Publishing Company, Boston, 1990.

Der Kiureghian, A., Sackman, J. L., and Hong, K-J., "Seismic Interaction in Linearly Connected Electrical Substation Equipment", Earthquake Engineering and Structural Dynamics, vol. 30, no. 3, pp. 327-347, March, 2001.

Del Vecchio, Robert M., Poulin, Bertrand, Feghali, Pierre T., Shah, Dilipkumar M., and Ahuja, Rajendra, Transformer Design Principles, With Applications to Core-Form Power Transformers, Taylor & Francis, New York, 2002.

DuPont, "NOMEX Pressboard, Technical Information", 2002, from http://Dupont.com/nomex/electapps/pressboard%204%20pager.pdf, Retrieved June, 2003.

Earthquake Protection Systems, Inc. (EPS), Technical Characteristics of Friction Pendulum Bearings, March, 1996.

Ersoy, Selahattin, "Seismic Response of Transformer Bushing Systems and Their Rehabilitation Using Friction Pendulum System", Doctoral Dissertation, New Jersey Institute of Technology, January, 2002.

Ersoy, Selahattin, "Simple Foundation Analysis of Transformers", Unpublished Manuscript, 2001.

Fan, Fa-Gung, and Ahmadi, Goodarz, "Floor Response Spectra for Base-Isolated Multi-Storey Structures", Earthquake Engineering and Structural Dynamics, vol. 19, no. 3, pp. 377-388, April, 1990.

Fan, Fa-Gung, and Ahmadi, Goodarz, "Seismic Responses of Secondary Systems in Base-Isolated Structures", Engineering Structures, vol. 14, no. 1, pp. 35-48, 1992.

Fleming, W. G. K., Weltman, A. J., Randolph, M. F., and Elson, W. K., Piling Engineering, Second Edition, John Wiley & Sons, Inc., New York, 1992.

Gilani, Amir S., Whittaker, Andrew S., Fenves, Gregory L., and Fujisaki, Eric, "Seismic Evaluation and Retrofit of 230-kV Porcelain Transformer Bushings" , Report No. PEER 1999/14, Pacific Earthquake Engineering Research Center, University of California, Berkeley, December, 1999.

Gilani, Amir S., Whittaker, Andrew S., Fenves, Gregory L., and Fujisaki, Eric, "Seismic Evaluation of 550-kV Porcelain Transformer Bushings", Report No. PEER 1999/05, Pacific Earthquake Engineering Research Center, University of California, Berkeley, October, 1999.

Heathcote, Martin J., J & P Transformer Book, Twelfth Edition, Newnes, Massachusetts, 1998.

Hong, K-J., Der Kiureghian, A., and Sackman, J. L., "Seismic Interaction in Cable-Connected Equipment Items", Journal of Engineering Mechanics, vol. 127, no. 11, pp. 1096-1105, November, 2001.

ICBO, Uniform Building Code, Volume 2, International Conference of Building Officials, 1997.

IEEE, IEEE Std. 693-1997, Recommended Practices for Seismic Design of Substations, Piscataway, New Jersey, 1998.

Kim, Young-Sang, and Lee, Dong-Guen, "Seismic Response of Support-Isolated Secondary Structures in a Multistorey Structure", Engineering Structures, vol. 15, no. 5, pp. 335-347, September, 1993.

KRYFS Laminations Pvt. Ltd., from http://www.transformercore.com/crgoMAIN.htm, Retrieved June, 2003.

Lambrou, V., and Constantinou, M. C., "Study of Seismic Isolation Systems for Computer Floors", Technical Report NCEER 94-0020, National Center for Earthquake Engineering Research, State University of New York, Buffalo, July, 1994.

Liu, Cheng, and Evett, Jack B., Soils and Foundations, second edition, Prentice Hall, New Jersey, 1987.

Mokha, A. S., Constantinou, M. C., and Reinhorn, A. M., "Experimental Study and Analytical Prediction of Earthquake Response of a Sliding Isolation System with a Spherical Surface", Technical Report NCEER 90-0020, National Center for Earthquake Engineering Research, State University of New York, Buffalo, October, 1990.

Mokha, A. S., Constantinou, M. C., and Reinhorn, A. M., "Verification of Friction Model of Teflon Bearings Under Triaxial Load", Journal of Structural Engineering, vol. 119, no. 1, pp. 240-261, Jan, 1993.

Nagarajaiah, S., Reinhorn, A. M., and Constantinou, M. C., "Nonlinear Dynamic Analysis of Three-Dimensional Base Isolated Structures (3D-BASIS)", Technical Report NCEER 89-0019, National Center for Earthquake Engineering Research, State University of New York, Buffalo, August, 1989.

Nagarajaiah, S., Reinhorn, A. M., and Constantinou, M. C., "3D-BASIS - Nonlinear Dynamic Analysis of Three-Dimensional Base Isolated Structures: Part II", Technical Report NCEER 91-0005, National Center for Earthquake Engineering Research, State University of New York, Buffalo, February, 1991.

Nagarajaiah, S., Li, C., Reinhorn, A. M., and Constantinou, M. C., "3D-BASIS-TABS: Computer Program for Nonlinear dynamic Analysis of Three Dimensional Base Isolated Structures", Technical Report NCEER 93-0011, National Center for Earthquake Engineering Research, State University of New York, Buffalo, August, 1993.

Pansini, A. J., Electrical Transformer and Power Equipment, Fairmont Press, Georgia, 1999.

PEER, PEER Strong Motion Database, from http://peer.berkeley.edu/smcat/, Retrieved November, 2002.

Prevost, Tom, Woodcock, David J., and Krause, Christoph, "The Effects on Winding Clamping Pressure Due to Changes in Moisture, Temperature and Insulation Age", WEIDMANN Electrical Technology, from http://www.weidmannb2b.biz/WACTI/pdf/WindingClampingPressure.pdf, Retrieved June, 2003.

Reinhorn, A. M., Nagarajaiah, S., Constantinou, M. C., and Tsopelas, P. C., "3D-BASIS-TABS Version 2.0: Computer Program for Nonlinear Dynamic Analysis of Three

Dimensional Base Isolated Structures", Technical Report NCEER 94-0018, National Center for Earthquake Engineering Research, State University of New York, Buffalo, June, 1994.

The Gund Company, Inc., "Material Data Sheet", from http://www.thegundcompany.com/DataPages/Electrical%20Insulation%20Materials/Pressboard%20and%20Kraft%20Papers/EHV%20Family%20of%20Pressboard%20Materials.pdf, Retrieved June, 2003.

Tsai, C. S., "Finite Element Formulation for Friction Pendulum Seismic Isolation Bearings", International Journal of Numerical Methods in Engineering, vol. 40, no. 1, pp. 29-49, January, 1997.

Tsopelas, P. C., Nagarajaiah, S., Constantinou, M. C., and Reinhorn, A. M., "3D-BASIS-M: Nonlinear Dynamic Analysis of Multiple Building Base Isolated Structures", Technical Report NCEER 91-0014, National Center for Earthquake Engineering Research, State University of New York, Buffalo, May, 1991.

Tsopelas, P. C., Constantinou, M. C., and Reinhorn, A. M., "3D-BASIS-ME: Computer Program for Nonlinear Dynamic Analysis of Seismically Isolated Single and Multiple Structures and Liquid Storage Tanks", Technical Report NCEER 94-0010, National Center for Earthquake Engineering Research, State University of New York, Buffalo, April, 1994.

Woodcock, David J., "Condition Appraisal of Power Transformers", Maintenance Strategies for the New Millennium, Indiana, November, 2000, from http://www.weidmannb2b.biz/WACTI/pdf/ConditionAppraisal.pdf, Retrieved June, 2003.

Zayas, V. A., Low, S. S., and Mahin, S. A., "The FPS Earthquake Resisting System, Experimental Report", Report No. UCB/EERC 87/01, Earthquake Engineering Research Center, University of California, Berkeley, June, 1987.

Zayas, V. A., Low, S., Bozzo, L., and Mahin, S., "Feasibility and Performance Studies on Improving the Earthquake Resistance of New and Existing Buildings Using the Friction Pendulum System", Report No. UCB/EERC 89/09, Earthquake Engineering Research Center, University of California, Berkeley, 1989.

Zayas, V., and Low, S., "Application of Seismic Isolation to a Four Story Wood Building", 1991 SEAOC Proceedings, SEAOC Convention, 1991.

Zayas, V., Piepenbrock, T. and Al-Hussaini, T., "Summary of Testing of the Friction Pendulum Seismic Isolation System: 1986-1993", Proceedings of ATC-17-1 Seminar on Seismic Isolation, Passive Energy Dissipation and Active Control, Applied Technology Council, San Francisco, March, 1993.

Zayas, V. A., Constantinou, M. C., Tsopelas, P., and Kartoum, A., "Testing of Friction Pendulum Seismic Isolation Bearings for Bridges", Proceedings of the Fourth World Congress on Joint Sealing and Bearing Systems for Concrete Structures, Sacramento, California, September, 1996.